UNIVERSITY OF
KWAZULU-NATAL

Simulating Thermal Fluctuations In Soft Matter Models

by

Emmanuel Omboga Obaga

Submitted in partial fulfilment of the academic requirements for the degree of Doctor of Philosophy in the

School of Physics,

University of KwaZulu-Natal

Pietermaritzburg

December, 2015

As the candidate's supervisor I have approved this thesis for submission.

Signed: Alessandro Sergi Name: **Prof. Alessandro Sergi** Date: March 31, 2016

Signed: Name: **Prof. F. Petruccione**(co-supervisor) Date: 31.3.2016

Abstract

The research carried out in this work is in two parts: In the first part, we derive a configurational temperature Nosé-Hoover thermostat by reformulating the original Braga and Travis thermostat [J. Chem. Phys. **123** (134101), 2005] in phase space using a quasi-Hamiltonian approach introduced by Sergi and Ferrario [Phys. Rev. E **64** (056125), 2001]. We also present a reversible integrator based on the symmetric Trotter decomposition of propagator for harmonic potentials and for more complicated potentials, a harmonic approximation of the potential is performed locally resulting in a position-dependent harmonically approximated propagator for a general system. In the second part of our work, we present a phonostat methodology based on classical molecular dynamics and Wigner approach to quantum mechanics. We introduce quantum effects into our system by generating a thermal profile using different 'effective' temperature for the modes and coupling each one of the modes to a thermal bath. We test our phonostat algorithm against the range of temperatures and densities explored by Mausbach and May [Fluid Phase Equil. **249** (17), 2006].

Preface

All the work / numerical experiments / analysis presented in this thesis are the results of the collaborative effort within the School of Physics, University of KwaZulu-Natal, Pietermaritzburg, from July 2012 to December 2015, under the supervision of Prof. Alessandro Sergi.

Declaration

I, **Emmanuel Omboga Obaga** declare that

1. The research reported in this thesis, except where otherwise indicated, is my original research.

2. This thesis has not been submitted for any degree or examination at any other university.

3. This thesis does not contain other persons' data, pictures, graphs or other information, unless specifically acknowledged as being sourced from other persons.

4. This thesis does not contain other persons' writing, unless specifically acknowledged as being sourced from other researchers. Where other written sources have been quoted, then:

   (a) Their words have been re-written but the general information attributed to them has been referenced

   (b) Where their exact words have been used, then their writing has been placed in italics and inside quotation marks, and referenced.

5. This thesis does not contain text, graphics or tables copied and pasted from the Internet, unless specifically acknowledged, and the source being detailed in the thesis and in the References sections.

Signed: 

Acknowledgments

I thank Almighty God for all I have achieved this far in my life. By His grace, my dreams have become realities laid bare for all to witness.

With the completion of three years of hard work, I now come to the end, and perhaps the most apprehensive part of acknowledging all stakeholders including the family, supervisor, academic staff, friends, colleagues and other resource members that have been key in keeping me focused throughout my time as a postgraduate and PhD student. Their love, guidance, interest, patience, and encouragement during this study period considerably influenced and enhanced my research.

As this may be my only opportunity to thank these individuals in writing, I may be a bit more verbose in my thanks than necessary. First and foremost,I would like to express my eternal gratitude to my supervisor Prof. Alessandro Sergi. His insight, invaluable guidance, enthusiastic interest, constructive criticism, tireless efforts and encouragement during this study period are unsurpassed. He has provided guidance at key moments in my work while also allowing me to work independently the majority of the time.

My deep heartfelt gratitude to my parents for their perpetual support which has kept the lighted flame within me throughout the past years.

Finally, I register my special gratitude to my entire family, relatives and friends and all those that I did not mention by name for their great support and encouragement. May the good Lord bless you all and always.

Contents

List of Figures

List of Tables

Chapter 1

Introduction

From as early as the 19^{th} century, soft matter has been of considerable research interest in the field of condensed matter physics. Soft matter is made up of macromolecular materials which are on a length scale of tens of nanometers existing in a variety of physical states. Such materials include polymers [1–3], liquid crystals [4, 5], amphiphiles, colloids [6–8] and bio-molecules. Usually these large molecules are easily deformed by thermal fluctuations or thermal stresses and show predominant physical behaviors at energy scales comparable to room temperature thermal energy. Many soft matter materials are ubiquitous in our every day lives from a wide range of technical applications in the commercial and medical fields, for example in food technology and personal to home-care products such as cosmetics and detergents, pharmaceutical industries especially in drug delivery among other.

In the academic field, especially in biology, chemistry and physics, soft matter systems are extensively studied by both experimentalists and theoreticians since they have special properties that make them valuable model systems for research. For instance, one can define a precise interaction potential from the effective interactions of the molecules within the system which can be tuned in a controlled way by changing relevant properties of the suspension [9, 10], such as the temperature, the salt concentration, the solvent quality or by altering the physical and chemical composition of the dispersed particles. Also, the dispersed particles are comparatively larger in size when compared to their

atomic counterparts thus experimental investigations can be carried out using indirect measurement techniques such as X-ray scattering [11] and small-angle neutron scattering (SANS) or through modern real-time tools such as video microscopy[12, 13] which are capable of providing insight to the particles' motion and behavior.

Computer simulations have recently been used to model soft matter systems using molecular dynamics (MD) simulation. Despite the challenges faced using computers for simulations such as limited computational resources as the case of modelling a system using only a finite number of atoms as opposed to a large Avogradro's number of atoms [14], computational simulations capture the essential features of molecular systems. If the numerical results are in agreement to the theoretical predictions based on approximated theories, the models can be extended to study system behaviours with conditions which are not feasibly achievable experimentally [14]. This provides further insights into how processes evolve at a molecular level. The computational models use suitably chosen interacting potentials such as the Lennard-Jones and the Gaussian Core potentials capable of mimicking the atomic forces in polymer chains, liquid crystals, crystals and bio-molecules among others.

In our work, we use MD simulation techniques for systems in nonequilibrium to test algorithms derived for new configurational thermostats based on the original Braga and Travis thermostat [15] capable of controlling the temperature using only the configurational information of the system. Also, we introduce a new phonostat algorithm which is tested against a standard MD simulation and compared with literature results with excellent agreement.

The structure of the thesis is organised as follows: In Chapter 2, a brief introduction of molecular dynamics is given. Also, the static and dynamical properties investigated within the thesis are briefly discussed. In Chapter 3, a new configurational Nosé-Hoover thermostat(CTNH) based on the original Braga-Travis thermostat is presented. This new thermostat is formulated in phase space using a quasi-Hamiltonian approach introduced by Sergi and Ferrario [16]. To integrate the equations of motion for this thermostat, a reversible integrator based on the symmetric Trotter decomposition of the propagator (STP) is presented for systems with quadratic potentials. However, for a general

system with a more complicated potential, a position-dependent harmonically approximated propagator (PDHA-STP) is presented. Furthermore, we perform simulations on system coupled to the CTNH thermostat using a Weeks-Chandler-Andersen(WCA) potential with the PDHA-STP integration algorithm. In Chapter 4, a new phonostat methodology is presented. The thermostat is able to maintain the temperature of each mode via a thermostat coupled to each mode effectively maintaining the energy of the system. The classical description of the phonostat algorithm is tested against a standard molecular dynamics simulation. Moreover, using the Wigner approach to quantum mechanics, the 'effective' temperatures of the modes can be obtained and with the phonostat algorithm quantum effects are easily introduced to the system. A system with an interacting Gaussian Core potential is investigated with a range of similar state points explored by Mausbach and May [17]. In Chapter 5, a brief summary of the research work is presented and the main conclusions highlighted from the two different cases investigated within this thesis and discuss possible future work.

Chapter 2

Molecular Dynamics

2.1 Introduction

Molecular Dynamics (MD) is a type of computer simulation technique generally used to investigate the dynamical evolution of a system comprising of many interacting particles. This is achieved through numerical integration of Newtons classical equations of motion.

MD was first derived and implemented in the late 1950's by Alder and Wainwright[18–20], in their work, they performed numerical simulations on a system of hard and elastic spheres which lead to important insights concerning the behavior of simple liquids. Following their success, many other simulation models have been proposed and extensively investigated providing comprehensive insight into their structural and dynamical properties. Examples of these models include, the Lennard-Jones (LJ) by Rahman in 1964 [21, 22] where he studied the thermodynamic properties of liquid Argon and the Gaussian-Core model (GCM) introduced by Stillinger in 1976 [23, 24]. Such systems have been used in the study of polymers, liquid crystals, amphiphiles, colloids and biomolecules.

Naturally, MD simulations are performed at constant energy conditions which correspond to the constant energy conditions, NVE ensemble (constant number of particles, volume and energy). However, real-life results are obtained from experiments performed at constant pressure or constant temperature conditions. This poses a problem when

comparing results from computer simulations (MD) and those obtained from real-life experiments. Anderson, in 1980, proposed a constant pressure method which enables MD simulations to be performed under the NPH [25] ensemble (constant number of particles, pressure and enthalpy). Nosé, in 1984, introduced a method to maintain constant temperature within MD simulations which made use of a thermal reservoir (thermostat). With the use of such thermostats, MD simulations could be performed under NVT [26] (constant number of particles, volume and temperature) ensembles or NPT [27] (constant number of particles, pressure and temperature) ensembles.

This thesis shall concern itself with MD simulations performed under constant temperature (NVT ensemble).

2.2 Molecular Dynamics ensembles

MD simulation techniques are widely used in the theoretical study of biological and chemical systems. MD simulations study the dynamical evolution of particles within a molecular system in time by numerically integrating Newton equations of motion. At a given time within an MD simulation, the microscopic information of the particles such as position and velocities are known, by using statistical mechanics [28] this information can be converted to macroscopic quantities such as pressure and temperature. However, different microscopic states can yield the same macroscopic or thermodynamics states. Thus, information about macroscopic quantities are always obtained from ensembles. An ensemble is a statistical average over all the possible microscopic states explored by a system such that an identical macroscopic or thermodynamic states are obtained. Examples of such ensembles include the microcanonical ensemble and the canonical ensemble.

For a given N-body system with a dynamical quantity, $A(\mathbf{x})$, where $\mathbf{x}$ defines the phase space points of the system, the ensemble averages are evaluated as,

$$\langle A \rangle_{ensemble} = \int dx^{2N} \rho\left(\mathbf{x}\right) A\left(\mathbf{x},t\right) \ . \tag{2.2.1}$$

This integral, however, is very difficult to evaluate as one has generally explores all possible regions of phase space for the system. In MD simulations, this microscopic states are explored sequentially in time, with the time averages evaluated as,

$$\langle A \rangle_{time} = \lim_{T \to \infty} \frac{1}{T} \int_0^T dt \, A\left(\mathbf{x}\left(t\right)\right) \ , \tag{2.2.2}$$

where T is the total time interval. However, due to the finite computational resources it is not feasible to explore all regions of phase space. This difficulty is solved by the use of the ergodic hypothesis [29], a fundamental axiom of statistical mechanics, which states that the ensemble average equals the time average,

$$\langle A \rangle_{ensemble} = \langle A \rangle_{time} \ . \tag{2.2.3}$$

2.2.1 Microcanonical ensemble

This statistical ensemble is characterized by a system having fixed thermodynamical parameters N, V, E which correspond to the number of particles, the volume and the energy respectively. Such a system has an equilibrium distribution function f_m given by

$$f_m\left(q, p\right) = Z^{-1} \delta\left(H - E\right), \tag{2.2.4}$$

where Z is the partition function given by

$$Z = \int d^N q \, d^N p \, \delta\left(H - E\right), \tag{2.2.5}$$

and $\delta\left(H - E\right)$ is the delta of Dirac which is characterized as having a zero value except when $H - E = 0$, in which case it is infinite. The delta of Dirac function mathematically enforces energy conservation within this ensemble as it ensures $\delta\left(H - E\right) \neq 0$ when $H = E$.

Under the principle of equal *a priori* probabilities one can realize that all the microscopic states (q, p) with energy $H = E$ are equally probable. It follows that all the

microstates must have the same energy E. However, given E little will be known about the microstates. This inadvertently leads to a system where some of the microstates are preferred and assigned higher probabilities than others. Hence in order to obtain averages in the microcanonical ensemble, all possible microstates have to be considered. This, however, proves to be extremely difficult to evaluate since ensemble averages (see Eq. (2.2.1)) require knowledge of all possible microscopic states. Using the ergodic hypothesis, ensemble averages are equivalent to time averages (see Eq. (2.2.2)) obtained when performing experiments numerically under MD simulation. In reality, experiments are carried out with knowledge of the macroscopic properties such as temperature or pressure. Thus, results from numerical experiments can be compared with real ones if one performs the calculations in the canonical ensemble.

2.2.2 Canonical ensemble

This statistical ensemble is characterized by a system having the macrostates N, V, T which correspond to the number of particles, the volume and the temperature respectively. Temperature control within this ensemble is achieved by placing the system of interest in contact with a heat bath, which in the thermodynamic limit is represented using an infinite number of degrees of freedom. Such a system has an equilibrium distribution function f_c that is dependent on the temperature given by

$$f_c\,(q,p) = Z^{-1} e^{-\beta H}, \tag{2.2.6}$$

where Z is the partition function given by

$$Z = \int d^N q\, d^N p\, e^{-\beta H}, \tag{2.2.7}$$

and

$$\beta = \frac{1}{k_B T}, \tag{2.2.8}$$

where k_B is the Boltzmann constant.

Using the canonical distribution function, given by Eq. (2.2.6), one can easily show how to obtain the famous Maxwell distribution function. This function governs the probability distribution of particle velocities in a system in contact with a thermal bath. It also forms the basis for deriving the celebrated Equipartition theorem expressed as

$$\left\langle \frac{p_i^2}{2m_i} \right\rangle = \frac{k_B T}{2}. \tag{2.2.9}$$

Eq. (2.2.9), states that the equilibrium average of the kinetic energy of an arbitrary particle is constant and equal to $k_B T/2$.

2.2.3 Estimating temperature in MD simulations

Temperature, under MD simulation is estimated using the equipartition theorem while assuming ergodicity. Hence for a system with N degrees of freedom, the equipartition theorem can be rewritten as

$$\left\langle \sum_{i=1}^{N} \frac{p_i^2}{2m_i} \right\rangle = N \left\langle \frac{p_i^2}{2m_i} \right\rangle = N \frac{k_B T}{2}. \tag{2.2.10}$$

Thus the temperature can be given using the following equation,

$$T = \frac{2}{N k_B} \left\langle \sum_{i=1}^{N} \frac{p_i^2}{2m_i} \right\rangle. \tag{2.2.11}$$

The instantaneous temperature can also be calculated using

$$T_t = \frac{2}{N k_B} \sum_{i=1}^{N} \frac{p_i^2}{2m_i}. \tag{2.2.12}$$

The instantaneous temperature times the Boltzmann constant $k_B T_t$ is only an estimate of the inverse of the fixed parameter β of the distribution function which can fluctuate.

However for non-equilibrium MD simulations, temperature within the system is evaluated using the configurational information of the particles, this idea was introduced by Rugh [30] in 1998. Thus, temperature can be evaluated as follows,

$$T_{\text{conf}} = \frac{1}{k_{\text{B}}} \frac{\langle |\nabla U|^2 \rangle}{\langle \nabla^2 U \rangle} , \tag{2.2.13}$$

where ∇ is the spacial gradient and U is the potential energy of the system.

2.3 Basic Approach to MD Simulation

In order to carry out a MD simulation, one has to take into account of the following three phases, the initialization phase, the equilibration phase and lastly the production phase. In the initialization phase, the system parameters (simulation time-step, cut-off distances, potential energy function parameters etc.) are set, and all the particles within the system are assigned initial positions and velocities. In the equilibration phase, simulations are carried out for a given number of time-steps while the systems thermodynamic properties such as the potential energy and the hamiltonian function are periodically checked for conservation. Once the system has reached equilibration, the production phase follows. This phase is similar to the equilibration phase, with the exception that the properties of interest are calculated during the dynamical evolution of the system with time. New particle trajectories are generated in MD by solving Newton's equations of motion numerically. A flowchart showing a typical MD simulation is shown in Fig. (2.1).

2.4 Reduced Units

Comparison and verification of results from experiments, simulations and different theories is of fundamental importance when comparing scientific work. However, this task can be inherently difficult if one does not consider a way of unifying different measurements and values. Historically, there exists various systems of measurements that are well established for defining and interpreting input data and results in systems, this has led to an ongoing debate over which systems of measurements are preferable over others. This problem has been avoided especially where theoretical considerations are taken for system values that have been expressed in terms of "natural" units which correspond

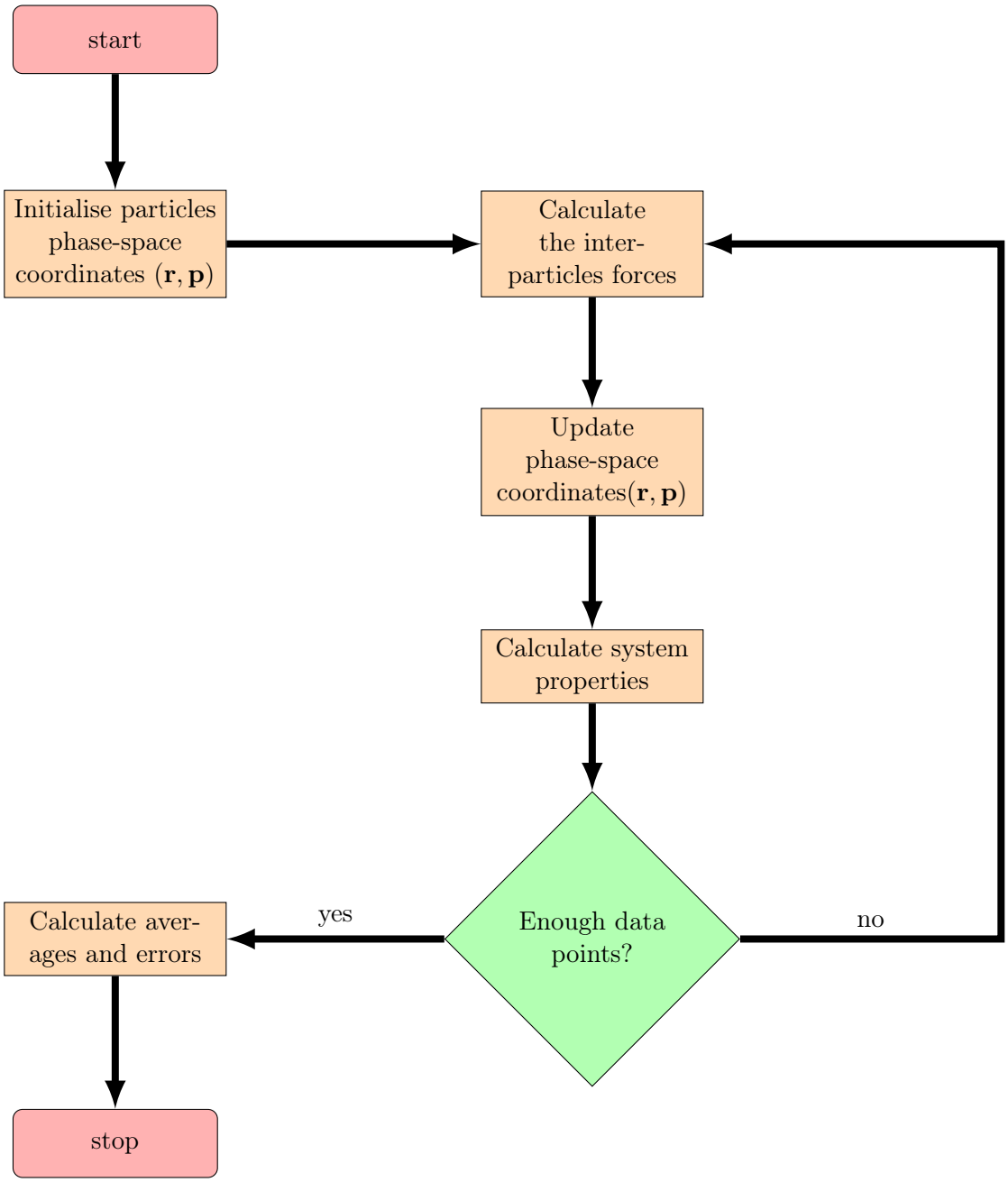

Figure 2.1: A figure showing typical algorithmic steps for a molecular dynamics simulation. Starting off with a set of initial conditions for the phase-space coordinates of the system, new phase-space coordinates are calculated at every iteration within the MD loop.

to characteristic length and energy scales of the model under consideration. Moreover, reduced units are generally preferred when performing computer simulations in order to preserve the accuracy of results by avoiding round-off errors associated with arithmetical calculations between very large and small numbers since the values are roughly of the

same order.

For the systems which are described within this thesis, ϵ and σ define their characteristic energy and length scale respectively. Thus, reduced units for the temperature, density and pressure are marked with a prime to distinguish them from physical quantities as follows:

The reduced temperature is defined as,

$$T' = \frac{k_B T}{\epsilon}, \tag{2.4.1}$$

the reduced density is expressed as,

$$\rho' = \rho\sigma^3, \tag{2.4.2}$$

and the reduced pressure,

$$P' = \frac{P\sigma^3}{\epsilon}, \tag{2.4.3}$$

where k_B is the well known Boltzmann's constant, ρ is the particle density, P is the pressure and T is the ensemble temperature.

Throughout this thesis only reduced units will be used, and for convenience the primes on the notations will be disregarded.

2.5 Analysis of Simulation Data

When performing molecular dynamics simulations it is common practice to generate data files periodically for analysis at the end of each simulation run. The analysis of these data files produce useful information dependent on the quantities of interest to be investigated within the system. Here, we outline the radial distribution function and the diffusion coefficient which have been calculated and reported in this work.

2.5.1 Radial Distribution Function

For a fixed density, the radial distribution function $g(r)$ defines the probability of a particle being found at a distance r away from a reference particle in comparison to the expected probability of such a particle in a completely random distribution such as the ideal gas state. From this definition, one can deduce that for an ideal gas state the $g(r)$ will be unity and any deviations from unity signifies correlations between particles[**?**]. The equation used when evaluating $g(r)$ is derived by integrating the configurational distribution function over all particle positions within a system with the exception of two positions [14],

$$g\left(\overrightarrow{r_1}, \overrightarrow{r_2}\right) = \frac{N(N-1)}{\rho^2 Z_{NVT}} \int d\overrightarrow{r_3}\; d\overrightarrow{r_4} \ldots d\overrightarrow{r_N}\; \exp\left(-\beta U\left(\overrightarrow{r_1}, \overrightarrow{r_2}, \ldots, d\overrightarrow{r_N}\right)\right), \tag{2.5.1}$$

where N is the number of particles, ρ is the density, $\beta = \frac{1}{k_B T}$. Here, k_B is the Boltzmann constant and T is the temperature of the system. U is the potential energy of the system and the configurational integral is given by

$$Z_{NVT} = \int d\overrightarrow{r_1}\; d\overrightarrow{r_2} \ldots d\overrightarrow{r_N}\; \exp\left(-\beta U\left(\overrightarrow{r_1}, \overrightarrow{r_2}, \ldots, d\overrightarrow{r_N}\right)\right). \tag{2.5.2}$$

For a classical system, $g\left(\overrightarrow{r_1}, \overrightarrow{r_2}\right)$ depends only on the inter-particle distance $r = |\overrightarrow{r_1} - \overrightarrow{r_2}|$, thus equation (2.5.1) can be expressed as

$$g(r) = \frac{1}{\rho^2} \left\langle \sum_i \sum_{j \neq i} \delta(\overrightarrow{r_i}) \delta(\overrightarrow{r_j} - \overrightarrow{r}) \right\rangle \tag{2.5.3}$$

$$= \frac{V}{N^2} \left\langle \sum_i \sum_{j \neq i} \delta(\overrightarrow{r} - \overrightarrow{r_{ij}}) \right\rangle \tag{2.5.4}$$

where r_{ij} is the displacement vector pointing from particle i to j whereas $\langle \cdot \rangle$ denotes the ensemble average (an average over all possible states).

Peculiar characteristic patterns of $g(r)$ emerge when considering the distribution of particles across different states. The $g(r)$ pattern for solids are characterised with high,

sharp peaks whereas for liquids there are no sharp peaks but $g(r)$ has regions of low and high intensity. Such distinct patterns help distinguish solids from liquids when obtaining $g(r)$ through computer simulations. Moreover, for a system of interacting particles, the thermodynamic properties such as energy and pressure can be calculated from the $g(r)$, using the general relation,

$$\langle \mathcal{A} \rangle = \left\langle \sum_i \sum_{j>i} a(r_{ij}) \right\rangle = \frac{1}{2} N\rho \int_0^\infty a(r) g(r) 4\pi r^2 dr, \tag{2.5.5}$$

where $\langle \mathcal{A} \rangle$ is the expectation value of $a(r_{ij})$, and $a(r_{ij})$ is a function dependent only on the inter-particle distance of particle i and particle j. For example, the total internal energy for a system with an isotropic pair potential $u(r)$, can be expressed as [14],

$$E = \frac{3}{2} N k_B T + 2\pi N \rho \int_0^\infty r^2 u(r) g(r) dr, \tag{2.5.6}$$

where in the first term, N, k_B and T are the number of particles, Boltzmann distribution and the temperature respectively. The pressure can be calculated by [14],

$$P = \rho k_B T - \frac{2}{3}\pi\rho^2 \int_0^\infty r^3 \frac{du(r)}{dr} g(r) dr. \tag{2.5.7}$$

2.5.2 Diffusion Coefficient

Diffusion coefficient is a macroscopic property that describes the random motion of a molecule in the absence of any gradients that would cause a mass flux. There are two common ways to obtain a self-diffusion coefficient. The first is from molecule positions and the second is from velocities. Theoretically, both methods yield the same result. Obtaining the diffusion coefficient from the velocities involves integrating the velocity autocorrelation function, an example from what is called Green-Kubo relations.

$$D = \frac{1}{3} \int_0^\infty \langle v_j(t) \cdot v_j(0) \rangle \tag{2.5.8}$$

Einstein related the self-diffusion coefficient to the mean square displacement of a particle as a function of observation time. The mean square displacement is proportional to the observation time in the limit that the observation time goes to infinity. The proportionality constant that relates the MSD to the observation time is called the self-diffusivity. The diffusion coefficient is expressed as

$$D = \lim_{t \to \infty} \frac{1}{2d} \left\langle \frac{\left[r_j\left(t\right) - r_j\left(0\right)\right]^2}{t} \right\rangle \tag{2.5.9}$$

where D is the self-diffusion coefficient, and d is the dimensionality of the system. The numerator of Eq. (2.5.9) is the mean square displacement. The angled brackets indicate an ensemble average has been taken. The ensemble average is an average over all molecules in the simulation and all origins. By origins it is implied that any time step can be considered the time zero in Eq. (2.5.9), because Eq. (2.5.9) is only looking at observation times (relative times or elapsed times) rather than some absolute time.

Chapter 3

Configurational Thermostat

3.1 Introduction

Temperature control in molecular dynamics simulations is of particular importance especially if one is interested with the thermodynamic properties of a molecular system. This is generally achieved by coupling the system of interest to a thermal heat bath or thermostat. The value of the temperature can be calculated from the fluctuation velocities $\mathbf{c}_i$ of the particles according to the equipartition function. Most thermostats which have been developed for MD simulations rely on the thermal fluctuation velocities of the system to achieve temperature control.

In nonequilibrium molecular dynamics(NEMD) simulations, the fluctuation velocities $\mathbf{c}_i = \mathbf{v}_i - \mathbf{u}(\mathbf{r}_i)$ are obtained by the difference between the actual velocities $\mathbf{v}_i$ of the fluid particles and the streaming velocity $\mathbf{u}$. It should be noted that although temperature estimates from the kinetic energy is a good measure, one has to correctly take into account the streaming velocity which is generally not known beforehand and is difficult to distinguish from the fluctuation velocities. Thermostatting schemes based on the assumption of the streaming velocity are known as "profile-biased" thermostat (PBT). If one, for example, assumes a linear shear flow with a streaming velocity profile $\mathbf{u}(\mathbf{r}) = (\dot{\gamma}_y, 0, 0)$, where the shear rate $\dot{\gamma} = \partial u_x / \partial y$ is infinitesimal whereby the system maintains a steady state then one can obtain an almost identical thermodynamic and kinetic

temperature as noted by Evans and Morriss [31]. In the case where the shear rate is large, the streaming velocity profile can become a position dependent function resulting in non-physical phenomena such as the string phases [32–34] being observed within the system. This was discovered by Erpenbeck [32] in 1984.

Instead of making assumptions about the streaming velocity profile, one can evaluate the actual profile during the dynamical evolution of the system. In this case, the instantaneous streaming velocity profile is expressed as,

$$\mathbf{u}(\mathbf{r}) \equiv \frac{\sum_{i=1}^{N} m_i \mathbf{v}_i \delta(\mathbf{r} - \mathbf{r}_i)}{\sum_{i=1}^{N} m_i \delta(\mathbf{r} - \mathbf{r}_i)}. \tag{3.1.1}$$

Thermostatting schemes based on this approach are referred to as profile-unbiased thermostats(PUT) [33]. This thermostat has been used to overcome the difficulty of the string phase phenomena [35] associated with PBT. However, a draw-back with this type of thermostatting approach is that they are more computationally expensive and difficult to implement compared to a PBT approach.

To overcome the aforementioned difficulties, a new way of describing temperature was developed which relies on the configurational information of the system instead of the kinetic information was introduced in 1998 by Rugh [30]. Following this initial breakthrough, a series of configurational type thermostats started emerging, with Lue and Evans [36] presenting their first thermostat in 2000, followed by Delhommelle and Evans [37] using a different approach later in 2001. This earlier thermostats, however, were difficult to implement and as in the case of Delhommelle-Evans approach [37], their thermostatting scheme failed to reproduce correctly the canonical distribution in the equilibrium case. By modifying this earlier thermostats, Braga and Travis [15] introduced a Nosé-Hoover-type configurational thermostat which was not only easier to implement but also capable of overcoming the problems plagued by the approach presented by Delhommelle-Evans [37].

Initially configurational temperature was used to compare the accuracy of the results obtained from Monte Carlo codes [38]. However, with the recent developments on configurational approaches the dynamics of different systems can now be studied by using

the configurational information, for example in systems subject to an external pressure constraint and in understanding conformational dynamics of biomolecules.

Our work is based on the original formulation of the configurational thermostat presented by Braga and Travis. However, it is worth to give a brief introduction of the Nosé-Hoover thermostat as the work by Braga and Travis is derived in spirit of the Nosé-Hoover thermostat.

3.2 Nosé-Hoover Thermostat

Introduced in the 1980s by Nosé [39] and later improved by Hoover[40], the Nosé-Hoover thermostat is a golden standard thermostat used in controlling temperature within Molecular dynamics simulations. The conserved energy function for the Nosé-Hoover thermostat is given as,

$$H^{NH} = \sum_{i=1}^{N} \frac{p_i^2}{2m_i} + U(q) + \frac{p_\eta^2}{2m_\eta} + g k_B T \eta, \tag{3.2.1}$$

where q and p represent the coordinates and momenta respectively. U is the inter-particle interaction potential and m is the mass of particles. η is the fictitious thermostat variable, p_η and m_η are the thermostat momenta and mass respectively. k_B represents the Boltzmann constant while T is the external temperature and g is the systems' degrees of freedom.

The equations of motion which define the Nosé-Hoover dynamics are given as,

$$\dot{q}_i = \frac{p_i}{m_i}\,, \tag{3.2.2}$$

$$\dot{p}_i = F_i - \frac{p_\eta}{m_\eta} p_i\,, \tag{3.2.3}$$

$$\dot{\eta} = \frac{p_\eta}{m_\eta}\,, \tag{3.2.4}$$

$$\dot{p}_\eta = \frac{p_i^2}{m_i} - k_B T \tag{3.2.5}$$

3.3 Braga-Travis Thermostat

Braga and Travis [15] developed a configurational temperature Nosé-Hoover type thermostat (B-T thermostat in short) capable of controlling the temperature of the system using only configurational variables where the temperature is defined by Eq. (2.2.13).

For the original formulation as presented by Braga and Travis [15], let us consider a system defined by the following conserved energy function,

$$H_\eta = \frac{p_i^2}{2m_i} + U(\mathbf{r}) + \frac{1}{2}M_\eta\eta^2 + k_BT\int_0^t \left[\eta(\tau)\sum_j \frac{\partial}{\partial \mathbf{r}_j}\cdot\frac{\partial U}{\partial \mathbf{r}_j}d\tau\right], \tag{3.3.1}$$

where r and p represent the coordinates and momenta respectively. U is the inter-particle interaction potential and m is the mass of particles. η plays the role of a fluctuating mobility: that is, a proportionality between force and drift velocity, as seen in the "position Langevin equation" or Schmoluchowski equation [15]. M_η is the thermostat mass, k_B represents the Boltzmann constant while T is the external temperature.

The equations of motion for the B-T thermostat are given as follows

$$\dot{\mathbf{r}}_i = \frac{\mathbf{p_i}}{m_i} - \eta\frac{\partial U}{\partial \mathbf{r_i}}, \tag{3.3.2}$$

$$\dot{\mathbf{p}}_i = -\frac{\partial U}{\partial \mathbf{r_i}}, \tag{3.3.3}$$

$$\dot{\eta} = \frac{F_\eta(\mathbf{r})}{M_\eta}, \tag{3.3.4}$$

where

$$F_\eta = \sum_j \left(\left|\frac{\partial U}{\partial \mathbf{r_j}}\right|^2 - k_BT\frac{\partial}{\partial \mathbf{r}_j}\cdot\frac{\partial U}{\partial \mathbf{r}_j}\right). \tag{3.3.5}$$

A simple integration algorithm presented by Braga and Travis based on the velocity-Verlet algorithm [14] which is capable of numerically integrating Eqs. (3.3.2-3.3.4) is

explicitly written as

$$r(t+\delta t) = r(t) + \delta t \frac{p(t)}{m} + \delta t \left[\eta(t) + \frac{\delta t}{2m}\right] F(t) \ , \tag{3.3.6}$$

$$p(t+\delta t) = p(t) + \frac{\delta t}{2}\left[F(t) + F(t+\delta t)\right] \ , \tag{3.3.7}$$

$$\eta(t+\delta t) = \eta(t) + \frac{\delta t}{2M_\eta}\left[F_\eta(t) + F_\eta(t+\delta t)\right] \ , \tag{3.3.8}$$

here, $F(t) = -\partial U/\partial \mathbf{r}$ and δt is the integration time step with p and $\dot{p}$ being distinctively explicit.

As previously mentioned, the B-T thermostat are easier to implement than previously derived configurational thermostat schemes as presented by Delhommelle-Evans [37]. However, there are problems associated with this thermostat such as nonergodicity for stiff systems and it is difficult to derive a general formalism of the equations of motions without losing the characteristic conserved nature of the Hamiltonian. In this chapter we aim to solve this problems associated with the B-T thermostat. We start by reformulating the B-T thermostat in phase space. For this, we use the antisymmetric matrix formalism as presented by Sergi and Ferrario [16] with which we extend our system to generate a dynamics that is ergodic. Using the phase space formulation, we are able to integrate the equations of motion using a reversible symmetric Trotter based algorithm which we shall refer to as STP.

3.4 Configurational Temperature Nosé-Hoover thermostat

Braga and Travis presented the original configurational temperature Nosé-Hoover thermostat (CTNH) as presented with the hamiltonian described by Eq. (3.3.1) with its equations of motion represented by Eqs. (3.3.2 - 3.3.4). To enable further generalisation, we start by first reformulating the original B-T thermostat in phase-space. From the B-T thermostat hamiltonian, given by Eq. (3.3.1), we can make the following substitutions, let

$$\zeta = \int_0^t \left[\eta(\tau) \cdot G \cdot d\tau\right] \ , \tag{3.4.1}$$

where

$$G = \sum_j \frac{\partial}{\partial \mathbf{q}_j} \cdot \frac{\partial U}{\partial \mathbf{q}_j} \,, \tag{3.4.2}$$

and

$$p_\zeta = M_\zeta \eta \,, \tag{3.4.3}$$

thus we can define a system with the phase space coordinates $x = (p, q, p_\zeta, \zeta)$ with the Hamiltonian of the system given as,

$$H = \frac{\mathbf{p}_i^2}{2m_i} + U(\mathbf{q}) + \frac{p_\zeta^2}{2M_\zeta} + k_B T \zeta \,, \tag{3.4.4}$$

where ζ is the fictitious thermostat variable with its associated momenta p_ζ. M_ζ is the thermostat mass, k_B is the Boltzmann constant and T is the temperature of the thermal bath. The equations of motion may be expressed in matrix form [16] as,

$$\dot{x}_i = \sum_j \mathcal{B}_{ij} \frac{\partial H}{\partial x_j} \,, \tag{3.4.5}$$

where the anti-symmetric matrix $\mathcal{B}_{ij}$ is,

$$\boldsymbol{\mathcal{B}}^{\mathrm{CTNH}} = \begin{bmatrix} 0 & 0 & 1 & -\frac{\partial \mathcal{U}}{\partial \mathbf{q}} \\ 0 & 0 & 0 & G \\ -1 & 0 & 0 & 0 \\ \frac{\partial \mathcal{U}}{\partial \mathbf{q}} & -G & 0 & 0 \end{bmatrix} . \tag{3.4.6}$$

where G is defined as

$$G = \sum_j \frac{\partial}{\partial \mathbf{q}_j} \cdot \frac{\partial U}{\partial \mathbf{q}_j} \,. \tag{3.4.7}$$

Thus the explicit form of the equations of motion can be written as,

$$\dot{\mathbf{q}} = \frac{p_i}{m_i} - \frac{p_\zeta}{2M_\zeta} \frac{\partial U}{\partial q_i} \,, \tag{3.4.8}$$

$$\dot{\mathbf{p}} = -\frac{\partial U}{\partial q_i} \,, \tag{3.4.9}$$

$$\dot{\zeta} = G(\mathbf{q}) \frac{p_\zeta}{M_\zeta} \,, \tag{3.4.10}$$

$$\dot{p}_\zeta = F_\zeta(q), \tag{3.4.11}$$

where G and F_η are defined as

$$G = \sum_j \frac{\partial}{\partial \mathbf{q}_j} \cdot \frac{\partial U}{\partial \mathbf{q}_j} \,, \tag{3.4.12}$$

and

$$F_\eta = \sum_j \left(\left| \frac{\partial U}{\partial \mathbf{q_j}} \right|^2 - k_B T \frac{\partial}{\partial \mathbf{q}_j} \cdot \frac{\partial U}{\partial \mathbf{q}_j} \right) \,. \tag{3.4.13}$$

Under the ergodic assumption and using standard techniques Eqs. (3.4.8 - 3.4.11) with the conserved quantity Eq. (3.4.4) can be shown to sample correctly the canonical distribution for non-stiff systems. The associated phase space compressibility [16], is given by

$$\begin{aligned} \kappa &= \frac{\partial \mathcal{B}_{ij}}{\partial x_i} \frac{\partial H}{\partial x_j} && (3.4.14) \\ &= -\dot{\zeta} && (3.4.15) \end{aligned}$$

The Liouville operators functions are given as,

$$\begin{aligned} L_1^{\mathrm{CTNH}} &= \left(\frac{\mathbf{p}}{m} + F(\mathbf{q}) \frac{p_\zeta}{M_\zeta} \right) \frac{\partial}{\partial \mathbf{q}} \,, && (3.4.16) \\ L_2^{\mathrm{CTNH}} &= F(\mathbf{q}) \frac{\partial}{\partial p} \,, && (3.4.17) \\ L_3^{\mathrm{CTNH}} &= G(\mathbf{q}) \frac{p_\zeta}{M_\zeta} \frac{\partial}{\partial \zeta} \,, && (3.4.18) \\ L_4^{\mathrm{CTNH}} &= F_\zeta(\mathbf{q}) \frac{\partial}{\partial p_\zeta} \,, && (3.4.19) \end{aligned}$$

where $F(q)$ is the force acting on the system coordinates q and

$$\begin{aligned} G &= \sum_j \frac{\partial}{\partial \mathbf{q}_j} \cdot \frac{\partial U}{\partial \mathbf{q}_j} \,, && (3.4.20) \\ F_\zeta &= \sum_j \left(\left| \frac{\partial U}{\partial \mathbf{q_j}} \right|^2 - k_B T \frac{\partial}{\partial \mathbf{q}_j} \cdot \frac{\partial U}{\partial \mathbf{q}_j} \right) \,. && (3.4.21) \end{aligned}$$

Thus the symmetric Trotter factorization of the Liouville propagator is given as,

$$\begin{aligned} U^{\mathrm{CTNH}}(\tau) &= U_4^{\mathrm{CTNH}}\left(\frac{\tau}{4}\right) U_3^{\mathrm{CTNH}}\left(\frac{\tau}{2}\right) U_4^{\mathrm{CTNH}}\left(\frac{\tau}{4}\right) U_2^{\mathrm{CTNH}}\left(\frac{\tau}{2}\right) U_1^{\mathrm{CTNH}}(\tau) \\ &\times U_2^{\mathrm{CTNH}}\left(\frac{\tau}{2}\right) U_4^{\mathrm{CTNH}}\left(\frac{\tau}{4}\right) U_3^{\mathrm{CTNH}}\left(\frac{\tau}{2}\right) U_4^{\mathrm{CTNH}}\left(\frac{\tau}{4}\right) . \end{aligned} \tag{3.4.22}$$

The action of the propagators U_α^{CTNH} for $\alpha = 2, 3, 4$ can be easily determined giving the following reversible algorithm:

$$p \to p + \tau F(q)\} \quad : \quad U_2^{\mathrm{CTNH}}(\tau) , \tag{3.4.23}$$

$$\left.\zeta \to \zeta + \tau G(q)\frac{p_\zeta}{M_\zeta}\right\} \quad : \quad U_3^{\mathrm{CTNH}}(\tau) , \tag{3.4.24}$$

$$p_\zeta \to p_\zeta + \tau F_\zeta(q)\} \quad : \quad U_4^{\mathrm{CTNH}}(\tau) . \tag{3.4.25}$$

Using the operator formula as shown in Appendix (A.1), the action of the propagator on Eq. (3.4.16) can be as derived analytically for a quadratic potential ($U(q) = \frac{1}{2}kq^2$) such that $F(q)$ is linear in q given as,

$$q \to q\exp\left(-\tau k\frac{p_\zeta}{M_\zeta}\right) + \tau\frac{p}{m}\exp\left(-\tau\frac{k}{2}\frac{p_\zeta}{M_\zeta}\right)\left[\frac{\sinh\left(\tau\frac{k}{2}\frac{p_\zeta}{M_\zeta}\right)}{\tau\frac{k}{2}\frac{p_\zeta}{M_\zeta}}\right]\Bigg\} : U_{1,\mathrm{h}}^{\mathrm{CTNH}}(\tau) . \tag{3.4.26}$$

The reversible algorithms derived using Eqs. (3.4.23 - 3.4.26) for a linear force $F(q)$ shall be referred to as STP algorithms.

In the case of a general potential, the application of the operator formula becomes difficult unless the calculated force is linearly approximated about a certain position say q_t such that,

$$F(q) \approx F(q_t) + \tilde{k}(q - q_t) , \tag{3.4.27}$$

where we define $\tilde{k}$ as,

$$\tilde{k} = \frac{1}{2}\frac{\partial \mathcal{U}}{\partial q}|_{q=q_t} . \tag{3.4.28}$$

In such a case, by applying the operator formula, the action of the propagator on Eq.

(3.4.16) for a general continuous potential can be approximated as,

$$q \;\rightarrow\; q\exp\left(-\tau\tilde{k}\frac{p_\zeta}{M_\zeta}\right)+\tau\left(\frac{p}{m}+F(q_t)+\tilde{k}q_t\right)\exp\left(-\tau\frac{\tilde{k}}{2}\frac{p_\zeta}{M_\zeta}\right)\left[\frac{\sinh\left(\tau\frac{\tilde{k}}{2}\frac{p_\zeta}{M_\zeta}\right)}{\tau\frac{\tilde{k}}{2}\frac{p_\zeta}{M_\zeta}}\right]\Bigg\}:\tilde{U}_{1,\mathrm{h}}^{\mathrm{CTNH}}(\tau)\;. \tag{3.4.29}$$

The reversible algorithms derived using Eqs. (3.4.23 - 3.4.25) and Eq.(3.4.29) for a linearly approximated force $F(q)$ shall be referred to as position-dependent harmonically approximated (PDHA) STP algorithms.

In the work of Beckedhal *et al* [41], it has been shown that the CTNH thermostat is incapable of sampling the canonical distribution function correctly for stiff systems such as a harmonic oscillator. However, by attaching a standard Nosé-Hoover thermostat which effectively regulates the kinetic energy of the configurational thermostat one can create a chain of thermostats that is capable of producing an ergodic system for such stiff systems. This thermostat is referred to as a hybrid configurational-kinetic temperature Nosé-Hoover chain thermostat (CKTNHC). Also, Beckedhal *et al* [41] showed that the derived STP and PDHA STP algorithms are stable over long times when compared against symplectic position Verlet and symplectic velocity Verlet integration algorithms. In this work we apply the CTNH thermostat to a three-dimensional system interacting using a Weeks-Chandler-Andersen (WCA) potential [42]. This potential was originally devised as a reference fluid in a perturbation treatment for the Lennard-Jones fluid [42–45].

3.5 CTNH Dynamics in a WCA Potential

In this section, we shall consider a general system of N particles interacting via a Weeks-Chandler-Andersen(WCA) potential in three-dimensional space using the CTNH thermostat. The WCA potential is a Lennard-Jones (LJ) potential that is shifted by ϵ and truncated at its minimum $2^{1/6}\sigma$. It is known that the CTNH thermostat is unable to sample correctly the canonical distribution function for small or stiff systems such as the case with the simple harmonic oscillator. However, thermostatting a system with

many degrees of freedom, one can reasonably assume that the dynamics of the system will be ergodic. For a general system with phase space coordinates q_i and p_i, where $i = 1, ..., 3N$, the WCA pairwise potential is thus given as,

$$\mathcal{U}^{\mathrm{WCA}}(r_{ij}) = \begin{cases} 4\epsilon\left[\left(\frac{\sigma}{r_{ij}}\right)^{12} - \left(\frac{\sigma}{r_{ij}}\right)^{6}\right] + \epsilon & \text{if } r_{ij} \leq r_{\min} \equiv \sigma\sqrt[6]{2}\,, \\ 0 & \text{otherwise}\,, \end{cases} \tag{3.5.1}$$

where r_{ij} is the inter-particle separation distance between particle i and j given by,

$$r_{ij} = |\mathbf{r}_i - \mathbf{r}_j| = \left(x_{ij}^2 + y_{ij}^2 + z_{ij}^2\right)^{\frac{1}{2}}. \tag{3.5.2}$$

The equations of motion using the CTNH thermostat are given as,

$$\dot{r}_i = \frac{p_i}{m_i} - \frac{p_\zeta}{M_\zeta}\frac{\partial U}{\partial r_i}\,, \tag{3.5.3}$$

$$\dot{p}_i = -\frac{\partial U}{\partial r_i}\,, \tag{3.5.4}$$

$$\dot{\zeta} = \sum_{i=1}^{3N}\left(\frac{\partial^2 U}{\partial r_i^2}\right)\frac{p_\zeta}{M_\zeta} = G(r)\frac{p_\zeta}{M_\zeta}\,, \tag{3.5.5}$$

$$\dot{p}_\zeta = = \left[\sum_{i=1}^{3N}(F_i)^2 - k_{\mathrm{B}}TG(r)\right]\,, \tag{3.5.6}$$

were the G and F_η functions are given as,

$$G = \sum_j \frac{\partial}{\partial \mathbf{r}_j}\cdot\frac{\partial U}{\partial \mathbf{r}_j}\,, \tag{3.5.7}$$

and

$$F_\zeta = \sum_j\left(\left|\frac{\partial U}{\partial \mathbf{r_j}}\right|^2 - k_B T\frac{\partial}{\partial \mathbf{r}_j}\cdot\frac{\partial U}{\partial \mathbf{r}_j}\right)\,. \tag{3.5.8}$$

Since the WCA considered is a pairwise function, one has to solve the spatial gradient and the second derivative functions which appear in Eqs. (3.5.7) and (3.5.8). The spacial

gradient is expressed as,

$$\frac{\partial U}{\partial \mathbf{r}_i} = \frac{\mathbf{r}_{ij}}{r_{ij}} \frac{\partial U}{\partial r_{ij}} = -\frac{\partial U}{\partial \mathbf{r}_j} \tag{3.5.9}$$

where r_{ij} is the inter-particle separation distance between particle i and j given by the scalar expression,

$$r_{ij} = |\mathbf{r}_i - \mathbf{r}_j| = \left(x_{ij}^2 + y_{ij}^2 + z_{ij}^2\right)^{\frac{1}{2}}. \tag{3.5.10}$$

The second order derivative of the potential is expressed as,

$$\frac{\partial^2 U}{\partial \mathbf{r}_i^2} = \frac{\partial^2 U}{\partial x_i^2} + \frac{\partial^2 U}{\partial y_i^2} + \frac{\partial^2 U}{\partial z_i^2} \tag{3.5.11}$$

It can easily be shown that the second partial derivative of the potential with respect to x is given by the following expression,

$$\frac{\partial^2 U}{\partial x_i^2} = \left(\frac{1}{r_{ij}} - \frac{x_{ij}^2}{r_{ij}^3}\right) \frac{\partial U}{\partial r_{ij}} + \frac{x_{ij}^2}{r_{ij}^2} \frac{\partial^2 U}{\partial r_{ij}^2}, \tag{3.5.12}$$

similarly, expressions for the partial derivatives with respect to y and z coordinates can be obtained. The problem now reduces into solving the scalar quantities $\frac{\partial U}{\partial r_{ij}}$ and $\frac{\partial^2 U}{\partial r_{ij}^2}$ which for the WCA potential are expressed as,

$$\frac{\partial U}{\partial r_{ij}} = -24\frac{\epsilon}{\sigma}\left[2\left(\frac{\sigma}{r_{ij}}\right)^{13} - \left(\frac{\sigma}{r_{ij}}\right)^{7}\right], \tag{3.5.13}$$

and

$$\frac{\partial^2 U}{\partial r_{ij}^2} = 24\frac{\epsilon}{\sigma^2}\left[26\left(\frac{\sigma}{r_{ij}}\right)^{14} - 7\left(\frac{\sigma}{r_{ij}}\right)^{8}\right]. \tag{3.5.14}$$

The total Liouville operator is given by $L^{\mathrm{HCKTNHC}} = \sum_{n=1}^{4} L_n^{\mathrm{HCKTNHC}}$ with the explicit L_n^{HCKTNHC} functions given as,

$$L_1 = \left(\frac{p}{m} + F(r)\frac{p_\zeta}{M_\zeta}\right)\frac{\partial}{\partial r} \tag{3.5.15}$$

$$L_2 = F(r)\frac{\partial}{\partial p} \tag{3.5.16}$$

$$L_3 = G(r)\frac{p_\zeta}{M_\zeta}\frac{\partial}{\partial \zeta} \tag{3.5.17}$$

$$L_4 = F_\zeta(r)\frac{\partial}{\partial p_\zeta} \tag{3.5.18}$$

With the symmetric Trotter factorization of the Liouville propagator is given as,

$$\begin{aligned} U(\tau) &= U_4\left(\frac{\tau}{4}\right) U_3\left(\frac{\tau}{2}\right) U_4\left(\frac{\tau}{4}\right) \\ &\times U_2\left(\frac{\tau}{2}\right) U_1\left(\tau\right) U_2\left(\frac{\tau}{2}\right) \\ &\times U_4\left(\frac{\tau}{4}\right) U_3\left(\frac{\tau}{2}\right) U_4\left(\frac{\tau}{4}\right) . \end{aligned} \tag{3.5.19}$$

The action of the Liouville propagators $U_\alpha(\tau)$ for $\alpha = 2, 3, 4$ is given in Eqs. (3.4.23-3.4.25). The propagator $U_1(\tau)$ is resolved through a quasi-harmonic approximation of the WCA potential since the force F is not linear about every configuration q. Thus the numerical algorithm devised for the WCA is a PDHA-STP scheme.

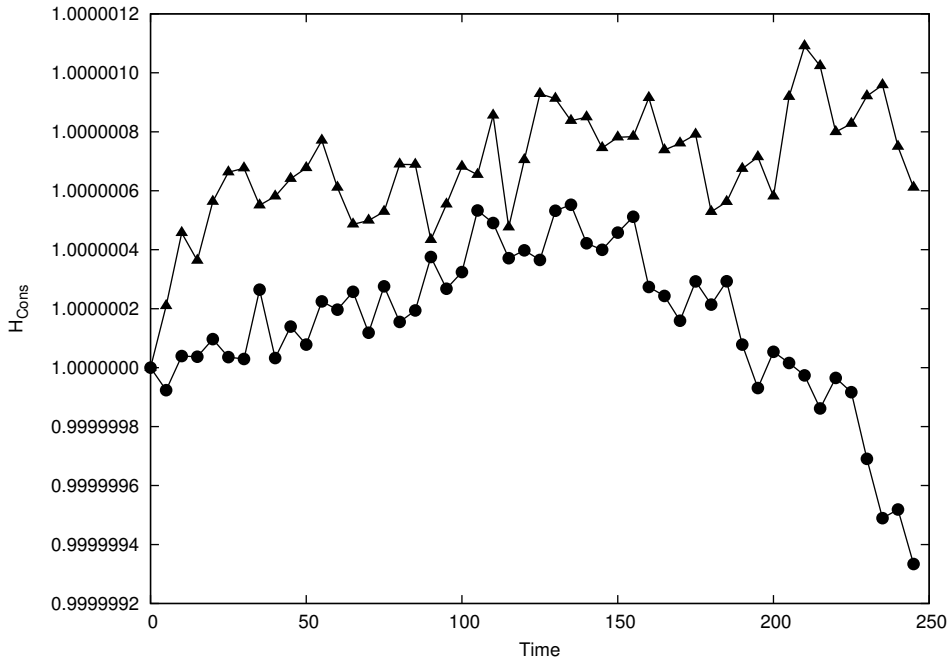

Figure 3.1: Comparison of the normalized hamiltonian function for the WCA potential function coupled to a configurational temperature Nosé-Hoover thermostat shown by the filled circles (●) and the Nosé-Hoover thermostat shown by the filled triangles (▲). The plot displays the results for a system with 1000 particles, external temperature set as $T_{ext} = 0.722$ and density of $\rho = 0.8442$. The time step was set as $\delta t = 2.5 \times 10^{-4}$. The configurational temperature Nosé-Hoover thermostat mass was set as $M_\zeta = 10^{20}$ while the Nosé-Hoover thermostat mass was set as $M_\zeta = 1.0$.

In our work, simulations of the CTNH thermostat using the WCA potential with the PDHA-STP algorithm was carried out. The results of this simulation was compared

against simulations performed on system using a standard Nose-Hoover thermostat with a WCA interacting potential. The following system parameters were used in the simulations, the number of particles used was set as 1000 with an external temperature $T_{ext} = 0.722$ and density $\rho = 0.8442$, the CTNH thermostat mass was set as $M_\zeta = 10^{20}$ and the Nosé-Hoover thermostat mass was set as $M_\zeta = 1$, an integration time-step $\delta t = 1 \times 10^{-4}$ was used for a total time of $t = 1 \times 10^9$ steps. Fig. (3.1) shows the normalized conserved quantity of the CTNH thermostat and the Nosé-Hoover thermostats. From this figure it can be observed that the system conserves the hamiltonian to a high degree of accuracy given the calculated standard deviation for the CTNH is 1.060×10^{-7} while that of the standard NH thermostat is 1.523×10^{-7}. Moreover, different temperature regions ranging from $T = 0.2$ to $T = 0.8$ were explored and the normalized conserved hamiltonian for the CTNH and the NH thermostats compared. It was observed that the CTNH conserves the hamiltonian to a higher degree of accuracy when compared to the NH thermostat as seen in Table 3.1. Furthermore, the PDHA-STP scheme proves to be sufficient for producing good dynamics when propagating particle positions for general systems where the potential energy is harmonically approximated. It is worth mentioning that the error introduced by the linearization of the forces is $\lll 1\%$. This can be seen from the percentage error calculated for different particles within the system as shown in tables 3.2, 3.3 and 3.4. The percentage error is calculated from first order approximation of the forces and linearly approximated forces along the x, y and z directions. The simulation times for the CTNH thermostat was also compared with the standard NH thermostat, and it was found that the NH thermostat was 10% faster than the run times of the CTNH thermostat.

Temperature	σ_{CTNH}	σ_{NH}
0.2	4.075×10^{-9}	1.192×10^{-7}
0.3	8.533×10^{-8}	5.681×10^{-8}
0.4	4.948×10^{-8}	5.243×10^{-7}
0.5	8.964×10^{-8}	9.732×10^{-8}
0.6	6.706×10^{-8}	9.220×10^{-8}
0.7	4.331×10^{-8}	4.927×10^{-7}
0.8	4.023×10^{-7}	3.641×10^{-7}

Table 3.1: Standard deviation of the normalized conserved quantity for the CTNH and NH thermostats for different temperature values.

Particle	$F_{x_{1^{st}order}}$	$F_{x_{linear\ approx}}$	$\%Error$
1	147.85179509668470	147.85179509668450	0.00000000000014
10	0.10266460681494	0.10266460681495	0.00000000001239
100	90.21099214584918	90.21099214584922	0.00000000000005
1000	26.77319283224203	26.77319283224208	0.00000000000018

Table 3.2: Table showing the linear approximation, first order approximation and the percentage error of the forces acting along the x direction on different particles within the system.

Particle	$F_{y_{1^{st}order}}$	$F_{y_{linear\ approx}}$	$\%Error$
1	62.41716673469524	62.41716673469558	0.00000000000056
10	726.80039460039575	726.80039460039563	0.00000000000001
100	404.46315981982906	404.46315981982895	0.00000000000003
1000	0.11336264341379	0.11336264341379	0.00000000000000

Table 3.3: Table showing the linear approximation, first order approximation and the percentage error of the forces acting along the y direction on different particles within the system.

Particle	$F_{z_{1^{st}order}}$	$F_{z_{linear\ approx}}$	$\%Error$
1	96.29243868904805	96.29243868904791	0.00000000000014
10	493.20915590451625	493.20915590451625	0.00000000000000
100	287.12463365611740	287.12463365611768	0.00000000000010
1000	259.14316562815299	259.14316562815327	0.00000000000011

Table 3.4: Table showing the linear approximation, first order approximation and the percentage error of the forces acting along the z direction on different particles within the system.

3.6 Conclusion

Temperature control in molecular dynamics simulations is of fundamental importance especially when one studies the rheological properties of molecular systems [46]. By coupling the system to a thermal heat bath, temperature control within the MD simulation can be achieved. However, many present thermostatting schemes use the thermal fluctuation velocities of the molecules within the system to achieve temperature control. This becomes increasingly difficult for NEMD simulations. Rugh [30] introduced a method of representing temperature using configurational information of the system. With this definition of temperature, a new breed of configurational thermostats emerged which are capable of controlling temperature in NEMD simulations which use the configurational information, one such thermostat was presented by Braga and Travis [15] referred as the B-T thermostat which is a configurational temperature Nosé-Hoover thermostat. One of the draw backs of the B-T thermostat is its inability to sample the phase space uniformly.

In our work, we solve this problem by reformulating the B-T thermostat in phase space using a quasi-Hamiltonian approach introduced by Sergi and Ferrario [16], we call this thermostat a CTNH thermostat. For stiff systems, Beckedhal *et al* [41] have recently demonstrated that the CTNH is incapable of achieving ergodicity using a simple harmonic oscillator in one dimension. However, by considering a three-dimensional type of system with the Weeks-Chandler-Anderson (WCA) potential, it can be reasonably assumed that no stiff modes will be expected thus uniform sampling is expected from the CTNH thermostat. A system which uses the WCA potential coupled to the CTNH thermostat was tested providing good results against a standard Nosé-Hoover thermostat. One can conclude that the CTNH thermostat can be reliably used to control temperature in NEMD simulations for systems with general potentials in three dimension.

Chapter 4

Gaussian-Core Model (GCM)

4.1 Introduction

The Gaussian-Core Model(GCM) is a core-softened potential first introduced by Stillinger in the mid-seventies. This potential has been widely used in research in modelling 'effective' repulsive particle interactions which can be described through a Gaussian law [9] within soft-matter systems. The GCM potential is bounded which means that a full of overlap of the particles is possible resulting in a range of unusual properties emerging in the solid and liquid phases. Examining the phase-diagram of the GCM as shown in Fig.(4.1), we can observe unusual features which are present in the phase-diagram of water. Such features include re-entrant melting and maximum freezing temperature. Re-entrant melting of the GCM can be observed from the phase diagram when the system is isothermally compressed from state P to Q, it undergoes two state changes. The system first freezes into a solid as it crosses the coexistence line and upon further compression the system melts back into a liquid until it reaches point Q. Moreover, the maximum freezing temperature is observed to be at a temperature value of $T^* = 0.00874$ with a density value of $\rho^* = 0.239$. Also, at sufficiently low temperature, the system can exhibit different crystalline structures dependent on the density, the symmetry of the structure can either be face-centred or body-centred [47].

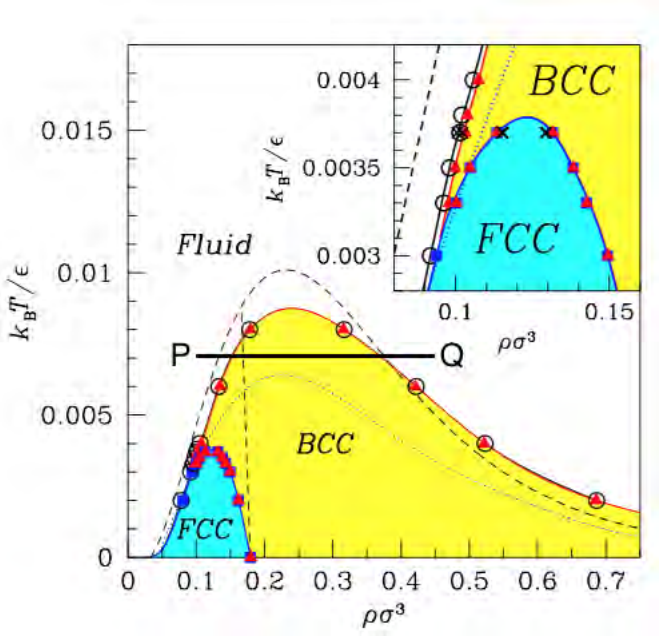

Figure 4.1: Gaussian-Core phase diagram [47]

In this work, the form of the potential for the GCM is expressed as the following,

$$U(r_{ij}) = \epsilon \exp\left[-\frac{r_{ij}}{\sigma}\right]^2, \tag{4.1.1}$$

where r_{ij} is the inter-particle separation distance between particle i and j given by the scalar expression,

$$r_{ij} = |\mathbf{r}_i - \mathbf{r}_j| = \left(x_{ij}^2 + y_{ij}^2 + z_{ij}^2\right)^{\frac{1}{2}}. \tag{4.1.2}$$

The aim of our study is to investigate the significance of the zero-point effects on the GCM within the range of temperatures and densities explored by Mausbach and May[17]. We start by presenting a phonostat methodology which will enable us to regulate the 'effective' temperature of a given vibrational mode ω_n thereby regulate the total energy of the system. The phonostat algorithm is able to achieve this in the following ways; First we obtain the normal modes and their vibrational frequencies using the Normal Coordinate Analysis method, then we project the displacements and velocities of the particles within the system onto the normal modes to obtain modal velocities and amplitudes. These modes are each coupled to a single Nosé-Hoover chain thermostat which regulates the 'effective' temperature of each mode. Using this methodology, we derive

phonostat algorithms comparing the simulation results to literature results as presented by Mausbach and May[17].

4.2 Phonostat Methodology

We use normal coordinate analysis to decouble the Hamiltonian into $3N$ modes with vibrational frequency ω_n. The motion of each mode is analogous to a simple harmonic oscillator. Using the eigenvectors as a reference frame, we project the cartesian coordinates onto the normal modes by carefully mapping them onto the eigenvectors and vice versa. Since each normal mode has a characteristic frequency ω_n, we can obtain frequency dependent 'effective' temperature using the Wigner approach to quantum mechanics and effectively thermalize each mode by coupling it to a Nosé-Hoover chain thermostat. In this sense, we can describe such a system as being thermostatted 'locally'. A major draw-back of 'local' thermostatting compared to 'global' thermostatting is their inability to recover the dynamical properties of the system [48]. The term 'local' used here is to describe a system where a single thermostat is coupled to each degree of freedom as opposed to 'global' where a single thermostat is coupled to the entire system degrees of freedom.

4.2.1 Normal Coordinate Analysis

Normal Coordinate Analysis(NCA) is a widely used methodology successfully applied in the early 1980s [49–51] for studying chemical systems, such as polymers and biological molecules, in order to obtain in-depth understanding to their structures and dynamics [49–54]. Using the NCA method, one obtains the characteristic frequencies associated to the natural vibrational motion of the system [55]. This follows from the assumption that the molecular potential energy of the system is approximately quasi-harmonic about an energy minimum, yielding a generalised eigenvalue problem which can be solved giving an analytical description of the motion [56, 57]. What follows is a basic approach into performing Normal Coordinate analysis to a general system.

Basic NCA Theory

Consider a general system of N-particles in 3-dimensions with an interacting potential $V(\mathbf{r})$. A Taylor series expansion of the potential can be performed about an equilibrium position $\mathbf{r}^0$,

$$V(\mathbf{r}) = V(\mathbf{r}^0) + \sum_{i=1}^{3N} \left|\frac{\partial V}{\partial \mathbf{r}_i}\right|_0 \left(\mathbf{r}_i - \mathbf{r}_i^0\right) + \frac{1}{2}\sum_{i=1}^{3N} \left|\frac{\partial^2 V}{\partial \mathbf{r}_i \partial \mathbf{r}_j}\right|_0 \left(\mathbf{r}_i - \mathbf{r}_i^0\right)\left(\mathbf{r}_j - \mathbf{r}_j^0\right) + \cdots \quad (4.2.1)$$

The first term on the right-hand side of Eq. (4.2.1) is a constant. This value represents the minimum potential energy for the system which can be set to zero by simply redefining the zero of the energy. The second term represents the sum of all the inter-atomic forces. This sum is zero for a structure that is in equilibrium. Now,

$$V(\mathbf{r}^0) \;=\; 0 \quad \text{and} \quad \left|\tfrac{\partial V}{\partial \mathbf{r}_i}\right|_0 \; . \quad (4.2.2)$$

Considering only finite displacements about the minimum, the higher order terms may be neglected thus Eq. (4.2.1) can be re-written as,

$$V(\mathbf{r}) = \frac{1}{2}\sum_{i=1}^{3N} F'_{ij}\left(\mathbf{r}_i - \mathbf{r}_i^0\right)\left(\mathbf{r}_j - \mathbf{r}_j^0\right) \; , \quad (4.2.3)$$

where

$$F'_{ij} = \left|\frac{\partial^2 V}{\partial \mathbf{r}_i \partial \mathbf{r}_j}\right|_0 \; , \quad (4.2.4)$$

is the force constant analogous to the expression for a harmonic oscillator.

Equation. 4.2.3 can be rewritten in matrix form as,

$$V(\mathbf{r}) = \frac{1}{2}\mathbf{r}\cdot\mathbf{F'}\cdot\mathbf{r} \; , \quad (4.2.5)$$

where, $\mathbf{F'}$, the force constant is a $3N\times 3N$ matrix made up of the second order derivative of the potential evaluated at the local minimum. $\mathbf{r}$ is a $3N$ matrix made up of the coordinates $(\mathbf{r}_i - \mathbf{r}_i^0)$.

If we consider a generalized dynamical evolution of a system, the Lagrangian, $L =$

$L(\mathbf{r}, \dot{\mathbf{r}}, t)$, which is a function of the time dependent functions $\mathbf{r} = \mathbf{r}(t)$, $\dot{\mathbf{r}} = \dot{\mathbf{r}}(t)$ and time t can be expressed as,

$$L = T - V \ , \tag{4.2.6}$$

where T is the kinetic energy of the system and V is the potential energy. Substituting Eq. (4.2.5) into Eq. (4.2.6) and realizing that the kinetic energy term T can be expressed as,

$$T = \frac{1}{2}\dot{\mathbf{r}} \cdot \mathbf{M} \cdot \dot{\mathbf{r}} \ , \tag{4.2.7}$$

where, $\mathbf{M}$, is a diagonal matrix made up of the particles masses, an expression for the Euler-Lagrange equation of motion follows as,

$$\mathbf{M} \cdot \ddot{\mathbf{r}} = - \mathbf{F}' \cdot \mathbf{r} \ . \tag{4.2.8}$$

Equation (4.2.8) can further be simplified by using mass-weighted coordinates such that the dependence of the mass matrix $\mathbf{M}$ present on the left hand side of the equation is removed. If the set of coordinates are defined as,

$$\mathbf{q} = \mathbf{M}^{\frac{1}{2}} \cdot \mathbf{r} \ , \tag{4.2.9}$$

Eq. (4.2.8) can be re-written as,

$$\ddot{\mathbf{q}} = - \mathbf{H} \cdot \mathbf{q} \ . \tag{4.2.10}$$

where $\mathbf{H}$ is a $3N \times 3N$ mass-weighted force constant matrix also known as the Hessian matrix. It should be noted that the differential equations shown by Eq. (4.2.10) are all linearly coupled. Also, this equation is synonymous to the harmonic oscillator problem for linearly coupled systems with the general solution given as,

$$\mathbf{q} = \mathbf{A} \exp[i\lambda t] \ . \tag{4.2.11}$$

Substituting Eq. (4.2.11) into Eq. (4.2.10) we obtain the following eigenproblem,

$$\mathbf{HA} = \lambda^2 \mathbf{A} \ , \tag{4.2.12}$$

where the eigenvalues are λ^2 and eigenvectors are $\mathbf{A}$. Moreover, the solution to this equation is found by diagonalising the Hessian matrix. It should be noted that λ^2 has $3N$ eigenvalues which correspond to the squares of the vibrational frequencies ω_n and $\mathbf{A}$ which is a $3N \times 3N$ matrix of the eigenvectors correspond to the normal modes. Also, by diagonalizing the Hessian we are able to seperate the potential energy into a linear combination of uncoupled quadratic terms.

In this work we use the normal mode analysis method to obtain the normal modes and corresponding vibrational frequencies for our system.

4.2.2 Normal mode calculation

As previously mentioned, in order for the normal modes to be calculated, the equilibrium geometry of the system first has to be evaluated. Then by diagonalising the Hessian matrix, one can find the normal modes and the associated vibrational frequencies. The problem one will be faced with is how to evaluate the elements of the Hessian matrix. This matrix contains mass-weighted second-order derivatives of the potential energy with respect to the atomic displacements expressed as

$$\mathbf{H} = \begin{pmatrix} \frac{\partial^2 V}{\partial q_1 \partial q_1} & \frac{\partial^2 V}{\partial q_1 \partial q_2} & \cdots & \frac{\partial^2 V}{\partial q_1 \partial q_{3N}} \\ \frac{\partial^2 V}{\partial q_2 \partial q_1} & \frac{\partial^2 V}{\partial q_2 \partial q_2} & \cdots & \frac{\partial^2 V}{\partial q_2 \partial q_{3N}} \\ \vdots & \vdots & \ddots & \vdots \\ \frac{\partial^2 V}{\partial q_{3N} \partial q_1} & \frac{\partial^2 V}{\partial q_{3N} \partial q_2} & \cdots & \frac{\partial^2 V}{\partial q_{3N} \partial q_{3N}} \end{pmatrix} . \tag{4.2.13}$$

For this work, the elements of the Hessian matrix are calculated numerically using a small-displacement method which is commonly referred to as the frozen-phonon approximation [58, 59] given by the following expression,

$$h_{ij} = -\frac{f_i(q_i + \tilde{s}e_j) - f_i(q_i - \tilde{s}e_j)}{2\tilde{s}} , \tag{4.2.14}$$

where h_{ij} is the Hessian matrix element, e_j is the unit vector along the direction j and $\tilde{s}$ is the magnitude of the atomic displacement. In this work, $\tilde{s} = 10^{-6}$. q corresponds to the mass-weighted coordinates in the x, y and z directions for atom i. The force f_i

in the above equation is given by,

$$f_i = -\frac{\partial V}{\partial q_i} \, . \tag{4.2.15}$$

Once the normal modes and their associated vibrational frequencies are evaluated, the cartesian phase-space coordinates are carefully mapped onto the normal modes to obtain the normal mode phase-space coordinates. Also, the cartesian phase-space coordinates can be recovered back by projecting the normal mode phase-space coordinates onto the inverse matrix of the normal modes. This aforementioned procedure forms a fundamental step within the phonostat algorithm.

4.2.3 Modal Temperature using the Wigner distribution function

Introduced by Eugene Wigner[60] in 1932, the Wigner function is defined as an integral transform of the density matrix $\tilde{\rho}$[60–62], for a given quantum system expressed in the position basis as,

$$W(r,p,t) = \frac{1}{2\pi\hbar} \int_{-\infty}^{+\infty} dy e^{-\frac{ipy}{\hbar}} \left\langle r + \frac{y}{2} \middle| \tilde{\rho}(t) \middle| r - \frac{y}{2} \right\rangle \, , \tag{4.2.16}$$

Quantum mechanical averages under the Wigner representation are calculated as integrals in phase space[63] as

$$\langle \chi \rangle = \int_{-\infty}^{+\infty} \int_{-\infty}^{+\infty} W(r,p) \chi_W(r,p) dr dp \, , \tag{4.2.17}$$

where $\chi_W(r,p)$ is the Wigner representation of the quantum operator $\hat{\chi}$. Moreover, it should be noted that the Wigner function is not a true probability distribution function since it is not positively defined as a result of quantum interference[64], and as such, it is referred to as a quasi-probability distribution[60–62, 64, 65]. Under the Wigner representation of quantum mechanics, the quantum law of evolution is naturally transformed into the Wigner equations of motion. With its formulation in phase space, the Wigner distribution function is thus used as a basis to study the quantum to classical limit.

Starting with an initial quantum state, the Wigner distribution function is given as,

$$\rho_W = \prod_{n=1}^{3N} \left\{ \frac{1}{\pi\hbar} \tanh\left(\frac{\hbar\omega_n}{2}\beta\right) \exp\left[-\frac{2}{\hbar\omega_n}\tanh\left(\frac{\hbar\omega_n}{2}\beta\right) H_n\right]\right\} , \tag{4.2.18}$$

where $\beta = 1/(k_B T)$, $\hbar$ is the Plank's constant, ω_n is the frequency of mode n and T is the external temperature. H_n is the Hamiltonian of the n^{th} mode harmonic oscillator given by

$$H_n = \frac{P_n^2}{2m_n} + \frac{1}{2} m_n \omega_n^2 R_n^2 . \tag{4.2.19}$$

A full derivation for this function is presented in Appendix (B).

If we let

$$\tilde{\beta}_n = \frac{2}{\hbar\omega_n}\tanh\left(\frac{\hbar\omega_n}{2}\beta\right) , \tag{4.2.20}$$

then Eq. (4.2.18) can be re-written as,

$$\rho_W = \prod_{n=1}^{3N} \left\{ \frac{1}{Z_n^q} \exp\left[-\tilde{\beta}_n H_n\right]\right\} , \tag{4.2.21}$$

where the normalization constant Z_n^q is given by,

$$Z_n^q = \frac{2\pi}{\omega_n \tilde{\beta}_n} . \tag{4.2.22}$$

The frequency dependent 'effective' temperature of each mode is thus given as,

$$\tilde{T}_n = \frac{\hbar\omega_n}{2k_B}\coth\left(\frac{\hbar\omega_n}{2k_B T}\right) , \tag{4.2.23}$$

noting that $\tilde{\beta}_n = 1/(k_B \tilde{T}_n)$.

At high temperature, $T \to \infty \Rightarrow \beta \to 0$, the classical canonical distribution function is recovered, thus the Wigner distribution function

$$\rho_W = \prod_{n=1}^{3N} \left\{ \frac{1}{Z_n^c} \exp\left[-\beta H_n\right]\right\} , \tag{4.2.24}$$

where the normalization constant Z_n^c is given by,

$$Z_n^c = \frac{2\pi}{\omega_n \beta} \, . \tag{4.2.25}$$

The form in which Eq. (4.2.21) and Eq. (4.2.24) are expressed in, is analogous to the Maxwell distribution function,

$$f_c = \frac{1}{Z} \exp\left[-\beta H_c\right] \, , \tag{4.2.26}$$

where the normalization constant Z is given by,

$$Z = \int \exp\left[-\beta H_c\right] , \tag{4.2.27}$$

which is purely classical.

Classically, from the equipartition theory, the temperature of each mode is the same regardless of the vibrational frequency of the mode. This assertion is evident in the Wigner distribution function considered within the high temperature limit as expressed by Eq. (4.2.24). The temperature, $\beta = 1/(k_B T)$, is independent of the vibrational frequency ω_n of the modes. However, in quantum mechanics this assertion fails. The temperature of each mode depends on the vibrational frequency of the mode as expressed by Eq. (4.2.23). This is important as one can generate a thermal distribution according to this frequency dependent 'effective' temperature. We use this concept in our study to introduce quantum effects into a classical system.

4.2.4 Modal Temperature control using a Nosé-Hoover Chain thermostat

From the normal coordinate analysis one can obtain the normal modes of the system. Each mode can be treated as a simple harmonic oscillator with vibrational frequency ω_n. For a classical system the temperature of each mode is equivalent to the external temperature of the system since it is independent of the vibrational frequency ω_n but for a quantum system, one can obtain a frequency dependent 'effective' temperature following

the Wigner approach to quantum mechanics. Thermalisation of each vibrational mode was achieved through the coupling of a Nosé-Hoover Chain thermostat. This thermostat ensures that the dynamics of each mode is ergodic in nature.

Phonostat algorithm

Consider a system of N interacting particles represented in cartesian coordinates with the generalized simple hamiltonian,

$$\mathcal{H}_S = \sum_{i=1}^{N} \frac{p_i^2}{2m_i} + V(r), \tag{4.2.28}$$

where (r_i, p_i) are the phase-space points of the system with the interacting potential $V(r)$ and m_i is the mass of the i^{th} particle. The above hamiltonian can be represented in an alternative form as a sum of decoupled modes through a coordinate transformation into normal modes using the normal coordinate analysis method. Each normal mode represents the systems internal degree of freedom. Thus, an N particle 3 dimensional system will be characterized with $3N$ degrees of freedom. Here, we couple each degree of freedom to a Nosé-Hoover chain thermostat. This type of thermostatting technique using many Nosé-Hoover chain thermostats is commonly referred to in literature as "massive" Nosé-Hoover chain(MNHC)[66]. The thermostat hamiltonian is given by

$$\mathcal{H}_{NHC} = \sum_{j=1}^{3N} \left[\frac{p_{\eta_{1_j}}^2}{2m_{\eta_{1_j}}} + \frac{p_{\eta_{2_j}}^2}{2m_{\eta_{2_j}}} + g_j k_B T_j \eta_{1_j} + k_B T_j \eta_{2_j} \right], \tag{4.2.29}$$

where η_{1_j} and η_{2_j} are the two thermostat variables with the corresponding fictitious masses $m_{\eta_{1_j}}$ and $m_{\eta_{2_j}}$, and their associated momenta $p_{\eta_{1_j}}$ and $p_{\eta_{2_j}}$ for each j^{th} mode thermostat. k_B is the Boltzmann constant whereas T_j is the temperature of each j^{th} mode. g_j is the degrees of freedom. Since each mode is coupled to a thermostat, $g_j = 1$.

The following notations (r, p) and (R', P') have been used to denote cartesian and normal mode coordinates respectively.

We define the non-Hamiltonian equations of motion following Equation (4.3.2), as follows

$$\dot{r}_{i_j} = \frac{p_{i_j}}{m_{i_j}}, \tag{4.2.30}$$

$$\dot{\eta}_{1_j} = \frac{p_{\eta_{1_j}}}{m_{\eta_{1_j}}}, \tag{4.2.31}$$

$$\dot{\eta}_{2_j} = \frac{p_{\eta_{2_j}}}{m_{\eta_{2_j}}}, \tag{4.2.32}$$

$$\dot{p}_{i_j} = -\frac{\partial V(r)}{\partial r_{i_j}} - P'_j \frac{p_{\eta_{1_j}}}{m_{\eta_{1_j}}}, \tag{4.2.33}$$

$$\dot{p}_{\eta_{1_j}} = \left(\sum_{j=1}^{g_j} \frac{P'^2_j}{M'_j} - g_j k_B T_j \right) - p_{\eta_{1_j}} \frac{p_{\eta_{2_j}}}{m_{\eta_{2_j}}}, \tag{4.2.34}$$

$$\dot{p}_{\eta_{2_j}} = \frac{p^2_{\eta_{1_j}}}{m_{\eta_{1_j}}} - k_B T_j. \tag{4.2.35}$$

The Liouville operator $\mathcal{L}$ is associated with the equations of motion Eqs. (4.2.30) - (4.2.35), and split as

$$\mathcal{L} = \sum_{\alpha=1}^{5} \mathcal{L}_\alpha, \tag{4.2.36}$$

where the single terms are given as follows

$$\mathcal{L}_1 = \sum_{i=1}^{N} \frac{p_i}{m_i} \frac{\partial}{\partial r_i} + \frac{p_{\eta_{1_j}}}{m_{\eta_{1_j}}} \frac{\partial}{\partial \eta_{1_j}} + \frac{p_{\eta_{2_j}}}{m_{\eta_{2_j}}} \frac{\partial}{\partial \eta_{2_j}}, \tag{4.2.37}$$

$$\mathcal{L}_2 = F_i(r) \frac{\partial}{\partial p_i}, \tag{4.2.38}$$

$$\mathcal{L}_3 = -\frac{p_{\eta_{1_j}}}{m_{\eta_{1_j}}} P'_j \frac{\partial}{\partial p_j}, \tag{4.2.39}$$

$$\mathcal{L}_4 = \left[-\frac{p_{\eta_{2_j}}}{m_{\eta_{2_j}}} p_{\eta_{1_j}} + F_{p_{\eta_{1_j}}} \right] \frac{\partial}{\partial p_{\eta_{1_j}}}, \tag{4.2.40}$$

$$\mathcal{L}_5 = F_{p_{\eta_{2_j}}} \frac{\partial}{\partial p_{\eta_{2_j}}}, \tag{4.2.41}$$

where we have defined the following

$$F_i(r) = -\frac{\partial V(r)}{\partial r_i}, \tag{4.2.42}$$

$$F_{p_{\eta_{1_j}}} = \frac{P_j'^2}{M_j'} - k_B T_j, \tag{4.2.43}$$

$$F_{p_{\eta_{2_j}}} = \frac{p_{\eta_{1_j}}^2}{m_{\eta_{1_j}}} - k_B T_j. \tag{4.2.44}$$

At the start of the MD calculation, the initial normal mode coordinates and velocities (R', P') are obtained from the initial atoms' displacements and velocities (r, p) through a transformational matrix $\mathbf{C}$. The columns of $\mathbf{C}$ are the eigenvectors of the Hessian.

A propagator

$$U_\alpha(\tau) = exp\left[\tau \mathcal{L}_\alpha\right], \tag{4.2.45}$$

for $\alpha = 1, \ldots, 5$ is associated with each Liouville piece. The "massive" Nosé-Hoover chain propagator can be written explicitly using the symmetric Trotter formula as follows

$$\begin{aligned} U(\tau) &= U_5\left(\frac{\tau}{2}\right) U_4\left(\frac{\tau}{2}\right) U_3\left(\frac{\tau}{2}\right) U_2\left(\frac{\tau}{2}\right), \\ &\times U_1(\tau)\, U_2\left(\frac{\tau}{2}\right) U_3\left(\frac{\tau}{2}\right) U_4\left(\frac{\tau}{2}\right) U_5\left(\frac{\tau}{2}\right). \end{aligned} \tag{4.2.46}$$

Operators with the form

$$\mathcal{L}_i = \left(-\frac{p_k}{m_k} p_i + F_{p_i}\right) \frac{\partial}{\partial p_i}, \tag{4.2.47}$$

as seen in Equation (4.3.14) can be expanded as shown,

$$e^{\tau \mathcal{L}_i} p_i = p_i e^{-\tau(p_k/m_k)} + \tau F_{p_i} e^{-\tau(p_k/2m_k)} \left(\tau \frac{p_k}{2m_k}\right)^{-1} sinh\left[\tau \frac{p_k}{2m_k}\right]. \tag{4.2.48}$$

The function $\left(\tau \frac{p_k}{2m_k}\right)^{-1} sinh\left[\tau \frac{p_k}{2m_k}\right]$ is treated through an eighth order expansion.

Using the direct translation technique, the pseudo-code form of the time-reversible algorithm is:

$$p_{\eta 2_j} \rightarrow p_{\eta 2_j} + \tfrac{\tau}{2} F_{p_{\eta 2_j}} \Big\} : U_5\left(\tfrac{\tau}{2}\right)$$

$$p_{\eta 1_j} \rightarrow p_{\eta 1_j} e^{-\frac{\tau}{2}\left(p_{\eta 2_j}/m_{\eta 2_j}\right)} + \tfrac{\tau}{2} F_{\eta 1_j} e^{-\frac{\tau}{2}\left(p_{\eta 2_j}/2m_{\eta 2_j}\right)} \left(\tfrac{\tau}{2}\tfrac{p_{\eta 2_j}}{2m_{\eta 2_j}}\right)^{-1} \sinh\left[\tfrac{\tau}{2}\tfrac{p_{\eta 2_j}}{2m_{\eta 2_j}}\right] \Big\} : U_4\left(\tfrac{\tau}{2}\right)$$

$$P'_j \rightarrow P'_j \cdot exp\left[-\tfrac{\tau}{2}\tfrac{p_{\eta 1_j}}{m_{\eta 1_j}}\right] \Big\} : U_3\left(\tfrac{\tau}{2}\right)$$

Convert normal modes back to cartesian coordinates: $(R', P') \rightarrow (r, p)$

$$p_i \rightarrow p_i + \tfrac{\tau}{2} F_i(r) \Big\} : U_2\left(\tfrac{\tau}{2}\right)$$

$$\left.\begin{array}{rcl} r_i & \rightarrow & r_i + \tau \frac{p_i}{m_i} \\ \eta 1_j & \rightarrow & \eta 1_j + \tau \frac{p_{\eta 1_j}}{m_{\eta 1_j}} \\ \eta 2_j & \rightarrow & \eta 2_j + \tau \frac{p_{\eta 2_j}}{m_{\eta 2_j}} \end{array}\right\} : U_1(\tau)$$

$$p_i \rightarrow p_i + \tfrac{\tau}{2} F_i(r) \Big\} : U_2\left(\tfrac{\tau}{2}\right)$$

Convert cartesian coordinates to normal modes: $(r, p) \rightarrow (R', P')$

$$P'_j \rightarrow P'_j \cdot exp\left[-\tfrac{\tau}{2}\tfrac{p_{\eta 1_j}}{m_{\eta 1_j}}\right] \Big\} : U_3\left(\tfrac{\tau}{2}\right)$$

$$p_{\eta 1_j} \rightarrow p_{\eta 1_j} e^{-\frac{\tau}{2}\left(p_{\eta 2_j}/m_{\eta 2_j}\right)} + \tfrac{\tau}{2} F_{\eta 1_j} e^{-\frac{\tau}{2}\left(p_{\eta 2_j}/2m_{\eta 2_j}\right)} \left(\tfrac{\tau}{2}\tfrac{p_{\eta 2_j}}{2m_{\eta 2_j}}\right)^{-1} \sinh\left[\tfrac{\tau}{2}\tfrac{p_{\eta 2_j}}{2m_{\eta 2_j}}\right] \Big\} : U_4\left(\tfrac{\tau}{2}\right)$$

$$p_{\eta 2_j} \rightarrow p_{\eta 2_j} + \tfrac{\tau}{2} F_{p_{\eta 2_j}} \Big\} : U_5\left(\tfrac{\tau}{2}\right)$$

Convert normal modes back to cartesian coordinates: $(R', P') \rightarrow (r, p)$

4.3 Classical MD using Nosé-Hoover Chain thermostat with cartesian coordinates

In this section, we describe the classical MD algorithm with cartesian coordinates used to compare results from the phonostat algorithm.

Consider a system of N interacting particles coupled to a Nosé-Hoover chain thermostat with the following phase-space points $x_i = (r_i, \eta_1, \eta_2, p_i, p_{\eta_1}, p_{\eta_2})$. The hamiltonian of this system is given by

$$\mathcal{H}_{NHC} = \sum_{i=1}^{N} \frac{p_i^2}{2m_i} + V(r) + \frac{p_{\eta_1}^2}{2m_{\eta_1}} + \frac{p_{\eta_2}^2}{2m_{\eta_2}} + gk_BT\eta_1 + k_BT\eta_2, \tag{4.3.1}$$

where m_i and p_i are the mass and momenta of the i^{th} particle respectively, r_{ij} is the inter-particle distance between the i^{th} and j^{th} particle while η_1 and η_2 are the two thermostat variables with the corresponding fictitious masses m_{η_1} and m_{η_2}, and their associated momenta p_{η_1} and p_{η_2}. k_B is the Boltzmann constant whereas T is the external temperature of the system.

The generalized form of the equations of motion for the Nosé-Hoover chain can be expressed in the symplectic form as

$$\dot{x} = \sum_{j=1}^{5N} \mathcal{B}_{ij} \frac{\partial \mathcal{H}}{\partial x_j}, \qquad i = 1, 5N, \tag{4.3.2}$$

Where $\mathcal{B}_{ij}$ is the anti-symmetric matrix

$$\mathcal{B}_{ij} = \begin{bmatrix} 0 & 0 & 0 & 1 & 0 & 0 \\ 0 & 0 & 0 & 0 & 1 & 0 \\ 0 & 0 & 0 & 0 & 0 & 1 \\ -1 & 0 & 0 & 0 & -p_i & 0 \\ 0 & -1 & 0 & p_i & 0 & -p_{\eta_1} \\ 0 & 0 & -1 & 0 & p_{\eta_1} & 0 \end{bmatrix} \tag{4.3.3}$$

Using Equation (4.3.2), the non-Hamiltonian equations of motion can be derived as

$$\dot{r}_i = \frac{p_i}{m_i}, \tag{4.3.4}$$

$$\dot{\eta}_1 = \frac{p_{\eta_1}}{m_{\eta_1}}, \tag{4.3.5}$$

$$\dot{\eta}_2 = \frac{p_{\eta_2}}{m_{\eta_2}}, \tag{4.3.6}$$

$$\dot{p}_i = -\frac{\partial V(r)}{\partial r_i} - p_i \frac{p_{\eta_1}}{m_{\eta_1}}, \tag{4.3.7}$$

$$\dot{p}_{\eta_1} = \left(\sum_{i=1}^{N} \frac{p_i^2}{m_i} - g k_B T \right) - p_{\eta_1} \frac{p_{\eta_2}}{m_{\eta_2}}, \tag{4.3.8}$$

$$\dot{p}_{\eta_2} = \frac{p_{\eta_1}^2}{m_{\eta_1}} - k_B T. \tag{4.3.9}$$

The Liouville operator $\mathcal{L}$ is associated with the equations of motion Eqs. (4.3.4) - (4.3.9), and split as

$$\mathcal{L} = \sum_{\alpha=1}^{5} \mathcal{L}_\alpha, \tag{4.3.10}$$

where the single terms are given as follows

$$\mathcal{L}_1 = \sum_{i=1}^{N} \frac{p_i}{m_i} \frac{\partial}{\partial r_i} + \frac{p_{\eta_1}}{m_{\eta_1}} \frac{\partial}{\partial \eta_1} + \frac{p_{\eta_2}}{m_{\eta_2}} \frac{\partial}{\partial \eta_2}, \tag{4.3.11}$$

$$\mathcal{L}_2 = F_i(r) \frac{\partial}{\partial p_i}, \tag{4.3.12}$$

$$\mathcal{L}_3 = -\sum_{i=1}^{N} \frac{p_{\eta_1}}{m_{\eta_1}} p_i \frac{\partial}{\partial p_i}, \tag{4.3.13}$$

$$\mathcal{L}_4 = \left[-\frac{p_{\eta_2}}{m_{\eta_2}} p_{\eta_1} + F_{p_{\eta_1}} \right] \frac{\partial}{\partial p_{\eta_1}}, \tag{4.3.14}$$

$$\mathcal{L}_5 = F_{p_{\eta_2}} \frac{\partial}{\partial p_{\eta_2}}, \tag{4.3.15}$$

where we have defined the following

$$F_i(r) = -\frac{\partial V(r)}{\partial r_i}, \tag{4.3.16}$$

$$F_{p_{\eta_1}} = \sum_{i=1}^{N} \frac{p_i^2}{m_i} - g k_B T, \tag{4.3.17}$$

$$F_{p_{\eta_2}} = \frac{p_{\eta_1}^2}{m_{\eta_1}} - k_B T. \tag{4.3.18}$$

A propagator

$$U_\alpha(\tau) = exp\left[\tau \mathcal{L}_\alpha\right], \tag{4.3.19}$$

for $\alpha = 1, \ldots, 5$ is associated with each Liouville piece. The Nosé-Hoover chain propagator can be written explicitly using the symmetric Trotter formula as follows

$$\begin{aligned} U(\tau) &= U_5\left(\frac{\tau}{2}\right) U_4\left(\frac{\tau}{2}\right) U_3\left(\frac{\tau}{2}\right) U_2\left(\frac{\tau}{2}\right), \\ &\times U_1(\tau) U_2\left(\frac{\tau}{2}\right) U_3\left(\frac{\tau}{2}\right) U_4\left(\frac{\tau}{2}\right) U_5\left(\frac{\tau}{2}\right). \end{aligned} \tag{4.3.20}$$

Operators with the form

$$\mathcal{L}_i = \left(-\frac{p_k}{m_k} p_i + F_{p_i}\right) \frac{\partial}{\partial p_i}, \tag{4.3.21}$$

as seen in Equation (4.3.14) can be expanded as shown,

$$e^{\tau \mathcal{L}_i} p_i = p_i e^{-\tau(p_k/m_k)} + \tau F_{p_i} e^{-\tau(p_k/2m_k)} \left(\tau \frac{p_k}{2m_k}\right)^{-1} sinh\left[\tau \frac{p_k}{2m_k}\right]. \tag{4.3.22}$$

The function $\left(\tau \frac{p_k}{2m_k}\right)^{-1} sinh\left[\tau \frac{p_k}{2m_k}\right]$ is treated through an eighth order expansion. Using the direct translation technique, the pseudo-code form of the time-reversible algorithm is:

$$p_{\eta_2} \rightarrow p_{\eta_2} + \tfrac{\tau}{2} F_{p_{\eta_2}} \Big\} : U_5\left(\tfrac{\tau}{2}\right)$$

$$\left.\begin{array}{rcl} p_{\eta_1} & \rightarrow & p_{\eta_1} e^{-\frac{\tau}{2}\left(p_{\eta_2}/m_{\eta_2}\right)} + \frac{\tau}{2} F_{\eta_1} e^{-\frac{\tau}{2}\left(p_{\eta_2}/2m_{\eta_2}\right)} \left(\frac{\tau}{2}\frac{p_{\eta_2}}{2m_{\eta_2}}\right)^{-1} \sinh\left[\frac{\tau}{2}\frac{p_{\eta_2}}{2m_{\eta_2}}\right] \end{array}\right\} : U_4\left(\tfrac{\tau}{2}\right)$$

$$\left.\begin{array}{rcl} p_i & \rightarrow & p_i \cdot exp\left[-\frac{\tau}{2}\frac{p_{\eta_1}}{m_{\eta_1}}\right] \end{array}\right\} : U_3\left(\tfrac{\tau}{2}\right)$$

$$\left.\begin{array}{rcl} p_i & \rightarrow & p_i \ + \frac{\tau}{2} F_i\left(r\right) \end{array}\right\} : U_2\left(\tfrac{\tau}{2}\right)$$

$$\left.\begin{array}{rcl} r_i & \rightarrow & r_i + \tau\frac{p_i}{m_i} \\ \eta_1 & \rightarrow & \eta_1 + \tau\frac{p_{\eta_1}}{m_{\eta_1}} \\ \eta_2 & \rightarrow & \eta_2 + \tau\frac{p_{\eta_2}}{m_{\eta_2}} \end{array}\right\} : U_1\left(\tau\right)$$

4.4 Numerical Simulation

The system under study was composed of 1024 particles with the equations of motion integrated using the velocity Verlet algorithm with a time step of $\delta t = 0.003$. The system was first equilibrated using 20000 steps and a further 500000 steps were used for the production run. The system density was kept fixed at $\rho = 0.4$. Three different simulations were run; the first simulation which served as a benchmark for our MD code was performed using standard cartesian coordinates MD simulation for a system coupled to single NHC thermostat. The second system investigated used a classical MD simulation approach with the phonostat methodology, the temperature of each mode is the same and each mode was coupled to a NHC thermostat. The last system investigated used the Wigner approach to quantum mechanics to obtain frequency dependent 'effective' temperature for each mode. Each of the modes were also coupled to a NHC thermostat. The results from these simulations were compared with the published work by Mausbach and May [17].

We first set out to test and compare the dynamical, thermodynamical and structural results from a standard MD simulations with results already published by Mausbach and May [17]. The density of the system was fixed at $\rho = 0.4$ and the temperature values investigated $T = 0.008,\ 0.010,\ 0.015,\ 0.020,\ 0.030,\ 0.040,\ 0.060$ and 0.080. The Nosé-Hoover chain thermostat masses used were set as $m_\eta = 1$ and $m_\zeta = 1$. Using the

results from these simulations, we compared the self-diffusion coefficients (see Table 4.1) calculated using the Einstein and Green-Kubo relations expressed by Eqs. (2.5.9) and (2.5.8) respectively. We also compared the system pressure against various temperature values, the results of this comparison are shown in Fig. (4.2). For all the temperature values investigated, we obtained the radial distribution function which were compared against the published results. The results of the radial distribution function are shown in Figs. (4.3, 4.4, 4.5, 4.6, 4.7, 4.8, 4.9 and 4.10). From these results, we observe that the we are able to reproduce the published results to a high degree of accuracy.

Temperature	$D_{published}$	D_{MSD}	σ_{MSD}	D_{VACF}	σ_{VACF}
0.008	0.005432	0.0056237	0.0003535	0.0056280	0.0002498
0.010	0.009294	0.0087236	0.0002379	0.0087382	0.0002598
0.015	0.017984	0.0178199	0.0006936	0.0176800	0.0003699
0.020	0.028123	0.0275807	0.0009696	0.0274719	0.0007158
0.030	0.050332	0.0498590	0.0013496	0.0488982	0.0009140
0.040	0.073024	0.0725793	0.0021159	0.0718541	0.0018641
0.060	0.117924	0.1184242	0.0046397	0.1170794	0.0025314
0.080	0.167652	0.1671267	0.0045177	0.1648737	0.0037886

Table 4.1: Self diffusion coefficient obtained from published results by Mausbach and May [17] compared with classical molecular dynamics results obtained using Einstein ($D(msd)$) and Green-Kubo ($D(vacf)$) relations for a range of published temperature values. σ_{MSD} and σ_{VACF} show the standard deviation from the calculated mean values using the Einstein and Green-Kubo methods.

A classical MD simulation was performed using the phonostat methodology. From the equipartition theory, classically, the temperature of each mode is the same regardless of the vibrational frequency of the mode. Each mode was coupled to a Nosé-Hoover chain thermostat whose masses were set as $m_\eta = 1$ and $m_\zeta = 1$. Thermostatting the system locally results in the loss of the dynamical information [48]. Simulations were performed on the temperature ranges investigated by Mausbach and May [17]. We compared the pressure for the various temperature values as seen in Table (4.2) and Fig. (4.2). Also, for all the temperature values investigated, we obtained the radial distribution function which was compared against the published results and from results obtained using standard MD simulation. The results of the radial distribution function

are shown in Figs. (4.3, 4.4, 4.5, 4.6, 4.7, 4.8, 4.9, 4.10). From these results, we observe that the we are able to reproduce the both the published results and standard MD simulation results to a high degree of accuracy.

Table (4.2) shows the numerical values of the pressure and the corresponding percentage difference obtained from classical MD simulations using cartesian coordinates and classical MD simulation using the phonostat algorithm for the various temperature values investigated by Mausbach and May [17]. It can be observed that the percentage difference in the results is $\lll 1\%$. This comparison, highlights the level of accuracy of the phonostat algorithm used in reproducing classical results, in this case, when comparing the thermodynamical properties such as the pressure. Moreover, a comparison of the static properties is also shown by the radial distribution function in Figs. (4.3, 4.4, 4.5, 4.6, 4.7, 4.8, 4.9, 4.10) for the same temperature values explored by Mausbach and May[17].

Temperature	$Pressure_{CartMD}$	$Pressure_{ClassPhono}$	$\%Error$
0.008	0.419823647	0.420141399	0.075687104
0.010	0.419725537	0.420015663	0.069122696
0.015	0.419836909	0.420103490	0.063496507
0.020	0.420287222	0.420805782	0.123382388
0.030	0.422264338	0.422834396	0.135000466
0.040	0.424910039	0.425354719	0.104652847
0.060	0.430880189	0.431339175	0.106522783
0.080	0.437615931	0.438076407	0.105223702

Table 4.2: Percentage difference between the comparison of the pressure obtained from classical MD simulations using cartesian coordinates ($Pressure_{CartMD}$) and classical MD simulation using the phonostat algorithm ($Pressure_{ClassPhono}$) versus temperature.

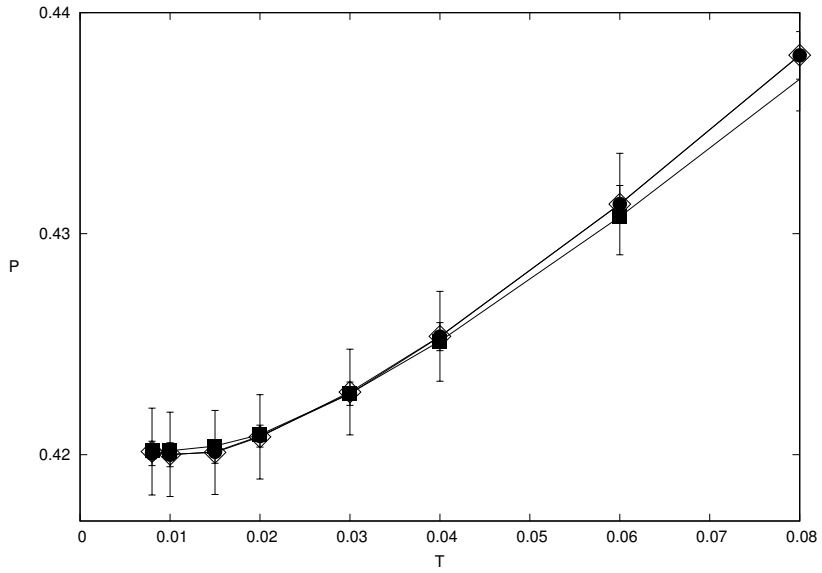

Figure 4.2: Comparison of the pressure versus temperature for results obtained from the work of Mausbach and May [17] (■), classical MD simulations using cartesian coordinates (●) and classical MD simulation using the phonostat algorithm (◇). The system parameters used for the simulations were 1024 particles for a fixed density (ρ) of 0.4 with a time-step $\delta t = 0.003$ for a production run of 5.0×10^5 steps.

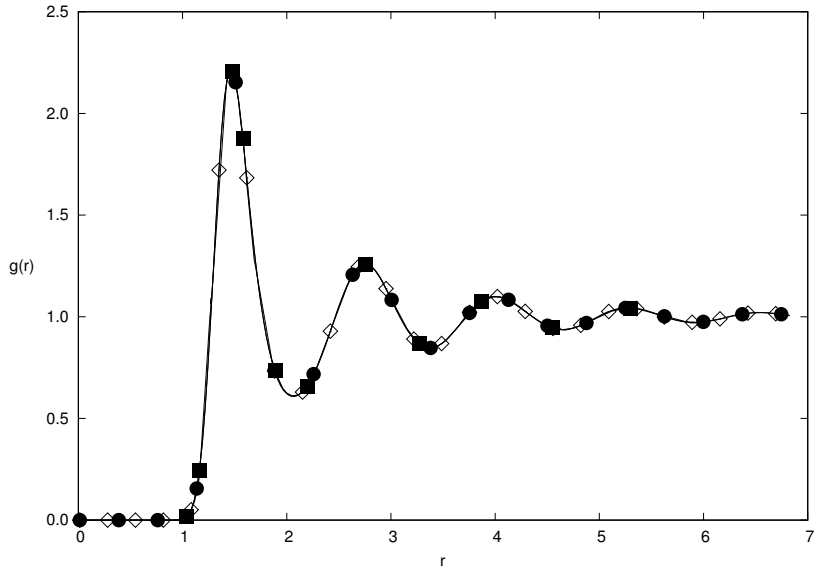

Figure 4.3: Comparison of the radial distribution function at a temperature value $T = 0.008$ from the work of Mausbach and May [17] (■), classical MD simulations using cartesian coordinates (●) and classical MD simulation using the phonostat algorithm (◇). The system parameters used for the simulations were 1024 particles for a fixed density (ρ) of 0.4 with a time-step $\delta t = 0.003$ for a production run of 5.0×10^5 steps.

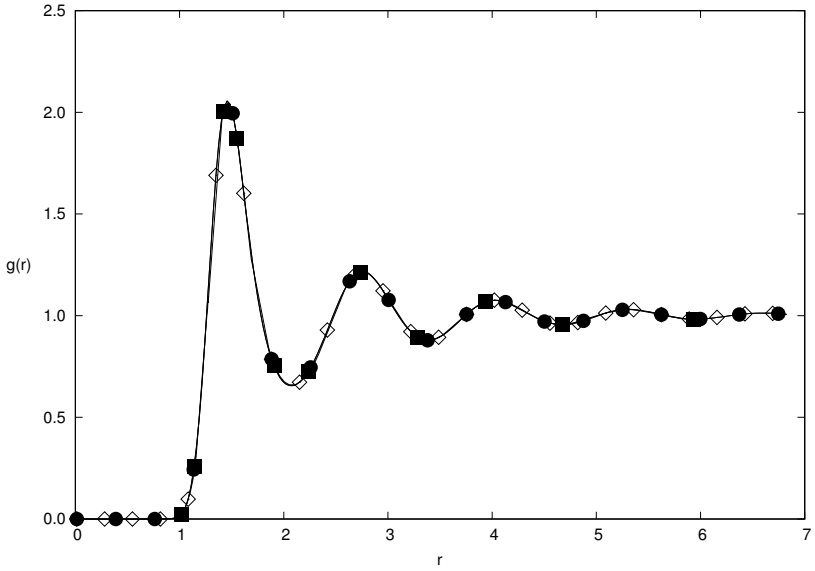

Figure 4.4: Comparison of the radial distribution function at a temperature value $T = 0.010$ from the work of Mausbach and May [17] (■), classical MD simulations using cartesian coordinates (●) and classical MD simulation using the phonostat algorithm (◇). The system parameters used for the simulations were 1024 particles for a fixed density (ρ) of 0.4 with a time-step $\delta t = 0.003$ for a production run of 5.0×10^5 steps.

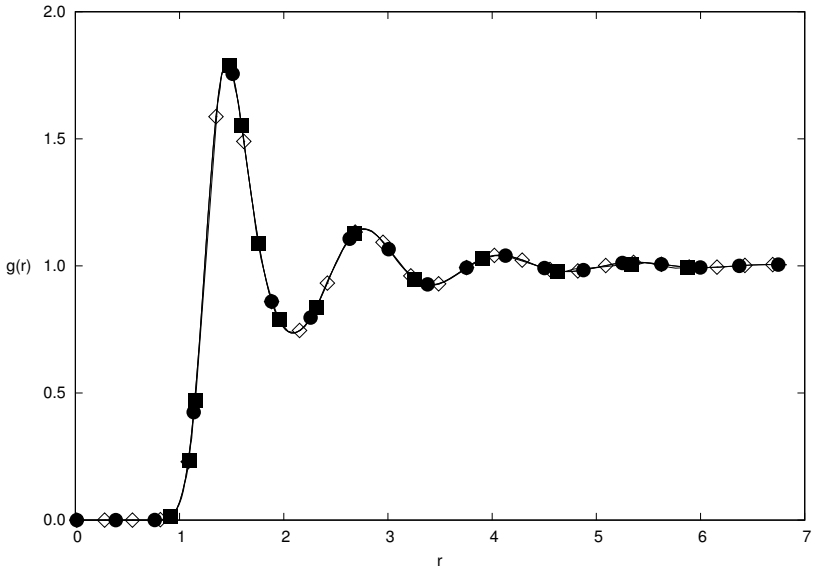

Figure 4.5: Comparison of the radial distribution function at a temperature value $T = 0.015$ from the work of Mausbach and May [17] (■), classical MD simulations using cartesian coordinates (●) and classical MD simulation using the phonostat algorithm (◇). The system parameters used for the simulations were 1024 particles for a fixed density (ρ) of 0.4 with a time-step $\delta t = 0.003$ for a production run of 5.0×10^5 steps.

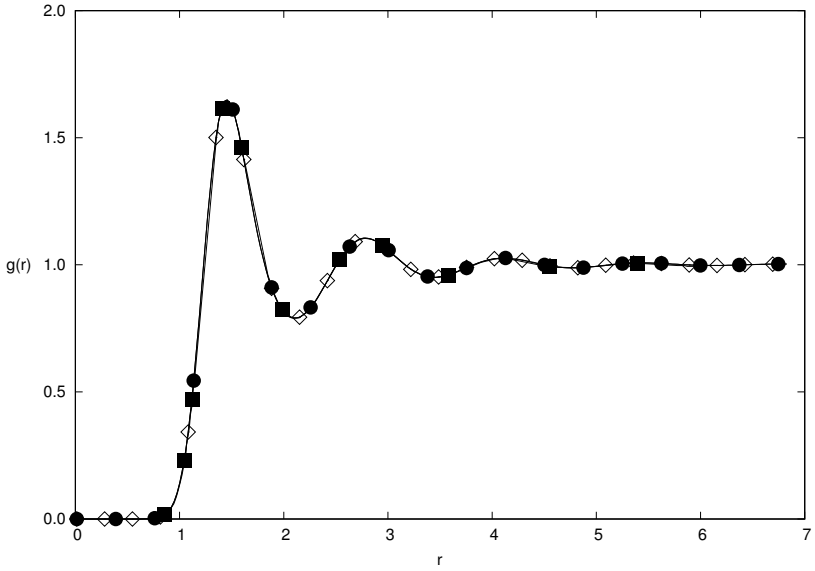

Figure 4.6: Comparison of the radial distribution function at a temperature value $T = 0.020$ from the work of Mausbach and May [17] (■), classical MD simulations using cartesian coordinates (●) and classical MD simulation using the phonostat algorithm (◇). The system parameters used for the simulations were 1024 particles for a fixed density (ρ) of 0.4 with a time-step $\delta t = 0.003$ for a production run of 5.0×10^5 steps.

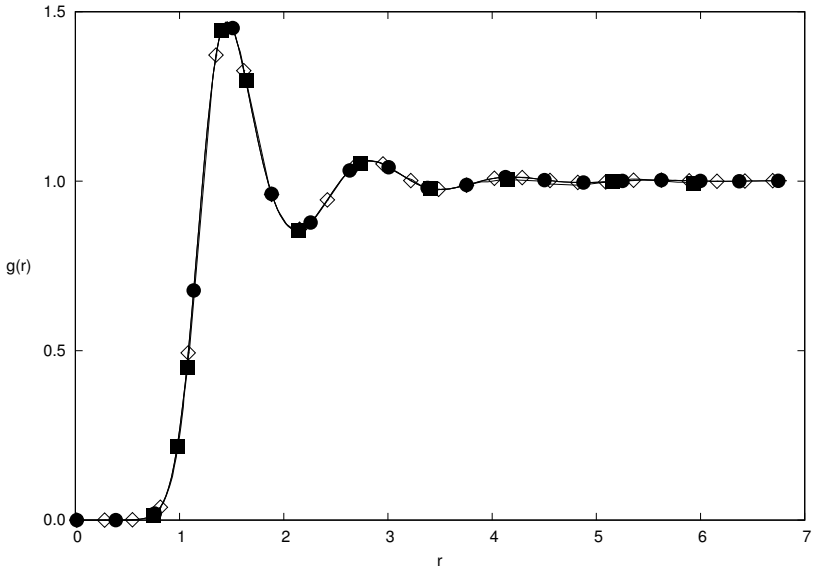

Figure 4.7: Comparison of the radial distribution function at a temperature value $T = 0.030$ from the work of Mausbach and May [17] (■), classical MD simulations using cartesian coordinates (●) and classical MD simulation using the phonostat algorithm (◇). The system parameters used for the simulations were 1024 particles for a fixed density (ρ) of 0.4 with a time-step $\delta t = 0.003$ for a production run of 5.0×10^5 steps.

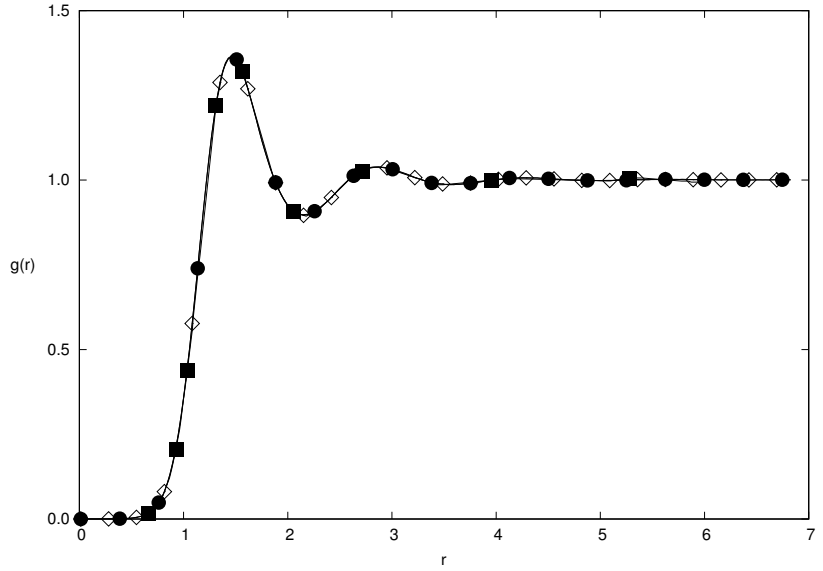

Figure 4.8: Comparison of the radial distribution function at a temperature value $T = 0.040$ from the work of Mausbach and May [17] (■), classical MD simulations using cartesian coordinates (●) and classical MD simulation using the phonostat algorithm (◇). The system parameters used for the simulations were 1024 particles for a fixed density (ρ) of 0.4 with a time-step $\delta t = 0.003$ for a production run of 5.0×10^5 steps.

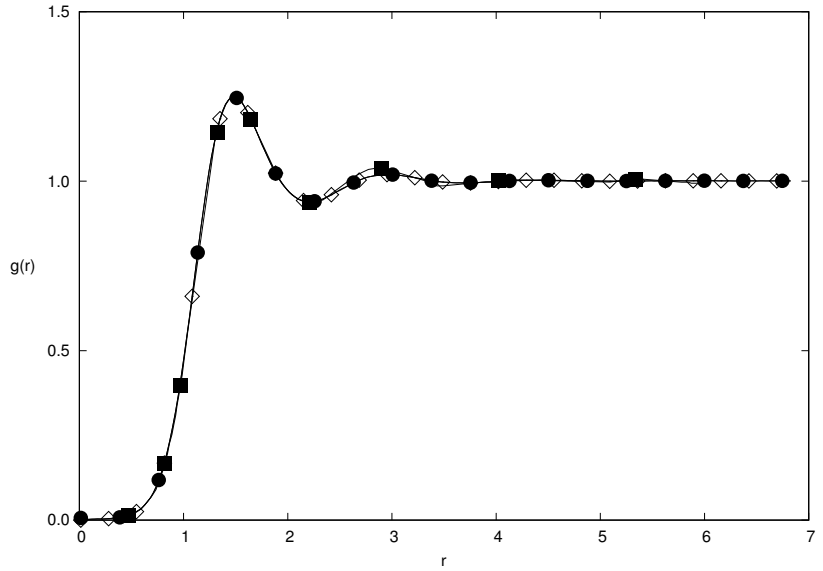

Figure 4.9: Comparison of the radial distribution function at a temperature value $T = 0.060$ from the work of Mausbach and May [17] (■), classical MD simulations using cartesian coordinates (●) and classical MD simulation using the phonostat algorithm (◇). The system parameters used for the simulations were 1024 particles for a fixed density (ρ) of 0.4 with a time-step $\delta t = 0.003$ for a production run of 5.0×10^5 steps.

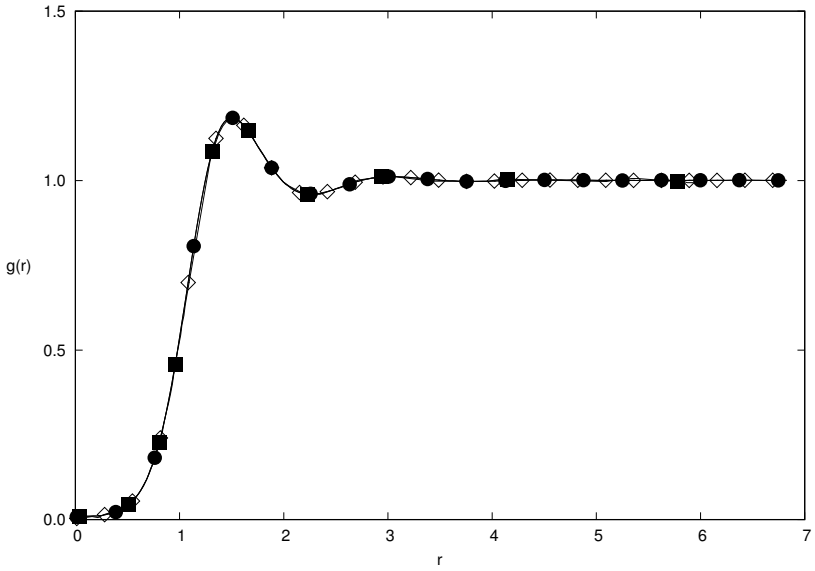

Figure 4.10: Comparison of the radial distribution function at a temperature value $T = 0.080$ from the work of Mausbach and May [17] (■), classical MD simulations using cartesian coordinates (●) and classical MD simulation using the phonostat algorithm (◇). The system parameters used for the simulations were 1024 particles for a fixed density (ρ) of 0.4 with a time-step $\delta t = 0.003$ for a production run of 5.0×10^5 steps.

Using the Wigner approach to quantum mechanics and the phonostat methodology, the frequency dependent effective temperatures for the modes were calculated. Each mode was thermalized by coupling to a Nosé-Hoover chain thermostat whose masses were set as $m_\eta = 1$ and $m_\zeta = 1$. Numerical simulations were carried out for the temperature ranges explored by Mausbach and May [17]. The results of this simulations were compared with those from standard MD simulations, classical MD simulations using the phonostat algorithm and from the published results from the work of Mausbach and May [17]. By observing the thermodynamic results of the pressure as seen in Table. (4.3) and Fig. (4.11) it can be observed that the quantum results differ from the classical results by a percentage difference of $\gg 45\%$ within the temperature ranges, $T = 0.008$ and $T = 0.080$, investigated by Mausbach and May[17]. Also, quantum effects are evident when investigating the structural properties of the fluid, this can be seen from the difference in the height of the peaks when comparing the radial distribution functions of the classical and quantum systems as seen in Figs. (4.12, 4.13, 4.14, 4.15, 4.16, 4.17, 4.18 and 4.19). The classical fluid is seen to have a distinct structure whereas the quantum fluid looses its structure.

At high temperatures, however, the Wigner approach to quantum mechanics is able to reproduce the classical results. By observing the trend in the pressure versus temperature as shown in Fig. (4.11) and the percentage error in the results from Table. (4.3), it can be noted that as the temperature is increased the graph showing the phonostat algorithm using the Wigner approach converges with that of the classical simulations. Moreover, the value of the percentage error decreases with an increase in temperature. Thus, at high temperatures, classical results can be obtained to a high degree of accuracy using the Wigner approach to quantum mechanics. To highlight this, as an example, we consider MD simulations performed at a temperature $T = 3.000$. From Table. (4.3), the pressure values obtained from the Wigner approach to quantum mechanics when compared to the classical MD simulation using the phonostat methodology are approximately the same having a percentage difference of less than 2%. Also, similar radial distribution function graphs are shown in Fig. (4.20) when comparing both the classical and quantum fluids.

Temperature	$Pressure_{ClassPhono}$	$Pressure_{QuantPhono}$	$\%Error$
0.008	0.420141399	0.643027723	53.05031223
0.010	0.420015663	0.643124163	53.11909054
0.015	0.420103490	0.643098712	53.08102092
0.020	0.420805782	0.643154323	52.83875614
0.030	0.422834396	0.643320620	52.14481736
0.040	0.425354719	0.643071234	51.18469486
0.060	0.431339175	0.643480897	49.18211351
0.080	0.438076407	0.643050790	46.78964217
0.100	0.445292592	0.643822491	44.58414594
0.150	0.464343607	0.645576537	39.02991800
0.200	0.484349310	0.649775743	34.15436536
0.300	0.525266647	0.663314819	26.28154152
0.400	0.566973090	0.683117390	20.48497566
0.500	0.608588576	0.707799137	16.30174541
0.700	0.691653013	0.767449498	10.95874427
1.000	0.815577745	0.870616674	6.748458904
1.200	0.897504568	0.943953335	5.175323763
1.500	1.020470738	1.057857752	3.663702645
2.000	1.223787427	1.251802206	2.289186706
3.000	1.628699541	1.647163630	1.133670636
4.000	2.031861067	2.046243668	0.707853555
6.000	2.834400177	2.843694687	0.327918053
8.000	3.638195276	3.643297195	0.140232142
10.00	4.441449642	4.440856457	0.013355671

Table 4.3: Percentage difference between the comparison of the pressure obtained from classical MD simulation using the phonostat algorithm ($Pressure_{ClassPhono}$) and the Wigner approach of quantum mechanics using the phonostat algorithm ($Pressure_{QuantPhono}$) versus temperature.

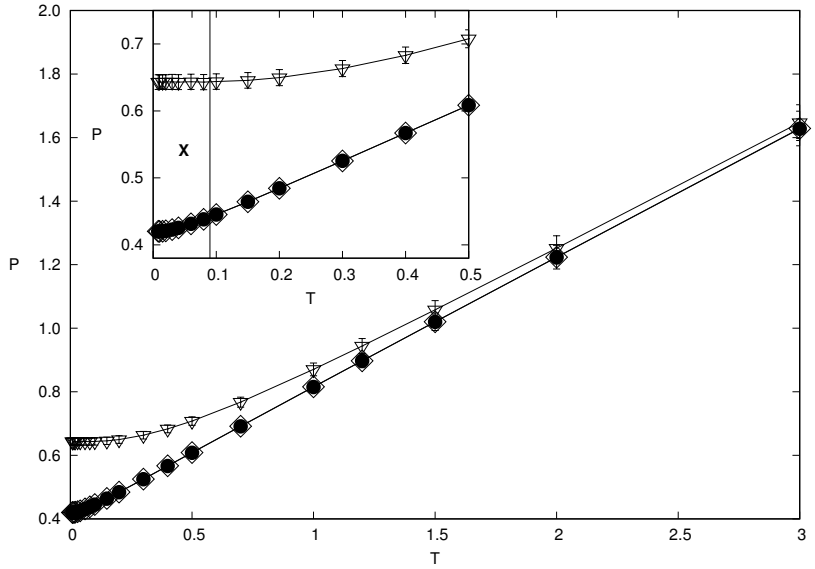

Figure 4.11: Comparison of the pressure versus temperature for results obtained from classical MD simulations using cartesian coordinates (●), classical MD simulation using the phonostat algorithm (◇) and the Wigner approach of quantum mechanics using the phonostat algorithm (▽). The system parameters used for the simulations were 1024 particles for a fixed density (ρ) of 0.4 with a time-step $\delta t = 0.003$ for a production run of 5.0×10^5 steps. The inset plot shows a zoom of the temperature region of 0 to 0.5, where the region marked as 'X' in the inset plot shows the temperature ranges investigated by Mausbach and May [17] in their work.

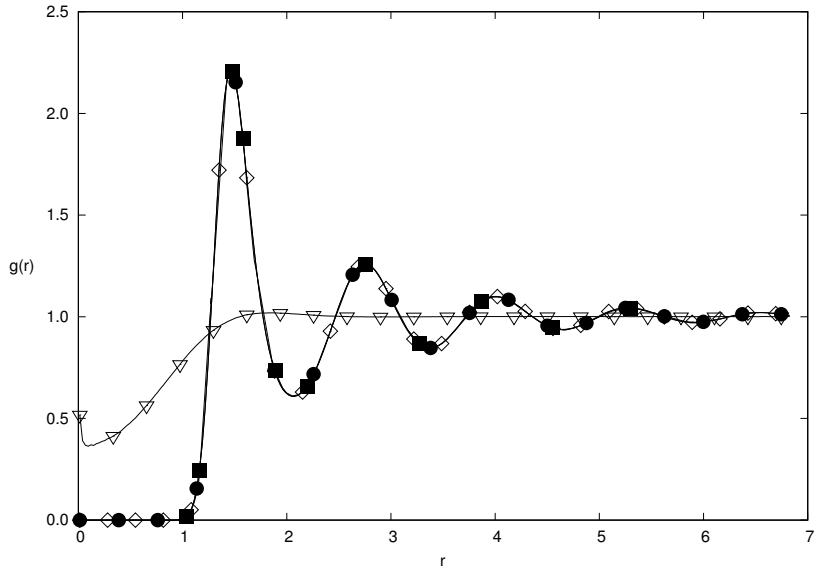

Figure 4.12: Comparison of the radial distribution function at a temperature value $T = 0.008$ from the work of Mausbach and May [17] (■), classical MD simulations using cartesian coordinates (●), classical MD simulation using the phonostat algorithm (◇) and the Wigner approach of quantum mechanics using the phonostat algorithm (▽). The system parameters used for the simulations were 1024 particles for a fixed density (ρ) of 0.4 with a time-step $\delta t = 0.003$ for a production run of 5.0×10^5 steps.

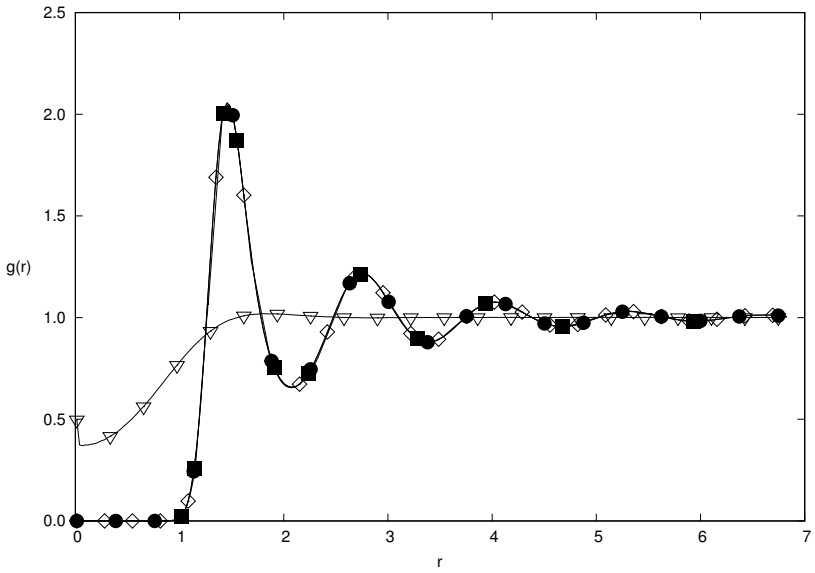

Figure 4.13: Comparison of the radial distribution function at a temperature value $T = 0.010$ from the work of Mausbach and May [17] (■), classical MD simulations using cartesian coordinates (●), classical MD simulation using the phonostat algorithm (◇) and the Wigner approach of quantum mechanics using the phonostat algorithm (▽). The system parameters used for the simulations were 1024 particles for a fixed density (ρ) of 0.4 with a time-step $\delta t = 0.003$ for a production run of 5.0×10^5 steps.

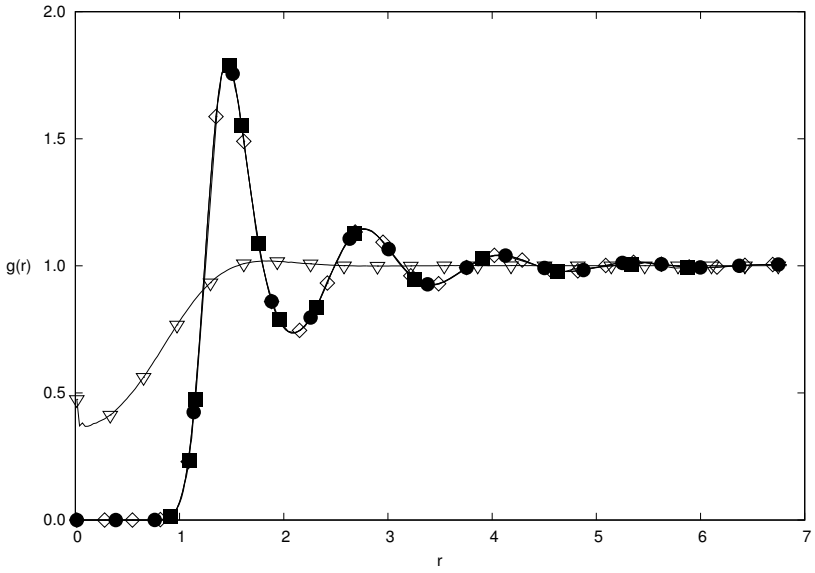

Figure 4.14: Comparison of the radial distribution function at a temperature value $T = 0.015$ from the work of Mausbach and May [17] (■), classical MD simulations using cartesian coordinates (●), classical MD simulation using the phonostat algorithm (◇) and the Wigner approach of quantum mechanics using the phonostat algorithm (▽). The system parameters used for the simulations were 1024 particles for a fixed density (ρ) of 0.4 with a time-step $\delta t = 0.003$ for a production run of 5.0×10^5 steps.

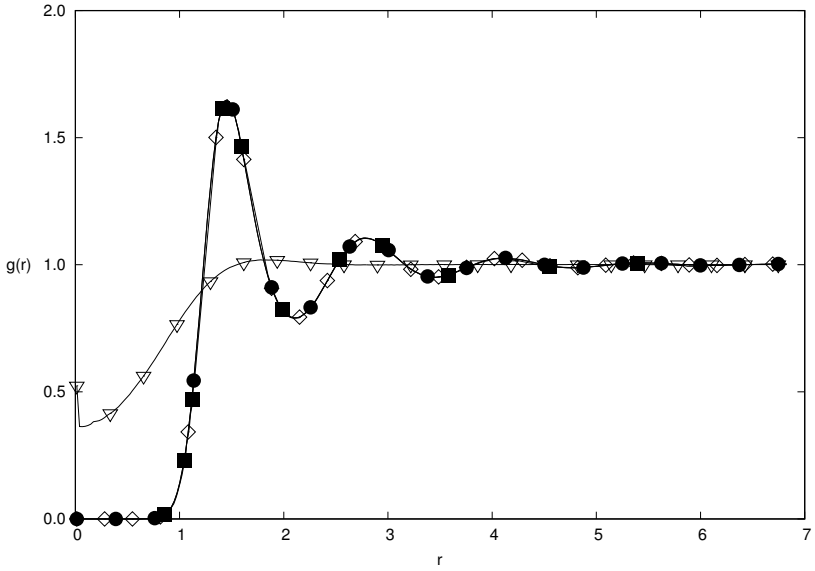

Figure 4.15: Comparison of the radial distribution function at a temperature value $T = 0.020$ from the work of Mausbach and May [17] (■), classical MD simulations using cartesian coordinates (●), classical MD simulation using the phonostat algorithm (◇) and the Wigner approach of quantum mechanics using the phonostat algorithm (▽). The system parameters used for the simulations were 1024 particles for a fixed density (ρ) of 0.4 with a time-step $\delta t = 0.003$ for a production run of 5.0×10^5 steps.

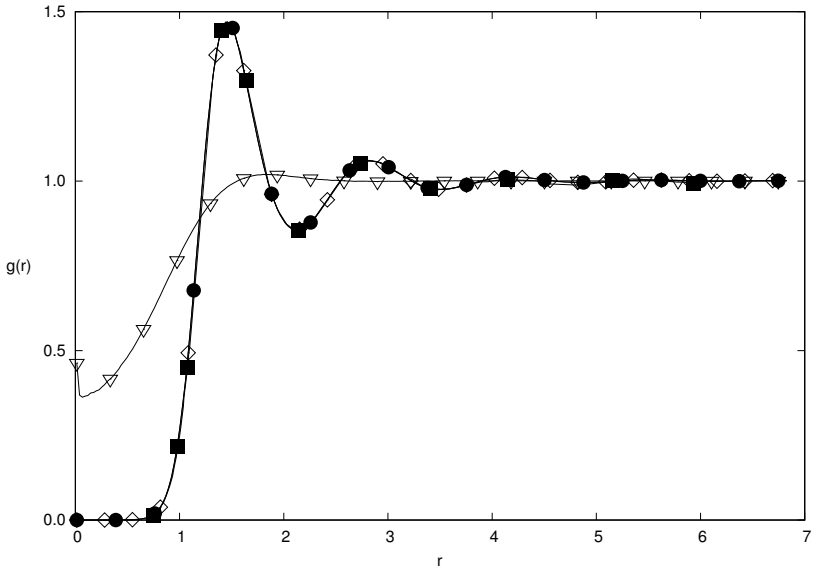

Figure 4.16: Comparison of the radial distribution function at a temperature value $T = 0.030$ from the work of Mausbach and May [17] (■), classical MD simulations using cartesian coordinates (●), classical MD simulation using the phonostat algorithm (◇) and the Wigner approach of quantum mechanics using the phonostat algorithm (▽). The system parameters used for the simulations were 1024 particles for a fixed density (ρ) of 0.4 with a time-step $\delta t = 0.003$ for a production run of 5.0×10^5 steps.

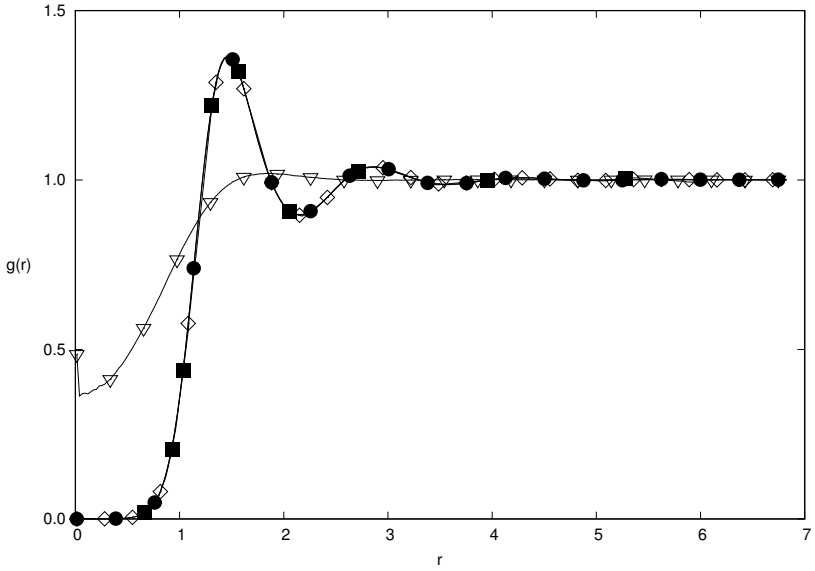

Figure 4.17: Comparison of the radial distribution function at a temperature value $T = 0.040$ from the work of Mausbach and May [17] (■), classical MD simulations using cartesian coordinates (●), classical MD simulation using the phonostat algorithm (◇) and the Wigner approach of quantum mechanics using the phonostat algorithm (▽). The system parameters used for the simulations were 1024 particles for a fixed density (ρ) of 0.4 with a time-step $\delta t = 0.003$ for a production run of 5.0×10^5 steps.

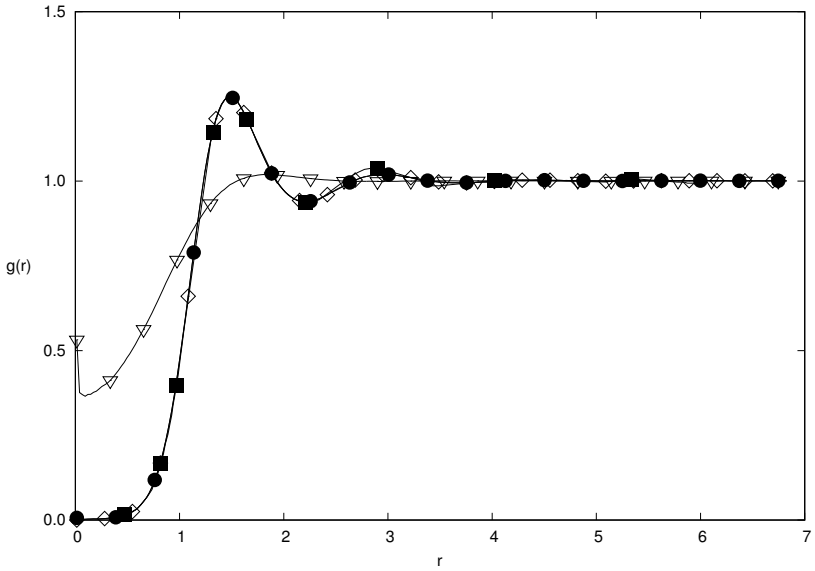

Figure 4.18: Comparison of the radial distribution function at a temperature value $T = 0.060$ from the work of Mausbach and May [17] (■), classical MD simulations using cartesian coordinates (●), classical MD simulation using the phonostat algorithm (◇) and the Wigner approach of quantum mechanics using the phonostat algorithm (▽). The system parameters used for the simulations were 1024 particles for a fixed density (ρ) of 0.4 with a time-step $\delta t = 0.003$ for a production run of 5.0×10^5 steps.

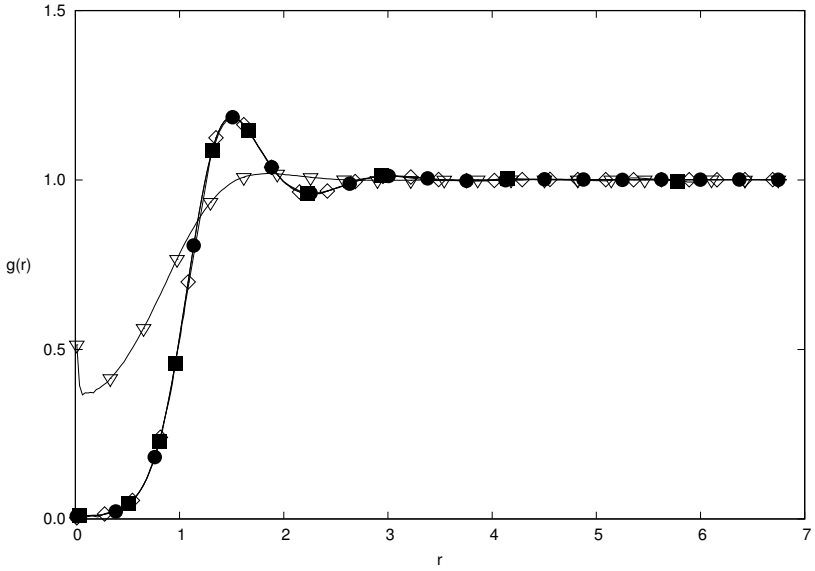

Figure 4.19: Comparison of the radial distribution function at a temperature value $T = 0.080$ from the work of Mausbach and May [17] (■), classical MD simulations using cartesian coordinates (●), classical MD simulation using the phonostat algorithm (◇) and the Wigner approach of quantum mechanics using the phonostat algorithm (▽). The system parameters used for the simulations were 1024 particles for a fixed density (ρ) of 0.4 with a time-step $\delta t = 0.003$ for a production run of 5.0×10^5 steps.

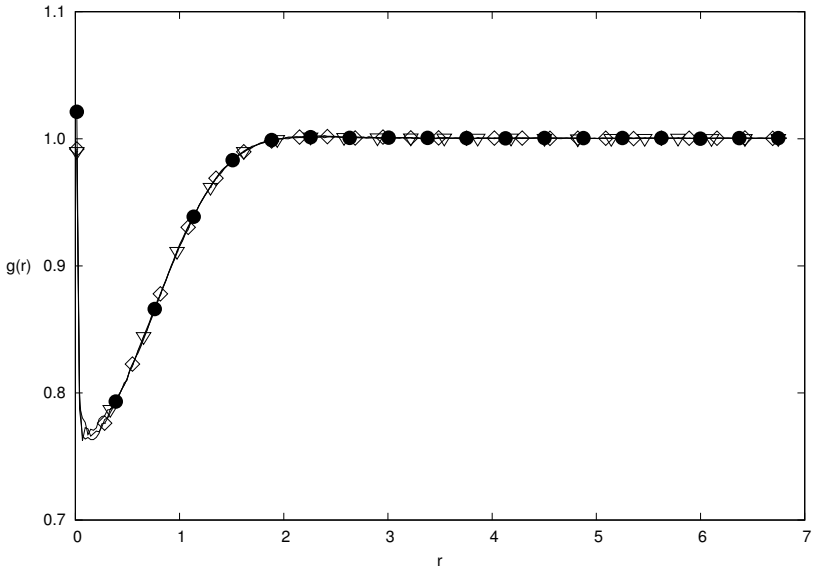

Figure 4.20: Comparison of the radial distribution function at a temperature value $T = 3.0$ for classical MD simulations using cartesian coordinates (●), classical MD simulation using the phonostat algorithm (◇) and the Wigner approach of quantum mechanics using the phonostat algorithm (▽). The system parameters used for the simulations were 1024 particles for a fixed density (ρ) of 0.4 with a time-step $\delta t = 0.003$ for a production run of 5.0×10^5 steps.

4.5 Conclusion

The Gaussian core is a bounded potential used widely in describing simulations of soft-matter models. In particular, the GCM is able to mimic the phase diagram of water. In this work, we have presented a phonostat methodology based on classical molecular dynamics and Wigner approach to quantum mechanics. We were also able to introduce quantum effects into our system by generating a thermal profile using different 'effective' temperature for the modes and coupling each one of the modes to a thermal bath. From our work we have found that quantum corrections are numerically quite important for the range of temperatures and densities explored by Mausbach and May [17]. This is contrary to what is usually assumed when simulating soft models, the quantum nature of motion cannot be disregarded.

Chapter 5

Conclusions and Perspectives

Soft matter has been of considerable research interest from as early as the 19^{th} century in the field of condensed matter physics. The concentrated interest in this particular field is due to two main reasons: first, soft matter is commonly found in our every day lives. This includes bio-organic substances such as protein solutions, blood, mayonnaise, milk among many others to inorganic substances such as different varieties of foam, paint, ink which are mainly used in industrial and technological applications. These substances are easily deformed by thermal fluctuations or thermal stresses due to their comparatively larger size when compared to atomic materials.

The second reason soft matter has received considerable attention is its role in academic research since they have special properties that make them valuable model systems for research. For instance, a precise definition of the effective interaction potential which can be obtained by carefully changing in a controlled way the relevant properties of the suspension such as the temperature and salt concentration. Also, through computer simulation, one can choose suitable interacting potentials which are capable of mimicking the atomic forces in polymer chains, liquid crystals, crystals and bio-molecules among others, such potentials include the Lennard Jones and the Gaussian core potential.

In this work we develop a new configurational thermostatting scheme [41] for controlling temperature in nonequilibrium molecular dynamics (NEMD). This thermostatting scheme also known as a configurational temperature Nosé-Hoover thermostat (CTNH)

is based on the original Braga-Travis thermostat and formulated in phase space using a quasi-Hamiltonian approach introduced by Sergi and Ferrario [16]. The equations of motion for this thermostat were integrated using a reversible integrator based on the symmetric Trotter decomposition of the propagator (STP) for simple potential energy functions such as quadratic functions. However for general systems with more complicated potentials, it was necessary to perform a harmonic approximation of the potential thereby yielding a position-dependent harmonically approximated (PDHA) STP propagator. Using a PDHA STP algorithm with the CTNH thermostat, a three dimensional system with a Weeks-Chandler-Anderson(WCA) interacting potential was tested close to the Lennard-Jones triple point ($\rho = 0.8442$, $T = 0.722$) and compared against a standard Nosé-Hoover thermostat with the same initial state point. It was found that the CTNH thermostat yielded very good results which were stable over long times for a general system when compared with the simulations from a standard Nosé-Hoover (NH) thermostat. Also the run times for the NH simulations were approximately 10% than the CTNH thermostat, this could have been attributed to the local harmonic approximation of the potential energy in each time step.

Also, we presented a new phonostat methodology that is capable of maintaining the temperature of each mode via a Nosé-Hoover chain thermostat coupled to each mode. This phonostat approach defined in the classical regime was tested against a standard molecular dynamics simulation and published results presented by Mausbach and May [17] with excellent agreement. It is also noted that thermostatting each degree of freedom results in the loss of the dynamical information of the system. With our phonostat algorithm, the nuclear quantum effects of a system can be investigated as one can use the Wigner approach to quantum mechanics to obtain the 'effective' temperatures of the modes. A system with an interacting Gaussian Core potential is investigated with a range of similar state points explored by Mausbach and May [17]. In our findings, the quantum effects of the GCM system were numerically quite important.

The phonostat methodology can be used in many other soft matter systems as a simple way to introduce quantum effects in such systems. A future perspective of this methodology would be to investigate the phase diagram of the Gaussian Core model.

Prespitino *et al* [47] have presented a comprehensive numerical analysis of the phase diagram of the Gaussian Core model which displays some similarities to the phase behavior of star-polymer solutions [67]. Using the phonostat algorithm, one can easily introduce quantum effects into the system and investigate their importance when compared to the similar range of state points presented in the work of Prespitino *et al* [47].

Appendix A

Miscellaneous Proofs and Derivations

A.1 Operator formula

Consider the following operator equation,

$$\dot{q} = Lq \ , \tag{A.1.1}$$

where L is the Liouville operator.

For an arbitrary initial condition q_0, the formal solution to the evolution of a system can be determined in time according to

$$q_t = e^{tL} q_0 \ , \tag{A.1.2}$$

where e^{tL} is the classical propagator.

For a given Liouville operator of the form,

$$L = (A - q\ B)\frac{\partial}{\partial q} \ , \tag{A.1.3}$$

equation (A.1.1) can be rewritten as,

$$\begin{aligned} \dot{q} &= Lq \,, \\ &= A - q\, B \,. \end{aligned} \tag{A.1.4}$$

Integrating Eq. (A.1.4),

$$\int_{t_1}^{t_2} dt = \int_{q(t_1)}^{q(t_2)} \frac{dq}{A - q\, B} \,. \tag{A.1.5}$$

From the left-hand side of Eq. (A.1.5),

$$\int_{t_1}^{t_2} dt = t_2 - t_1 = \tau \,. \tag{A.1.6}$$

To integrate the right-hand side of Eq. (A.1.5) we use the following change of variables, let

$$g = A - q\, B \,, \tag{A.1.7}$$

thus, we can find the differential of g as,

$$dg = -B\, dq \,, \tag{A.1.8}$$

hence the right-hand side of Eq. (A.1.5) can be written as,

$$-\frac{1}{B} \int_{A - B\, q(t_1)}^{A - B\, q(t_2)} dt \frac{dg}{g} = -\frac{1}{B}\, ln \left(\frac{A - B\, q(t_2)}{A - B\, q(t_1)} \right) \,. \tag{A.1.9}$$

From the results of Eq. (A.1.6) and Eq. (A.1.9), Eq(A.1.5) is finally solved as follows,

$$\begin{aligned}
\tau &= -\frac{1}{B}\, ln\left(\frac{A - B\, q(t_2)}{A - B\, q(t_1)}\right) , && \text{(A.1.10)}\\
q(t_2) &= \frac{A}{B} - \frac{A}{B}e^{-B\tau} + q(t_1)e^{-B\tau} , && \text{(A.1.11)}\\
q(t_2) &= Ae^{-\frac{B\tau}{2}}\left[\frac{e^{\frac{B\tau}{2}} - e^{-\frac{B\tau}{2}}}{B}\right] + q(t_1)e^{-B\tau} ,\\
&= Ae^{-\frac{B\tau}{2}}\tau\left[\frac{e^{\frac{B\tau}{2}} - e^{-\frac{B\tau}{2}}}{\frac{2B\tau}{2}}\right] + q(t_1)e^{-B\tau} , && \text{(A.1.12)}\\
q(t_2) &= A\tau e^{-\frac{B\tau}{2}}\tau \sinh\left[\frac{B\tau}{2}\right] + q(t_1)e^{-B\tau} . && \text{(A.1.13)}
\end{aligned}$$

For our work, the term $\sinh(x)$ is treated using a Maclaurin expansion for numerical stability as follows,

$$\sinh(x) = x + \frac{x^3}{3!} + \frac{x^5}{5!} + \frac{x^7}{7!} + \frac{x^9}{9!} + \mathcal{O}(x^{11}) . \qquad \text{(A.1.14)}$$

A.2 Deriving the Liouville operator for the Nosé-Hoover chain dynamics

Consider a system of N interacting particles coupled to a Nosé-Hoover chain thermostat with the following phase-space points $x_i = (r_i, \eta_1, \eta_2, p_i, p_{\eta_1}, p_{\eta_2})$. The hamiltonian of this system is given by

$$\mathcal{H}_{NHC} = \sum_{i=1}^{N}\frac{p_i^2}{2m_i} + V\left(q_{ij}\right) + \frac{p_{\eta_1}^2}{2m_{\eta_1}} + \frac{p_{\eta_2}^2}{2m_{\eta_2}} + gk_BT\eta_1 + k_BT\eta_2, \qquad \text{(A.2.1)}$$

where m_i and p_i are the mass and momenta of the i^{th} particle respectively, q_{ij} is the inter-particle distance between the i^{th} and j^{th} particle while η_1 and η_2 are the two thermostat variables with the corresponding fictitious masses m_{η_1} and m_{η_2}, and their associated momenta p_{η_1} and p_{η_2}. k_B is the Boltzmann constant whereas T is the external temperature of the system.

We can find the consequent splitting of the Liouville operator from

$$\mathcal{L}_\alpha = \sum_{i,j} \mathcal{B}_{ij} \frac{\partial H_\alpha}{\partial x_j} \frac{\partial}{\partial x_i}, \tag{A.2.2}$$

where is $\mathcal{B}_{ij}$ is the anti-symmetric matrix given as

$$\mathcal{B}_{NHC} = \begin{bmatrix} 0 & 0 & 0 & 1 & 0 & 0 \\ 0 & 0 & 0 & 0 & 1 & 0 \\ 0 & 0 & 0 & 0 & 0 & 1 \\ -1 & 0 & 0 & 0 & -p_i & 0 \\ 0 & -1 & 0 & p_i & 0 & -p_{\eta_1} \\ 0 & 0 & -1 & 0 & p_{\eta_1} & 0 \end{bmatrix}. \tag{A.2.3}$$

Thus the explicit Liouville operators can be calculated as follows:

For $\mathcal{L}_1$

$$\begin{aligned} \mathcal{L}_1 &= \sum_{i,j} \mathcal{B}_{ij} \frac{\partial H_1}{\partial x_j} \frac{\partial}{\partial x_i} = \sum_{i,j} \mathcal{B}_{ij} \frac{\partial V(q)}{\partial x_j} \frac{\partial}{\partial x_i} = \sum_i \mathcal{B}_{i1} \frac{\partial V(q)}{\partial x_1} \frac{\partial}{\partial x_i}, \\ &= \mathcal{B}_{21} \frac{\partial V(q)}{\partial x_1} \frac{\partial}{\partial x_2}, \\ &= -\frac{\partial V(q)}{\partial q} \frac{\partial}{\partial p}. \end{aligned} \tag{A.2.4}$$

For $\mathcal{L}_2$

$$\begin{aligned} \mathcal{L}_2 &= \sum_{i,j} \mathcal{B}_{ij} \frac{\partial H_2}{\partial x_j} \frac{\partial}{\partial x_i} = \sum_{i,j} \mathcal{B}_{ij} \frac{\partial}{\partial x_j} \left(\frac{p^2}{2m} \right) \frac{\partial}{\partial x_i} = \sum_i \mathcal{B}_{i2} \frac{\partial}{\partial x_2} \left(\frac{p^2}{2m} \right) \frac{\partial}{\partial x_i}, \\ &= \mathcal{B}_{12} \frac{\partial}{\partial x_2} \left(\frac{p^2}{2m} \right) \frac{\partial}{\partial x_1} + \mathcal{B}_{42} \frac{\partial}{\partial x_2} \left(\frac{p^2}{2m} \right) \frac{\partial}{\partial x_4}, \\ &= \mathcal{B}_{12} \frac{\partial}{\partial p} \left(\frac{p^2}{2m} \right) \frac{\partial}{\partial q} + \mathcal{B}_{42} \frac{\partial}{\partial p} \left(\frac{p^2}{2m} \right) \frac{\partial}{\partial p_{\eta_1}}, \\ &= \frac{p}{m} \frac{\partial}{\partial q} + \frac{p^2}{m} \frac{\partial}{\partial p_{\eta_1}}. \end{aligned} \tag{A.2.5}$$

For $\mathcal{L}_3$

$$\begin{aligned}
\mathcal{L}_3 &= \sum_{i,j} \mathcal{B}_{ij} \frac{\partial H_3}{\partial x_j} \frac{\partial}{\partial x_i} = \sum_{i,j} \mathcal{B}_{ij} \frac{\partial \left(k_B T \eta_1\right)}{\partial x_j} \frac{\partial}{\partial x_i} = \sum_{i} \mathcal{B}_{i3} \frac{\partial \left(k_B T \eta_1\right)}{\partial x_3} \frac{\partial}{\partial x_i} \,, \\
&= \mathcal{B}_{43} \frac{\partial \left(k_B T \eta_1\right)}{\partial x_3} \frac{\partial}{\partial x_4} = \mathcal{B}_{43} \frac{\partial \left(k_B T \eta_1\right)}{\partial \eta_1} \frac{\partial}{\partial p_{\eta_1}} \,, \\
&= -k_B T \frac{\partial}{\partial p_{\eta_1}} \,. \qquad \text{(A.2.6)}
\end{aligned}$$

For $\mathcal{L}_4$

$$\begin{aligned}
\mathcal{L}_4 &= \sum_{i,j} \mathcal{B}_{ij} \frac{\partial H_4}{\partial x_j} \frac{\partial}{\partial x_i} = \sum_{i,j} \mathcal{B}_{ij} \frac{\partial}{\partial x_j} \left(\frac{p_{\eta_1}^2}{2m_{\eta_1}} \right) \frac{\partial}{\partial x_i} = \sum_{i} \mathcal{B}_{i4} \frac{\partial}{\partial x_4} \left(\frac{p_{\eta_1}^2}{2m_{\eta_1}} \right) \frac{\partial}{\partial x_i} \,, \\
&= \mathcal{B}_{24} \frac{\partial}{\partial x_4} \left(\frac{p_{\eta_1}^2}{2m_{\eta_1}} \right) \frac{\partial}{\partial x_2} + \mathcal{B}_{34} \frac{\partial}{\partial x_4} \left(\frac{p_{\eta_1}^2}{2m_{\eta_1}} \right) \frac{\partial}{\partial x_3} + \mathcal{B}_{64} \frac{\partial}{\partial x_4} \left(\frac{p_{\eta_1}^2}{2m_{\eta_1}} \right) \frac{\partial}{\partial x_6} \,, \\
&= \mathcal{B}_{24} \frac{\partial}{\partial p_{\eta_1}} \left(\frac{p_{\eta_1}^2}{2m_{\eta_1}} \right) \frac{\partial}{\partial p} + \mathcal{B}_{34} \frac{\partial}{\partial p_{\eta_1}} \left(\frac{p_{\eta_1}^2}{2m_{\eta_1}} \right) \frac{\partial}{\partial \eta_1} + \mathcal{B}_{64} \frac{\partial}{\partial p_{\eta_1}} \left(\frac{p_{\eta_1}^2}{2m_{\eta_1}} \right) \frac{\partial}{\partial p_{\eta_2}} \,, \\
&= -p \frac{p_{\eta_1}}{m_{\eta_1}} \frac{\partial}{\partial p} + \frac{p_{\eta_1}}{m_{\eta_1}} \frac{\partial}{\partial \eta_1} + \frac{p_{\eta_1}^2}{m_{\eta_1}} \frac{\partial}{\partial p_{\eta_2}} \,. \qquad \text{(A.2.7)}
\end{aligned}$$

For $\mathcal{L}_5$

$$\begin{aligned}
\mathcal{L}_5 &= \sum_{i,j} \mathcal{B}_{ij} \frac{\partial H_5}{\partial x_j} \frac{\partial}{\partial x_i} = \sum_{i,j} \mathcal{B}_{ij} \frac{\partial \left(k_B T \eta_2\right)}{\partial x_j} \frac{\partial}{\partial x_i} = \sum_{i} \mathcal{B}_{i5} \frac{\partial \left(k_B T \eta_2\right)}{\partial x_5} \frac{\partial}{\partial x_i} \,, \\
&= \mathcal{B}_{65} \frac{\partial \left(k_B T \eta_2\right)}{\partial x_5} \frac{\partial}{\partial x_6} = \mathcal{B}_{65} \frac{\partial \left(k_B T \eta_2\right)}{\partial \eta_2} \frac{\partial}{\partial p_{\eta_2}} \,, \\
&= -k_B T \frac{\partial}{\partial p_{\eta_2}} \,. \qquad \text{(A.2.8)}
\end{aligned}$$

For $\mathcal{L}_6$

$$\begin{aligned}
\mathcal{L}_6 &= \sum_{i,j} \mathcal{B}_{ij} \frac{\partial H_6}{\partial x_j} \frac{\partial}{\partial x_i} = \sum_{i,j} \mathcal{B}_{ij} \frac{\partial}{\partial x_j} \left(\frac{p_{\eta_2}^2}{2m_{\eta_2}} \right) \frac{\partial}{\partial x_i} = \sum_{i} \mathcal{B}_{i6} \frac{\partial}{\partial x_6} \left(\frac{p_{\eta_2}^2}{2m_{\eta_2}} \right) \frac{\partial}{\partial x_i} \,, \\
&= \mathcal{B}_{46} \frac{\partial}{\partial p_{\eta_2}} \left(\frac{p_{\eta_2}^2}{2m_{\eta_2}} \right) \frac{\partial}{\partial x_4} + \mathcal{B}_{56} \frac{\partial}{\partial p_{\eta_2}} \left(\frac{p_{\eta_2}^2}{2m_{\eta_2}} \right) \frac{\partial}{\partial x_5} \,, \\
&= -p_{\eta_1} \frac{p_{\eta_2}}{m_{\eta_2}} \frac{\partial}{\partial p_{\eta_1}} + \frac{p_{\eta_2}}{m_{\eta_2}} \frac{\partial}{\partial \eta_2} \,. \qquad \text{(A.2.9)}
\end{aligned}$$

As a consequence of the splitting of the Hamiltonian, the corresponding Liouville pieces

are :

$$\mathcal{L}_1 = -\frac{\partial V(q)}{\partial q}\frac{\partial}{\partial p}\,, \tag{A.2.10}$$

$$\mathcal{L}_2 = \frac{p}{m}\frac{\partial}{\partial q} + \frac{p^2}{m}\frac{\partial}{\partial p_{\eta_1}}\,, \tag{A.2.11}$$

$$\mathcal{L}_3 = -k_B T\frac{\partial}{\partial p_{\eta_1}}\,, \tag{A.2.12}$$

$$\mathcal{L}_4 = -p\frac{p_{\eta_1}}{m_{\eta_1}}\frac{\partial}{\partial p} + \frac{p_{\eta_1}}{m_{\eta_1}}\frac{\partial}{\partial \eta_1} + \frac{p_{\eta_1}^2}{m_{\eta_1}}\frac{\partial}{\partial p_{\eta_2}}\,, \tag{A.2.13}$$

$$\mathcal{L}_5 = -k_B T\frac{\partial}{\partial p_{\eta_2}}\,, \tag{A.2.14}$$

$$\mathcal{L}_6 = -p_{\eta_1}\frac{p_{\eta_2}}{m_{\eta_2}}\frac{\partial}{\partial p_{\eta_1}} + \frac{p_{\eta_2}}{m_{\eta_2}}\frac{\partial}{\partial \eta_2}\,. \tag{A.2.15}$$

Appendix B

Analytic form of the Density Matrix, N independent oscillators

Using the Wigner distribution function of the density matrix, one can obtain the initial quantum conditions for an ensemble of oscillators in the canonical ensemble at a temperature T.

Let ρ denote the normalized density matrix, Ω the un-normalized density matrix and the temperature parameter $\beta = \frac{1}{k_B T}$. Thus $\hat{\rho}$ can be expressed as

$$\hat{\rho} = \frac{1}{Z(\beta)} e^{-\beta \hat{H}} \tag{B.0.1}$$

$$= \frac{1}{Z(\beta)} \hat{\Omega} \tag{B.0.2}$$

$$Z(\beta) = Tr(e^{-\beta \hat{H}}) \tag{B.0.3}$$

The un-normalized density matrix $\hat{\Omega}$ then satisfies the Bloch Equation

$$\frac{\partial \hat{\Omega}}{\partial \beta} = -\hat{H}\hat{\Omega} = -\hat{\Omega}\hat{H} \tag{B.0.4}$$

subject to the initial condition $\Omega(\beta = 0) = \hat{I}$ (Identity Operator).

Upon defining the operator

$$\Lambda = \frac{\overleftarrow{\partial}}{\partial R_i}\frac{\overrightarrow{\partial}}{\partial P_i} - \frac{\overleftarrow{\partial}}{\partial P_i}\frac{\overrightarrow{\partial}}{\partial R_i} \tag{B.0.5}$$

we can write the Wigner transform of the Bloch equation as

$$\begin{aligned}
\frac{\partial \Omega_W(R_n, P_n)}{\partial \beta} &= -H_W(R_n, P_n) e^{\frac{\hbar}{2i}\Lambda} \Omega_W(R_n, P_n) && \text{(B.0.6)} \\
&= -\Omega_W(R_n, P_n) e^{\frac{\hbar}{2i}\Lambda} H_W(R_n, P_n) && \text{(B.0.7)} \\
&= -H_W(R_n, P_n) e^{\frac{-\hbar}{2i}\Lambda} \Omega_W(R_n, P_n) && \text{(B.0.8)}
\end{aligned}$$

We introduce the notation

$$\begin{aligned}
\frac{\partial \Omega_W(q_n, P_n)}{\partial \beta} &= -H_W(q_n, P_n) e^{\frac{i\hbar}{2}\overleftarrow{\partial}\cdot B\cdot\overrightarrow{\partial}} \Omega_W(q_n, P_n) && \text{(B.0.9)} \\
&= -H_W(q_n, P_n) e^{\frac{-i\hbar}{2}\overleftarrow{\partial}\cdot B\cdot\overrightarrow{\partial}} \Omega_W(q_n, P_n) && \text{(B.0.10)} \\
& && \text{(B.0.11)}
\end{aligned}$$

This is possible if only even powers of the expansion of $e^{\frac{-i\hbar}{2}\overleftarrow{\partial}\cdot B\cdot\overrightarrow{\partial}}$ are taken into account. Therefore, the Wigner transform of the Bloch equation can be written as

$$\frac{\partial \Omega_W(R_n, P_n)}{\partial \beta} = -H_W(R_n, P_n)\cos\left(\frac{\hbar}{2}\overleftarrow{\partial}\cdot B\cdot\overrightarrow{\partial}\right)\Omega_W(R_n, P_n). \tag{B.0.12}$$

It's useful in the calculation of quantum mechanical corrections to classical statistical mechanics.

The initial condition for this equation is just the Wigner transform of

$\hat{\Omega}(\beta = 0) = \hat{I} \rightarrow \Omega_W(\beta = 0) = 1.$

$$\begin{aligned}
\Omega_W(\beta=0) &= \int dz e^{\frac{i}{\hbar}P_n z}\left\langle R_n - \frac{z}{2}|\hat{I}|R_n + \frac{z}{2}\right\rangle && \text{(B.0.13)}\\
&= \int dz e^{\frac{i}{\hbar}P_n z}\left\langle R_n - \frac{z}{2}|R_n + \frac{z}{2}\right\rangle && \text{(B.0.14)}\\
&= \int dz e^{\frac{i}{\hbar}P_n z}\delta\left(R_n - \frac{z}{2} - R_n - \frac{z}{2}\right) && \text{(B.0.15)}\\
&= \int dz e^{\frac{i}{\hbar}P_n z}\delta(-z) && \text{(B.0.16)}\\
&= \int dz e^{\frac{i}{\hbar}P_n z}\delta(z) && \text{(B.0.17)}\\
&= 1 && \text{(B.0.18)}
\end{aligned}$$

The Wigner transform of the Bloch equation can be simplified further.

Consider

$$\cos\left(\frac{\hbar}{2}\Lambda\right) = Re\left\{e^{\frac{i\hbar}{2}\Lambda}\right\} \tag{B.0.19}$$

Remember

$$Re\{z\} = \frac{z^* + z}{2} \tag{B.0.20}$$

Then

$$\begin{aligned}
Re\{e^{\frac{i\hbar}{2}}\Lambda\} &= \frac{e^{\frac{i\hbar}{2}\Lambda} + e^{\frac{-i\hbar}{2}\Lambda}}{2} && \text{(B.0.21)}\\
&= \cos\left(\frac{\hbar}{2}\Lambda\right) && \text{(B.0.22)}
\end{aligned}$$

Baker-Hausdorff Theorem

If $\hat{D}$ =[$\hat{A}$,$\hat{B}$] commutes with $\hat{A}$ and $\hat{B}$ then

$$\begin{aligned}
e^{A+B} &= e^A e^B e^{-\frac{D}{2}} && \text{(B.0.23)}\\
e^{A-B} &= e^A e^{-B} e^{\frac{D}{2}} && \text{(B.0.24)}
\end{aligned}$$

$$\Lambda = \frac{\overleftarrow{\partial}}{\partial P_n}\frac{\overrightarrow{\partial}}{\partial R_n} - \frac{\overrightarrow{\partial}}{\partial R_n}\frac{\overleftarrow{\partial}}{\partial P_n} \tag{B.0.25}$$

$$\hat{D} = \left[\frac{\overleftarrow{\partial}}{\partial P_n}\frac{\overrightarrow{\partial}}{\partial R_n}, \frac{\overleftarrow{\partial}}{\partial R_n}\frac{\overrightarrow{\partial}}{\partial P_n}\right] \tag{B.0.26}$$

$$= \frac{\overleftarrow{\partial}}{\partial P_n}\frac{\overrightarrow{\partial}}{\partial R_n}\frac{\overleftarrow{\partial}}{\partial R_n}\frac{\overrightarrow{\partial}}{\partial P_n} - \frac{\overleftarrow{\partial}}{\partial R_n}\frac{\overrightarrow{\partial}}{\partial P_n}\frac{\overleftarrow{\partial}}{\partial P_n}\frac{\overrightarrow{\partial}}{\partial R_n} \tag{B.0.27}$$

$$= 0 \tag{B.0.28}$$

Then since $\frac{\overleftarrow{\partial}}{\partial P_n}\frac{\overrightarrow{\partial}}{\partial R_n}$ and $\frac{\overleftarrow{\partial}}{\partial R_n}\frac{\overrightarrow{\partial}}{\partial P_n}$ commute

$$exp\left[\frac{i\hbar}{2}\left(\frac{\overleftarrow{\partial}}{\partial P_n}\frac{\overrightarrow{\partial}}{\partial R_n} - \frac{\overleftarrow{\partial}}{\partial R_n}\frac{\overrightarrow{\partial}}{\partial P_n}\right)\right] = exp\left[\frac{i\hbar}{2}\frac{\overleftarrow{\partial}}{\partial P_n}\frac{\overrightarrow{\partial}}{\partial R_n}\right] exp\left[-\frac{i\hbar}{2}\frac{\overleftarrow{\partial}}{\partial R_n}\frac{\overrightarrow{\partial}}{\partial P_n}\right] \tag{B.0.29}$$

To derive the Wigner transform of the density matrix for the general case of N independent harmonic oscillators, let us consider the Hamiltonian of a system of N independent harmonic oscillators

$$H_W = \sum_{n=1}^{N}\left(\frac{1}{2m_n}P_n^2 + \frac{1}{2}m_n\omega_n^2 R_n^2\right) \tag{B.0.30}$$

and the Bloch equation

$$\frac{\partial\Omega}{\partial\beta} = \left[-\sum_{n=1}^{N}\left(\frac{1}{2m_n}P_n^2 + \frac{1}{2}m_n\omega_n^2 R_n^2\right)\cos\left(\frac{\hbar}{2}\left[\frac{\overleftarrow{\partial}}{\partial R_n}\frac{\overrightarrow{\partial}}{\partial P_n} - \frac{\overleftarrow{\partial}}{\partial P_n}\frac{\overrightarrow{\partial}}{\partial R_n}\right]\right)\right]\Omega_W \tag{B.0.31}$$

Taylor series expansion of cos(x) up to fourth order

$$\begin{aligned}\cos x &= \cos(0) + \left(\frac{d\cos x}{dx}\right)_{x=0} x + \frac{1}{2!}\left(\frac{d^2\cos x}{dx^2}\right)_{x=0} x^2 + \\ &+ \frac{1}{3!}\left(\frac{d^3\cos x}{dx^3}\right)_{x=0} x^3 + \frac{1}{4!}\left(\frac{d^4\cos x}{dx^4}\right)_{x=0} x^4\end{aligned} \tag{B.0.32}$$

$$\frac{d\cos x}{dx} = -\sin x \tag{B.0.33}$$
$$\frac{d^2\cos x}{dx^2} = -\cos x \tag{B.0.34}$$
$$\frac{d^3\cos x}{dx^3} = \sin x \tag{B.0.35}$$
$$\frac{d^4\cos x}{dx^4} = \cos x \tag{B.0.36}$$

$$\cos(\mathrm{x}) \approx 1 - \frac{x^2}{2} + \frac{x^4}{4!} \tag{B.0.37}$$

Identifying $x = \frac{\hbar}{2}\left[\frac{\overleftarrow{\partial}}{\partial R_n}\frac{\overrightarrow{\partial}}{\partial P_n} - \frac{\overleftarrow{\partial}}{\partial P_n}\frac{\overrightarrow{\partial}}{\partial R_n}\right]$

$$\cos\left(\frac{\hbar}{2}\left[\frac{\overleftarrow{\partial}}{\partial R_n}\frac{\overrightarrow{\partial}}{\partial P_n} - \frac{\overleftarrow{\partial}}{\partial P_n}\frac{\overrightarrow{\partial}}{\partial R_n}\right]\right) = 1 - \frac{1}{2}\left(\frac{\hbar}{2}\right)^2\left[\frac{\overleftarrow{\partial}}{\partial R_n}\frac{\overrightarrow{\partial}}{\partial P_n} - \frac{\overleftarrow{\partial}}{\partial P_n}\frac{\overrightarrow{\partial}}{\partial R_n}\right]^2 + \\ + \frac{1}{4!}\left(\frac{\hbar}{2}\right)^4\left[\frac{\overleftarrow{\partial}}{\partial R_n}\frac{\overrightarrow{\partial}}{\partial P_n} - \frac{\overleftarrow{\partial}}{\partial P_n}\frac{\overrightarrow{\partial}}{\partial R_n}\right]^4$$

$$\begin{aligned}\left[\sum_{k=1}^{N}\left(\frac{\overleftarrow{\partial}}{\partial R_n}\frac{\overrightarrow{\partial}}{\partial P_n} - \frac{\overleftarrow{\partial}}{\partial P_n}\frac{\overrightarrow{\partial}}{\partial R_n}\right)\right]^2 &= \sum_{k=1}^{N}\sum_{l=1}^{N}\left[\left(\frac{\overleftarrow{\partial}}{\partial R_n}\frac{\overrightarrow{\partial}}{\partial P_n} - \frac{\overleftarrow{\partial}}{\partial P_n}\frac{\overrightarrow{\partial}}{\partial R_n}\right)\times\right. \\ &\quad \left.\times\left(\frac{\overleftarrow{\partial}}{\partial R_l}\frac{\overrightarrow{\partial}}{\partial P_l} - \frac{\overleftarrow{\partial}}{\partial P_l}\frac{\overrightarrow{\partial}}{\partial R_l}\right)\right] \\ &= \sum_{k=1}^{N}\sum_{l=1}^{N}\left[\frac{\overleftarrow{\partial}}{\partial R_n}\frac{\overrightarrow{\partial}}{\partial P_n}\frac{\overleftarrow{\partial}}{\partial R_l}\frac{\overrightarrow{\partial}}{\partial P_l} - \frac{\overleftarrow{\partial}}{\partial R_n}\frac{\overrightarrow{\partial}}{\partial P_n}\frac{\overleftarrow{\partial}}{\partial P_l}\frac{\overrightarrow{\partial}}{\partial R_l}\right. \\ &\quad \left.-\frac{\overleftarrow{\partial}}{\partial P_n}\frac{\overrightarrow{\partial}}{\partial R_n}\frac{\overleftarrow{\partial}}{\partial R_l}\frac{\overrightarrow{\partial}}{\partial P_l} + \frac{\overleftarrow{\partial}}{\partial P_n}\frac{\overrightarrow{\partial}}{\partial R_n}\frac{\overleftarrow{\partial}}{\partial P_l}\frac{\overrightarrow{\partial}}{\partial R_l}\right] \\ &= \sum_{k=1}^{N}\sum_{l=1}^{N}\left[\frac{\overleftarrow{\partial^2}}{\partial R_n\partial R_l}\frac{\overrightarrow{\partial^2}}{\partial P_n\partial P_l} - \frac{\overleftarrow{\partial^2}}{\partial R_n\partial P_l}\frac{\overrightarrow{\partial^2}}{\partial P_n\partial R_l} - \right. \\ &\quad \left.-\frac{\overleftarrow{\partial^2}}{\partial P_n\partial R_l}\frac{\overrightarrow{\partial^2}}{\partial R_n\partial P_l}\frac{\overleftarrow{\partial^2}}{\partial P_n\partial P_l}\frac{\overrightarrow{\partial^2}}{\partial R_n\partial R_l}\right]\end{aligned}$$

Therefore the Wigner Bloch equation becomes

$$\begin{aligned}
\frac{\partial \Omega_W}{\partial \beta} &= -\left[\sum_{n=1}^{N}\left(\frac{P_n^2}{2m_n}+\frac{1}{2}m_n\omega_n^2R_n^2\right)\right]\Omega_W + \\
&\quad +\frac{\hbar^2}{8}\left[\sum_{n=1}^{N}\left(\frac{P_n^2}{2m_n}+\frac{1}{2}m_n\omega_n^2R_n^2\right)\right]\sum_{k=1}^{N}\sum_{l=1}^{N}\left(\overleftarrow{\frac{\partial^2}{\partial R_n\partial R_l}}\overrightarrow{\frac{\partial^2}{\partial P_n\partial P_l}}-\right. \\
&\quad \left.-\overleftarrow{\frac{\partial^2}{\partial R_n\partial P_l}}\overrightarrow{\frac{\partial^2}{\partial P_n\partial R_l}}-\overleftarrow{\frac{\partial^2}{\partial P_n\partial R_l}}\overrightarrow{\frac{\partial^2}{\partial R_n\partial P_l}}+\overleftarrow{\frac{\partial^2}{\partial P_n\partial P_l}}\overrightarrow{\frac{\partial^2}{\partial R_n\partial R_l}}\right)\Omega_W \\
&= -\left[\sum_{n=1}^{N}\left(\frac{P_n^2}{2m_n}+\frac{1}{2}m_n\omega_n^2R_n^2\right)\right]\Omega_W + \\
&\quad +\sum_{k=1}^{N}\sum_{l=1}^{N}\sum_{n=1}^{N}\left(\frac{P_n^2}{2m_n}\overleftarrow{\frac{\partial^2}{\partial P_n\partial P_l}}\overrightarrow{\frac{\partial^2}{\partial R_n\partial R_l}}+\frac{1}{2}m_n\omega_n^2R_n^2\overleftarrow{\frac{\partial^2}{\partial R_n\partial R_l}}\overrightarrow{\frac{\partial^2}{\partial P_n\partial P_l}}\right)
\end{aligned}$$

The Wigner transformed Bloch equation for N independent harmonic oscillators becomes

$$\begin{aligned}
\frac{\partial \Omega_W}{\partial \beta} &= -\left[\sum_{n=1}^{N}\left(\frac{P_n^2}{2m_n}+\frac{1}{2}m_n\omega_n^2R_n^2\right)\right]\Omega_W \\
&\quad +\frac{\hbar^2}{8}\sum_{k=1}^{N}\sum_{l=1}^{N}\left(\frac{1}{m_n}\overrightarrow{\frac{\partial^2}{\partial R_n\partial R_l}}+m_n\omega_n^2\overrightarrow{\frac{\partial^2}{\partial P_n\partial P_l}}\right)\Omega_W \\
&= -\left[\sum_{n=1}^{N}\left(\frac{P_n^2}{2m_n}+\frac{1}{2}m_n\omega_n^2R_n^2\right)\right]\Omega_W \\
&\quad +\frac{\hbar^2}{8}\sum_{k=1}^{N}\sum_{l=1}^{N}\left(\frac{1}{m_n}\frac{\partial^2\Omega_W}{\partial R_n\partial R_l}+m_n\omega_n^2\frac{\partial^2\Omega_W}{\partial P_n\partial P_l}\right) \qquad \text{(B.0.38)}
\end{aligned}$$

To solve this equation we let

$$\Omega(R_n,P_n) = e^{-A(\beta)H+B(\beta)} \qquad \text{(B.0.39)}$$

$$\text{where} \qquad A(0) = B(0) = 0 \qquad \text{(B.0.40)}$$

and use the Baker-Hausdorff Theorem.

NB:

$$\begin{aligned}
\frac{\partial H}{\partial R_n} &= m_n\omega_n^2R_n \\
\frac{\partial H}{\partial P_n} &= \frac{P_n}{m_n}
\end{aligned}$$

We now find the required derivatives of Ω and substitute them into equation (B.0.38)

$$\begin{aligned}
\sum_{k=1}^{N}\frac{\partial\Omega}{\partial R_n} &= \sum_{k=1}^{N}\left[\Omega\left(-A(\beta)\frac{\partial H}{\partial R_n}\right)\right] \\
&= \Omega\left(-A(\beta)\sum_{k=1}^{N}m_n\omega_n^2R_n\right) \\
\sum_{k=1}^{N}\sum_{l=1}^{N}\frac{\partial^2\Omega}{\partial R_n\partial R_l} &= \left(\sum_{l=1}^{N}\frac{\partial\Omega}{\partial R_l}\right)\left[-A(\beta)\sum_{k=1}^{N}m_n\omega_n^2R_n\right]-A(\beta)\Omega\sum_{l=1}^{N}m_l\omega_l^2 \\
&= \left(-A(\beta)\sum_{k=1}^{N}m_n\omega_n^2R_n\right)^2\Omega-A(\beta)\Omega\sum_{k=1}^{N}m_n\omega_n^2 \\
&= \left[A^2(\beta)\left(\sum_{k=1}^{N}m_n\omega_n^2R_n\right)^2-A(\beta)\sum_{k=1}^{N}m_n\omega_n^2\right]\Omega \qquad \text{(B.0.41)} \\
\sum_{k=1}^{N}\frac{\partial\Omega}{\partial P_n} &= \Omega\left(-A(\beta)\sum_{k=1}^{N}\frac{\partial H}{\partial P_n}\right) \\
&= -\Omega A(\beta)\sum_{k=1}^{N}\left(\frac{P_n}{m_n}\right) \\
\sum_{k=1}^{N}\sum_{l=1}^{N}\frac{\partial^2\Omega}{\partial P_n\partial P_l} &= -A(\beta)\sum_{k=1}^{N}\sum_{l=1}^{N}\frac{\partial^2H}{\partial P_n\partial P_l}\Omega-A(\beta)\sum_{k=1}^{N}\sum_{l=1}^{N}\frac{\partial H}{\partial P_n}\frac{\partial\Omega}{\partial P_l} \\
&= -A(\beta)\sum_{k=1}^{N}\left(\frac{1}{m_n}\right)\Omega+A^2(\beta)\sum_{k=1}^{N}\left(\frac{P_n}{m_n}\right)\sum_{l=1}^{N}\left(\frac{P_l}{m_l}\right)\Omega \\
&= -A(\beta)\sum_{k=1}^{N}\left(\frac{1}{m_n}\right)\Omega+A^2(\beta)\left(\sum_{k=1}^{N}\frac{P_n}{m_n}\right)^2\Omega \qquad \text{(B.0.42)}
\end{aligned}$$

Upon substituting the calculated derivatives, the Wigner transformed Bloch equation becomes

$$\sum_{k=1}^{N}\Omega\left(P_n,R_n\right)\left[-\frac{\partial A}{\partial\beta}H+\frac{\partial B}{\partial\beta}\right]=-H\sum_{k=1}^{N}\Omega_W(P_n,R_n)+\frac{\hbar^2}{8}\sum_{k=1}^{N}\sum_{l=1}^{N}\left(\frac{1}{m_n}\frac{\partial^2\Omega}{\partial R_n\partial R_l}+m_n\omega_n^2\frac{\partial^2\Omega}{\partial P_n\partial P_l}\right) \qquad \text{(B.0.43)}$$

Consider the second term on the right hand side of equation (B.0.43)

$$\begin{aligned}
\frac{\hbar^2}{8}\sum_{k=1}^{N}\sum_{l=1}^{N}\left(\frac{1}{m_n}\frac{\partial^2\Omega}{\partial R_n\partial R_l}\right) &= \frac{\hbar^2}{8}\sum_{k=1}^{N}\left\{\frac{1}{m_n}\left[A^2(\beta)\left(m_n\omega_n^2R_n\right)^2-A(\beta)m_n\omega_n^2\right]\right\}\Omega \\
&= \frac{\hbar^2}{8}\sum_{k=1}^{N}\left[A^2(\beta)m_n\left(\omega_n^2R_n\right)^2-A(\beta)\omega_n^2\right]\Omega \qquad \text{(B.0.44)}
\end{aligned}$$

Now consider the third term on the right hand side of equation (B.0.43)

$$\begin{aligned}\frac{\hbar^2}{8}\sum_{k=1}^{N}\sum_{l=1}^{N} m_n\omega_n^2\left(\frac{\partial^2\Omega}{\partial P_n\partial P_l}\right) &= \frac{\hbar^2}{8}\sum_{k=1}^{N}\sum_{l=1}^{N} m_n\omega_n^2\left[-A(\beta)\frac{1}{m_n}\Omega + A^2(\beta)\left(\frac{P_n}{m_n}\right)^2\right]\Omega \\ &= \frac{\hbar^2}{8}\sum_{k=1}^{N}\left[-A(\beta)\omega_n^2 + A^2(\beta)\frac{1}{m_n}\left(P_n\omega_n\right)^2\right]\Omega \quad \text{(B.0.45)}\end{aligned}$$

We now simplify equation (B.0.43)

$$\begin{aligned}-\frac{\partial A}{\partial\beta}H + \frac{\partial B}{\partial\beta} &= -H + \frac{\hbar^2}{8}\sum_{k=1}^{N}\Big[A^2(\beta)m_n\left(\omega_n^2R_n\right)^2 - A(\beta)\omega_n^2 - A(\beta)\omega_n^2 \\ &\qquad + A^2(\beta)\frac{1}{m_n}\left(P_n\omega_n\right)^2\Big] \\ &= -H + \frac{\hbar^2}{8}\sum_{k=1}^{N}\left[A^2(\beta)\omega_n^2\left(m_n\left(\omega_nR_n\right)^2 + \frac{P_n^2}{m_n}\right) - 2\omega_n^2A(\beta)\right] \\ &= -H + \frac{\hbar^2}{4}\sum_{k=1}^{N}\left[-\omega_n^2A(\beta) + A^2(\beta)\omega_n^2\left(\frac{1}{2}m_n\omega_n^2R_n^2 + \frac{P_n^2}{2m_n}\right)\right] \\ &= -H + \frac{\hbar^2}{4}\sum_{k=1}^{N}\left[-\omega_n^2A(\beta) + A^2(\beta)\omega_n^2H\right] \\ -\frac{\partial A}{\partial\beta}H + H &= -\frac{\partial B}{\partial\beta} + \frac{\hbar^2}{4}\sum_{k=1}^{N}\left[-\omega_n^2A(\beta) + A^2(\beta)\omega_n^2H\right] \\ \left(-\frac{\partial A}{\partial\beta} + 1\right)H &= -\frac{\partial B}{\partial\beta} + \sum_{k=1}^{N}\left[\left(\frac{\hbar\omega_n}{2}\right)^2\left(-A(\beta) + A^2(\beta)H\right)\right] \\ \left[-\frac{\partial A}{\partial\beta} + 1 - \sum_{k=1}^{N}\left(\frac{\hbar\omega_nA(\beta)}{2}\right)^2\right]H &= -\frac{\partial B}{\partial\beta} - \sum_{k=1}^{N}\left[\left(\frac{\hbar\omega_n}{2}\right)^2A(\beta)\right]\end{aligned}$$

This equation must hold for all q and p, due to terms in the bracket are independent of q and p, therefore they must vanish independently.

$$\frac{dA}{d\beta} - 1 + \frac{(\hbar\omega_n)^2}{4}A^2 = 0 \quad \text{(B.0.46)}$$

$$\frac{\partial B}{\partial\beta} + \left(\frac{\hbar\omega_n}{2}\right)^2A = 0 \quad \text{(B.0.47)}$$

$$\frac{dA}{d\beta} = 1 - \left(\frac{\hbar\omega_n}{2}\right)^2 A^2 \tag{B.0.48}$$

$$\frac{dA}{1 - \left(\frac{\hbar\omega_n}{2}\right)^2 A^2} = d\beta \tag{B.0.49}$$

Consider the derivative of $\ln\left(\frac{1+x}{1-x}\right)$

$$\frac{d}{dx}\ln\left(\frac{1+x}{1-x}\right) = \frac{1-x}{1+x}\frac{d}{dx}\left(\frac{1+x}{1-x}\right) \tag{B.0.50}$$

$$= \frac{1-x}{1+x}\left(\frac{1}{1-x} - \frac{1+x}{(1-x)^2}(-1)\right) \tag{B.0.51}$$

$$= \frac{1-x}{1+x}\left(\frac{1}{1-x} + \frac{1+x}{(1-x)^2}\right) \tag{B.0.52}$$

$$= \frac{1}{1+x} + \frac{1}{1-x} \tag{B.0.53}$$

$$\frac{d}{dx}\ln\left(\frac{1+x}{1-x}\right) = \frac{1-x+1+x}{1-x^2} \tag{B.0.54}$$

$$= \frac{2}{1-x^2} \tag{B.0.55}$$

Therefore, we have the identity

$$\frac{1}{2}\frac{d}{dx}\ln\left(\frac{1+x}{1-x}\right) = \frac{1}{1-x^2} \tag{B.0.56}$$

Identifying

$$x = \frac{\hbar\omega_n}{2}A$$

$$dA = \frac{2}{\hbar\omega_n}dx$$

We can now integrate equation (B.0.49)

$$\int \frac{dA}{1-\left(\frac{\hbar\omega_n}{2}\right)^2 A^2} = \int d\beta \tag{B.0.57}$$

$$\frac{2}{\hbar\omega_n}\int \frac{1}{1-x^2} = \beta + C \tag{B.0.58}$$

$$\frac{2}{2\hbar\omega_n}\int dx \frac{d}{dx}\ln\left(\frac{1+x}{1-x}\right) = \beta + C \tag{B.0.59}$$

$$\frac{1}{\hbar\omega_n}\ln\left(\frac{1+x}{1-x}\right) = \beta \tag{B.0.60}$$

$$\beta = \frac{1}{\hbar\omega_n}\ln\left[\frac{1+\frac{\hbar\omega_n}{2}A}{1-\frac{\hbar\omega_n}{2}A}\right] \tag{B.0.61}$$

Inverting this equation gives

$$\hbar\omega_n\beta = \ln\left[\frac{1+\frac{\hbar\omega_n}{2}A}{1-\frac{\hbar\omega_n}{2}A}\right] \tag{B.0.62}$$

$$e^{\hbar\omega_n\beta} = \frac{1+\frac{\hbar\omega_n}{2}A}{1-\frac{\hbar\omega_n}{2}A} \tag{B.0.63}$$

$$e^{\hbar\omega_n\beta}\left(1-\frac{\hbar\omega_n}{2}A\right) = 1+\frac{\hbar\omega_n}{2}A \tag{B.0.64}$$

$$e^{\hbar\omega_n\beta} - e^{\hbar\omega_n\beta}\frac{\hbar\omega_n}{2}A - 1 = \frac{\hbar\omega_n}{2}A \tag{B.0.65}$$

$$e^{\hbar\omega_n\beta} - 1 = \frac{\hbar\omega_n}{2}\left(e^{\hbar\omega_n\beta}A + A\right) \tag{B.0.66}$$

$$= \frac{\hbar\omega_n}{2}\left(e^{\hbar\omega_n\beta}+1\right)A \tag{B.0.67}$$

We can now write A as

$$A = \frac{2}{\hbar\omega_n}\left(\frac{e^{\hbar\omega_n\beta}-1}{e^{\hbar\omega_n\beta}+1}\right) \tag{B.0.68}$$

$$= \frac{2}{\hbar\omega_n}\left(\frac{e^{\frac{\hbar}{2}\omega_n\beta}-e^{\frac{\hbar}{2}\omega_n\beta}}{e^{\frac{\hbar}{2}\omega_n\beta}+e^{\frac{\hbar}{2}\omega_n\beta}}\right) \tag{B.0.69}$$

$$A = \frac{2}{\hbar\omega_n}\left(\frac{e^{\frac{\hbar}{2}\omega_n\beta}-e^{\frac{\hbar}{2}\omega_n\beta}}{e^{\frac{\hbar}{2}\omega_n\beta}+e^{\frac{\hbar}{2}\omega_n\beta}}\right) \tag{B.0.70}$$

$$= \frac{2}{\hbar\omega_n}\tanh\left(\frac{\hbar\omega_n}{2}\beta\right) \tag{B.0.71}$$

We now use equation (B.0.47) to find B

$$\frac{\partial B}{\partial \beta} + \left(\frac{\hbar\omega_n}{2}\right)^2 A = 0 \tag{B.0.72}$$

$$\frac{\partial B}{\partial \beta} + \left(\frac{\hbar\omega_n}{2}\right)^2 \frac{2}{\hbar\omega_n} \tanh\left(\frac{\hbar\omega_n}{2}\beta\right) = 0 \tag{B.0.73}$$

$$B = -\frac{\hbar\omega_n}{2} \int d\beta \tanh\left(\frac{\hbar\omega_n}{2}\beta\right) \tag{B.0.74}$$

Let us recall the hyperbolic functions

$$\cosh x = \frac{e^x + e^{-x}}{2} \tag{B.0.75}$$

$$\sinh x = \frac{e^x - e^{-x}}{2} \tag{B.0.76}$$

$$\frac{d\cosh x}{dx} = \sinh x \tag{B.0.77}$$

$$\frac{d\sinh x}{dx} = \cosh x \tag{B.0.78}$$

$$\cosh^2 x - \sinh^2 x = 1 \tag{B.0.79}$$

Therefore we have the identity

$$\frac{d}{dx}\ln\left(\cosh x\right) = \frac{1}{\cosh x}\sinh x = \tanh x \tag{B.0.80}$$

Identifying

$$x = \frac{\hbar\omega_n}{2}\beta \tag{B.0.81}$$

$$dx = \frac{\hbar\omega_n}{2}d\beta \tag{B.0.82}$$

Therefore

$$B = -\frac{\hbar\omega_n}{2}\frac{2}{\hbar\omega_n}\int dx \tanh x \tag{B.0.83}$$

$$= -\int dx \frac{d}{dx}\ln(\cosh x) \tag{B.0.84}$$

$$= -\ln(\cosh x) \tag{B.0.85}$$

$$B = -\ln\left[\cosh\left(\frac{\hbar\omega_n}{2}\beta\right)\right] \tag{B.0.86}$$

Therefore from

$$\Omega = e^{-AH+B} = e^{-AH}e^{B} \tag{B.0.87}$$

the un-normalized density matrix is

$$\begin{aligned}
\Omega &= \exp\left[-\ln\left[\cosh\left(\frac{\hbar\omega_n}{2}\beta\right)\right]\right]\exp\left[-\frac{2}{\hbar\omega_n}\tanh\left(\frac{\hbar\omega_n}{2}\beta\right)H\right] && \text{(B.0.88)}\\
&= \exp\left[\ln\left[\cosh\left(\frac{\hbar\omega_n}{2}\beta\right)\right]^{-1}\right]\exp\left[-\frac{2}{\hbar\omega_n}\tanh\left(\frac{\hbar\omega_n}{2}\beta\right)H\right] && \text{(B.0.89)}\\
&= \frac{1}{\cosh\left(\frac{\hbar\omega_n}{2}\beta\right)}\exp\left[-\frac{2}{\hbar\omega_n}\tanh\left(\frac{\hbar\omega_n}{2}\beta\right)H\right] && \text{(B.0.90)}
\end{aligned}$$

To complete the derivation, one needs to normalize Ω

$$\begin{aligned}
Z(\beta) &= \int \mathrm{dq}_n\mathrm{dp}_n\Omega && \text{(B.0.91)}\\
\hat{\rho} &= \frac{\hat{\Omega}}{Z(\beta)} && \text{(B.0.92)}
\end{aligned}$$

The Wigner transform corresponds to

$$\rho_W = \frac{1}{Z(\beta)}W(\hat{\Omega}) \tag{B.0.93}$$

$$\begin{aligned}
Z(\beta) &= \frac{1}{\cosh\left(\frac{\hbar\omega_n}{2}\beta\right)}\int \mathrm{dq}_n\mathrm{dp}_n\exp\left[-\frac{2}{\hbar\omega_n}\tanh\left(\frac{\hbar\omega_n}{2}\beta\right)\left(\frac{p_n^2}{2m_n}+\frac{1}{2}m_n\omega_n^2q_n^2\right)\right]\\
&= \frac{1}{\cosh\left(\frac{\hbar\omega_n}{2}\beta\right)}\int \mathrm{dp}_n\exp\left[-\frac{2}{\hbar\omega_n}\tanh\left(\frac{\hbar\omega_n}{2}\beta\right)\frac{p_n^2}{2m_n}\right]*\\
&\quad *\int \mathrm{dq}_n\exp\left[-\frac{2}{\hbar\omega_n}\tanh\left(\frac{\hbar\omega_n}{2}\beta\right)\frac{m_n\omega_n^2q_n^2}{2}\right]
\end{aligned}$$

Gaussian integral

$$\int e^{-ax^2} = \sqrt{\frac{\pi}{a}} \tag{B.0.94}$$

$$\begin{aligned}
\int \mathrm{dp}_n\exp\left[-\frac{2}{\hbar\omega_n}\tanh\left(\frac{\hbar\omega_n}{2}\beta\right)\frac{p_n^2}{2m_n}\right] &= \sqrt{\frac{\pi}{\frac{1}{\hbar\omega_n m_n}\tanh\left(\frac{\hbar\omega_n}{2}\beta\right)}} && \text{(B.0.95)}\\
\int \mathrm{dq}_n\exp\left[-\frac{m_n\omega_n}{\hbar}\tanh\left(\frac{\hbar\omega_n}{2}\beta\right)q_n^2\right] &= \sqrt{\frac{\pi}{\frac{m_n\omega_n}{\hbar}\tanh\left(\frac{\hbar\omega_n}{2}\beta\right)}} && \text{(B.0.96)}
\end{aligned}$$

$$Z(\beta) = \frac{1}{\cosh\left(\frac{\hbar\omega_n}{2}\beta\right)} \frac{\pi}{\tanh\left(\frac{\hbar\omega_n}{2}\beta\right)} \frac{1}{\sqrt{\frac{1}{\hbar\omega_n m_n}\frac{m_n\omega_n}{\hbar}}} \tag{B.0.97}$$

$$= \frac{\pi\hbar}{\cosh\left(\frac{\hbar\omega_n}{2}\beta\right)\frac{\sinh\left(\frac{\hbar\omega_n}{2}\beta\right)}{\cosh\left(\frac{\hbar\omega_n}{2}\beta\right)}} \tag{B.0.98}$$

$$= \frac{\pi\hbar}{\sinh\left(\frac{\hbar\omega_n}{2}\beta\right)} \tag{B.0.99}$$

$$Z(\beta) = \frac{\pi\hbar}{\sinh\left(\frac{\hbar\omega_n}{2}\beta\right)} \tag{B.0.100}$$

Finally

$$\rho_W = \frac{\sinh\left(\frac{\hbar\omega_n}{2}\beta\right)}{\pi\hbar} \frac{\exp\left[-\frac{2}{\hbar\omega_n}\tanh\left(\frac{\hbar\omega_n}{2}\beta\right)H\right]}{\cosh\left(\frac{\hbar\omega_n}{2}\beta\right)}$$

$$= \frac{1}{\pi\hbar}\tanh\left(\frac{\hbar\omega_n}{2}\beta\right)\exp\left[-\frac{2}{\hbar\omega_n}\tanh\left(\frac{\hbar\omega_n}{2}\beta\right)H\right]$$

$$= \frac{1}{\pi\hbar}\tanh\left(\frac{\hbar\omega_n}{2}\beta\right)\exp\left[-\frac{2}{\hbar\omega_n}\tanh\left(\frac{\hbar\omega_n}{2}\beta\right)\sum_{k=1}^{N}\left(\frac{1}{2m_n}P_n^2+\frac{1}{2}m_n\omega_n^2R_n^2\right)\right]$$

$$\rho_W(R_n,P_n,\beta) = \prod_{k=1}^{N}\left\{\frac{1}{\pi\hbar}\tanh\left(\frac{\hbar\omega_n}{2}\beta\right)\exp\left[-\frac{2}{\hbar\omega_n}\tanh\left(\frac{\hbar\omega_n}{2}\beta\right)\left(\frac{1}{2m_n}P_n^2+\frac{1}{2}m_n\omega_n^2R_n^2\right)\right]\right\}$$

$$= \prod_{k=1}^{N}\left\{\frac{1}{\pi\hbar}\tanh\left(\frac{\hbar\omega_n}{2}\beta\right)\exp\left[-\frac{2}{\hbar\omega_n}\tanh\left(\frac{\hbar\omega_n}{2}\beta\right)H_{NORM}\right]\right\}$$

which is the Wigner distribution of the normalized density matrix for an ensemble of oscillators at temperature T.

NB: Each mode has a different temperature.

Bibliography

[1] B. Krüger, L. Schäfer, and A. Baumgärtner. *J. Phys.*, **50**(3191), 1989.

[2] J. Dautenhahn and C. K. Hall. *Macromolecules*, **27**(5399), 1994.

[3] A. A. Louis, P. G. Bolhuis, J.-P. Hansen, and E. J. Meijer. Can polymer coils be modeled as "soft colloids"? *Phys. Rev. Lett.*, **85**(2522), 2000.

[4] R. Hunter. *Foundations of Colloid Science*, volume **I**. Clarendon Press, Oxford, 1986.

[5] W.B. Russel, D.A. Saville, and W.R. Schowalter. *Colloidal Dispersions*. Cambridge University Press, Cambridge, 1990.

[6] A. Ashkin. Acceleration and trapping of particles by radiation pressure. *Phys. Rev. Lett.*, **24**(156), 1970.

[7] N. Osterman, D. Babic, I. Poberaj, J. Dobnikar, and P. Ziherl. Observation of condensed phases of quasiplanar core-softened colloids. *Phys. Rev. Lett.*, **99**(248301), 2007.

[8] D. G. Grier. A revolution in optical manipulation. *Nature*, **424**(810), 2003.

[9] C.N. Likos. Effective interactions in soft condensed matter physics. *Phys. Reports*, **348**(267), 2001.

[10] C. N. Likos. Soft matter with soft particles. *Soft Matter*, **2**(478), 2006.

[11] J. S. Higgins and H Benoit. *Polymers and neutron scattering*. Oxford University Press, Oxford, 1997.

[12] C. A. Murray and D. G Grier. Video microscopy of monodisperse colloidal systems. *Annu. Rev. Phys. Chem.*, **47**(421), 1996.

[13] P. Habdas and E. R. Weeks. Video microscopy of colloidal suspensions and colloidal crystals. *Curr. Opin. Colloid Interface Sci.*, **7**(196203), 2002.

[14] M. P. Allen and D. J. Tildesley. *Computer Simulation of Liquids.* Oxford University Press, 1987.

[15] C. Braga and K. P. Travis. A configurational temperature nosé-hoover thermostat. *J. Chem. Phys.*, **123**(134101), 2005.

[16] A. Sergi and M. Ferrario. Non-hamiltonian equations of motion with a conserved energy. *Phys. Rev. E*, **64**(056125), 2001.

[17] P. Mausbach and H. O. May. Static and dynamic anomalies in the gaussian core model liquid. *Fluid Phase Equilibria*, **249**(17), 2006.

[18] B.J. Alder and T.E. Wainwright. Phase transition for a hard sphere system. *J. Chem. Phys.*, **27**(1208), 1957.

[19] B.J. Alder and T.E. Wainwright. Studies in molecular dynamics, i. general method. *J. Chem. Phys.*, **31**(459), 1959.

[20] B.J. Alder and T.E. Wainwright. Studies in molecular dynamics, ii. behavior of a small number of elastic spheres. *J. Chem. Phys.*, **33**(1439), 1960.

[21] A. Rahman. Correlations in the motion of atoms in liquid argon. *Physical Review*, **136**(405), 1964.

[22] A. Rahman and T. E. Wainwright. *Phys. Rev. A*, **136**(405), 1964.

[23] F. H Stillinger. Phase transition in the gaussian core system. *J. Chem. Phys.*, **65**(3968), 1976.

[24] F.H. Stillinger and D.K. Stillinger. Negative thermal expansion in the gaussian core model. *Physica A*, **244**(358), 1997.

[25] H. C. Andersen. *J. Chem. Phys.*, **72**(2384), 1980.

[26] S. Nose. *Mol. Phys.*, **52**(255), 1984.

[27] S. Nose and M. L. Klein. *Mol. Phys.*, **50**(1055), 1983.

[28] R. Schneider H. Fehske and A. Weibe. *Computational Many-Particle Physics*. Springer, Berlin Heidelberg, 2008.

[29] H. Goldstein. *Classical Mechanics*. Addison-Wesley, London, 2nd edition, 1980.

[30] H. H. Rugh. A geometric, dynamical approach to thermodynamics. *J. Phys. A*, **31**(7761), 1998.

[31] D. J. Evans and G. P. Morriss. *Statistical Mechanics of Nonequilibrium Liquids*. Cambridge University Press, Cambridge, 2nd edition edition, 2008.

[32] J. J. Erpenbeck. Shear viscosity of the hard-sphere fluid via nonequilibrium molecular dynamics. *Phys. Rev. Lett.*, **52**(1333), 1984.

[33] D. J. Evans and G. P. Morriss. Shear thickening and turbulence in simple fluids. *Phys. Rev. Lett.*, **56**(2172), 1986.

[34] D. J. Evans, S. T. Cui, H. J. M. Hanley, and G. C. Straty. Conditions for the existence of a reentrant solid phase in a sheared atomic fluid. *Phys. Rev. A*, **46**(6731), 1992.

[35] B. D. Todd S. Bernardi and D. J. Searles. Thermostating highly confined fluids. *J. Chem. Phys.*, **132**(244706), 2010.

[36] L. Lue and Denis J. Evans. Configurational temperature for systems with constraints. *Phys. Rev. E*, **62**(4764), 2000.

[37] J. Delhommelle and D.J. Evans. Configurational temperature thermostat for fluids undergoing shear flow: application to liquid chlorine. *Mol. Phys.*, **99**(1825), 2001.

[38] B. D. Butler, G. Ayton, O. G. Jepps, and D. J. Evans. Configurational temperature: Verification of monte carlo simulations. *J. Chem. Phys.*, **109**(6519), 1998.

[39] S. Nose. A unified formulation of the constant temperature molecular dynamics methods. *J. Chem. Phys.*, **81**(511), 1984.

[40] W. G. Hoover. Canonical dynamics: Equilibrium phase-space distributions. *Phys. Rev. A*, **31**(1695), 1985.

[41] D. Beckedahl, E. O. Obaga, D. A. Uken, A. Sergi, and M. Ferrario. On the configurational temperature nosé-hoover thermostat. 2015.

[42] J. D. Weeks, D. Chandler, and H. C. Andersen. Role of repulsive forces in determining the equilibrium structure of simple liquids. *J. Chem. Phys.*, **54**(5237), 1971.

[43] H. C. Andersen, J. D. Weeks, and D. Chandler. Relationship between the hard-sphere fluid and fluids with realistic repulsive forces. *Phys. Rev. A*, **4**(1597), 1971.

[44] J. P. Hansen and I. R. McDonald. *Theory of Simple Liquids*. Academic Press, Amsterdam, London, 3rd edition, 2006.

[45] Y. Tang. Role of the barker-henderson diameter in thermodynamics. *J. Chem. Phys.*, **116**(6694), 2002.

[46] D. T. N. Chen, Q. Wen, P. A. Janmey, J. C. Crocker, and A. G. Yodh. Rheology of soft materials. *Ann. Rev. Cond. Mat. Phys*, 1, 2010.

[47] S. Prestipino, F. Saija, and P. V. Giaquinta. Phase diagram of the gaussian-core model. *Condensed Matter*, (0506012), 2005.

[48] M. Ceriotti, M. Parrinello, T. E. Markland, and D. E. Manolopoulos. Efficient stochastic thermostatting of path integral molecular dynamics. *J. Chem. Phys.*, **133**(124104), 2010.

[49] N Go, T Noguti, and T Nishikawa. Dynamics of a small globular protien in terms of low-frequency vibrational-modes. *Proc. Nati Acad. Sci*, **80**(3696), 1983.

[50] M. Levitt, C. Sander, and P. S. Stern. The normal modes of a protein: Native bovine pancreatic trypsin inhibitor. *Int. J. Quant. Chem*, **10**(181), 1983.

[51] B. Brooks and M. Karplus. Harmonic dynamics of proteins: Normal modes and fluctuations harmonic dynamics of proteins: Normal modes and fluctuations in bovine pancreatic trypsin inhibitor. *Proc. Natl. Acad. Sci. USA*, **80**(6571), 1983.

[52] D. I. Bower and W. F. Maddams. The vibrational spectroscopy of polymers. *Cambridge University Press, Cambridge*, 1989.

[53] R. Zbinden. Infrared spectroscopy of high polymers. *Academic Press, New York*, 1964.

[54] P. C. Painter, M. M. Coleman, and J. L. Koenig. The theory of vibrational spectroscopy and its application to polymeric materials. *Wiley, New York*, 1982.

[55] E. B. Wilson Jr., J. C. Decius, and P. C. Cross. Molecular vibrations. *Dover, New York*, 1980.

[56] M. Levitt, C. Sander, and P. S. Stern. Protein normal-mode dynamics: Trypsin inhibitor, crambin, ribonuclease and lysozyme. *Journal of molecular biology*, **181**(423), 1985.

[57] J. P. Ma. New advances in normal mode analysis of supermolecular new advances in normal mode analysis of supermolecular complexes and applications to structural refinement. *Curr. Protein Pept. Sci.*, **5**(119), 2004.

[58] G. Kresse, J. Furthmüller, and J. Hafner. Ab initio force constant approach to phonon dispersion relations of diamond and graphite. *Europhys. Lett.*, **32**(729), 1995.

[59] D. Alfé, G. D. Price, and M. J. Gillan. Thermodynamics of hexagonal-close-packed iron under earth's core conditions. *Phys. Rev. B*, **64**(045123), 2001.

[60] E. Wigner. On the quantum correction for thermodynamic equilibrium. *Phys. Rev.*, **40**(749), 1932.

[61] M. Hillery, R.F. O'Connell, M.O. Scully, and E.P. Wigner. Distribution functions in physics: fundamentals. *Phys. Reports*, **106**(121), 1984.

[62] H. Lee. Theory and application of the quantum phase-space distribution functions. *Phys. Reports*, **259**(147), 1995.

[63] L. E. Ballentine. Quantum mechanics a modern development. *Singapore: World scientific*, 1998.

[64] V. Zelevinsky. *Quantum Physics*, volume I. Wiley-VCH, Weinhein, 2011.

[65] L. E. Ballentine. *Quantum mechanics*. World Scientific, Amsterdam, 2005.

[66] D. J. Tobias, G. J. Martyna, and M. L. Klein. Molecular dynamics simulations of a protein in the canonical ensemble. *J. Phys. Chem*, **97**(12959), 1993.

[67] M. Watzlawek, C. N. Likos, and H. Löwen. Phase diagram of star polymer solutions. *Phys. Rev. Lett.*, **82**(5289), 1999.